APPLICATION OF FINITE ELASTIC THEORY TO THE DEFORMATION OF CYLINDRICAL TUBES

Thesis by
Jen-Shih Lee

In Partial Fulfillment of the Requirements
For the Degree of
Doctor of Philosophy

California Institute of Technology
Pasadena, California
1966
(Submitted April 27, 1966)

ACKNOWLEDGMENT

The author wishes to express his sincere appreciation to Professors Y. C. Fung and W. G. Frasher for their advice and encouragement throughout this work. The author is also grateful to Professor E. E. Sechler for his valuable suggestions regarding the work carried out in this investigation. The advice and suggestions of other members of the Department of Aeronautics are also appreciated.

Appreciation is expressed for the help received throughout the course of the experimental study from Dr. Kanji Kato and Mr. Joseph Johnson of the Cardiovascular Research Laboratory, and Mr. Marvin Jessey of the Electronics Laboratory and Mr. Milton Wood of the Structures Laboratory. Thanks are extended to Miss Helen Burrus and Miss Martha Fossum for helping with the preparation of the manuscript, to Miss Cecelia Lin for the data reduction and numerical calculations, to Mrs. Jewel Colbert for the reproduction of the manuscript. Very much appreciated was the help of Mrs. Philip Cassady for the typing of the thesis.

This study has been supported by the United States Air Force, Office of Scientific Research and this aid is gratefully acknowledged.

ABSTRACT

In Part I three types of symmetrical deformations of thin cylindrical rubber tubes are discussed. In the first type a rubber tube is deformed into another circular cylindrical tube of different length and diameter by simultaneous inflation and extension of the tube. This deformation is useful in determining the mechanical properties of tube-like material and it was found that Rivlin-Saunder form of strain-energy fitted a particular latex rubber used in our experiments. The second and third types of deformation are a tube deformed by a longitudinal stretching or an increase in internal pressure to a curved surface of revolution. A number of numerical examples were worked out with a view toward designing experiments to determine mechanical properties of short cylindrical tubes.

In Part II experimental studies on the overall mechanical properties of large blood vessels are presented. Two Lagrangian stresses and two extension ratios are used to describe the stress and strain states of the vessels subjected to symmetrical deformations. The interested deformation range is about ten to twenty percent in the neighborhood of the natural state.

Tests consisted of (1) a longitudinal stretching while the diameter of the vessels was maintained, (2) a lateral distension with the length of the vessels unchanged, and (3) repeated stretching of the vessels at low frequency.

The first two tests show that the stress-strain law of the vessels tested is highly nonlinear and the vessels behave more rigidly in the longitudinal direction than in the lateral direction. The last test shows that the vessels are more likely to behave as a plastic-elastic metal and a higher tangential modulus was observed for the vessels stretched at a smaller oscillation amplitude.

PART I

LARGE ELASTIC DEFORMATION OF THIN CYLINDRICAL TUBES

TABLE OF CONTENTS

LIST OF SYMBOLS

B	integration constant, Eq. (8)
C_1, C_2	physical constants (psi), $W = C_1(I_1 - 3) + C_2(I_2 - 3)$
$f(I_2 - 3)$	$W = C_1(I_1 - 3) + f(I_2 - 3)$, df/dI_2 is a decreasing function of I_2 as shown in Fig. 7
h_o, h	thicknesses of the undeformed and deformed tubes respectively
I_1, I_2	strain invariants, $I_1 = \sum_{r=1}^{3} \lambda_r^{\,2}$, $I_2 = \sum_{r=1}^{3} \lambda_r^{\,-2}$
ℓ_o, ℓ_f	lengths of the undeformed and deformed tubes
P	internal pressure (psi)
P'	$= PR_o/(2h_oC_1)$
R_o	radius of the middle surface S_o
(r, θ, z')	cylindrical polar system in the deformed state where z' is the axis of symmetry and r is the radius of S
r_e	radius at the ends of S
r_m	$= (r)_{z' = \ell_f/2}$, the radius at the equator of S
S_o, S	middle surfaces of the undeformed and deformed tube respectively
T_1, T_2	stress resultants per unit length in the meridional and latitudinal directions of S respectively

T	force, acting at the ends of the tube, required to keep it in equilibrium
T_1', T_2', T'	$= T_1/(2h_oC_1)$, $T_2/(2h_oC_1)$ and $T/(2\pi R_o h_o C_1)$ respectively
$W(I_1, I_2)$	strain-energy function of an isotropic incompressible material
Γ	$= C_2/C_1$
K_1, K_2	principal curvatures in the meridional and latitudinal directions of S
λ_1, λ_2, λ_3	principal extension ratios associated with meridians, the lines of the latitude and the normals of S respectively
λ_{1m}	$= (\lambda_1)_{z'} = \ell_f/2$
ξ	arc length measured along a meridian of S
(ξ, θ, N)	orthogonal curvilinear coordinates system in the deformed state where N is the normal coordinate of S
(ρ, θ, Z)	cylindrical polar system in the undeformed state where z is the axis of symmetry of the undeformed middle surface S_o

PART I

LARGE ELASTIC DEFORMATION OF THIN CYLINDRICAL TUBES

1. INTRODUCTION

We shall consider an elastic, incompressible, isotropic material whose constitutive law is specified by a strain-energy function W which is a function of two strain invariants I_1 and I_2. In the mathematical theory of large deformations of axially symmetrical elastic membranes, the governing equations are a set of nonlinear ordinary differential equations. In a few cases, such as the inflation of a circular plane sheet (Ref. 1), these differential equations can be numerically integrated for a general form of W. In other cases, e.g. the inflation of a thin-walled tube, it has been necessary to simplify the calculation by assuming the Mooney-Rivlin form for W

$$W = C_1(I_1 - 3) + C_2(I_2 - 3) \tag{1}$$

where I_1 and I_2 are defined in terms of the principal extension ratios λ_1, λ_2 and λ_3 by

$$I_1 = \lambda_1^2 + \lambda_2^2 + \lambda_3^2 \quad , \quad I_2 = \lambda_1^{-2} + \lambda_2^{-2} + \lambda_3^{-2} \tag{2}$$

and C_1 and C_2 are physical constants.

In this report we shall discuss three types of deformation of thin circular cylindrical rubber tubes. In the first type a rubber tube is deformed into another circular cylindrical tube of different length and diameter by simultaneous inflation and extension of the tube. Due to the simplicity in geometry, the governing differential equations are reduced to a set of algebraic equations in terms of the derivatives of the strain-energy function W. This simple deformation may be used in determining the strain-energy function from experimental data. The following Rivlin-Saunder's form for W

$$W = C_1 (I_1 - 3) + f(I_2 - 3) \tag{2}$$

where df/dI_2 , a decreasing function of $I_2 - 3$, was found to fit a particular latex rubber used in our experiments.

The second type of deformation considered is a stretching of the tube without internal pressure. The third type is a tube inflated by internal pressure, with or without a change in total length or end diameter. In these two types, the deformed tube is a curved surface of revolution; the analysis is more complicated, and our calculations are restricted to the Mooney-Rivlin materials specified by a strain-energy function in the form of Eq. (1).

With a view toward designing experiments to determine material properties, a number of numerical examples were worked out. When the tubes are stretched without internal pressure, results for $C_2/C_1 = 0,\ 0.46$ and some other suitable values were obtained. It was found that the numerical solutions are insensitive to the chosen values of C_2/C_1. The results of calculation were compared with measurements and good agreement was obtained.

It is shown further, by calculation, that for each state of deformation of the tube, the values of I_1 and I_2 vary only slightly along the tube. This has the effect that any slight dependence of $\partial W/\partial I_1$ and $\partial W/\partial I_2$ on I_1 and I_2, such as that indicated by the first type of deformation, would not be reflected in disagreement between the experimental results and those calculated on the basis of a strain-energy function of the form (1), provided C_2/C_1 is given an appropriate value for each state of deformation of the tube. In contrast, the third type of deformation, in which the tube was fixed at the ends and was inflated by internal pressure, a slight change in C_2/C_1 would affect the deformation of the tube considerably. Hence an inflation experiment is useful in determining the values of the ratio C_2/C_1.

2. THEORETICAL CONSIDERATIONS

Let us choose a set of cylindrical polar coordinates (ρ, θ, Z) to be our frame of reference in the undeformed state in which the z-axis is taken as the axis of symmetry of the tube. The undeformed middle surface S_o is taken to be the surface $\rho = R_o$. We assume that a point $P(R_o, \theta, z)$ in S_o is carried by the deformation to a point $P(r, \theta, z')$ in the deformed middle surface S. The deformation is considered to be entirely symmetric with respect to the z-axis, so that any point initially lying on the plane θ = constant remains on that plane as the deformation proceeds (Fig. 1). The arc length in the surface S between a point P and an end of the tube, measured along a meridian θ = constant, is denoted by ξ. We take the meridians, θ = constant, the lines of the latitude, ξ = constant, and the normals N to the deformed middle surface S as a set of orthogonal curvilinear coordinates to describe the deformed state. From symmetry of the problem and the assumption that the membrane is very thin compared with the cylinder radius, so that the state of strain is nearly constant throughout the thickness, it follows that the principal directions at any point in the membrane coincide with the coordinate axes (ξ, θ, N) and we denote the principal extension ratios in these directions by λ_1, λ_2 and λ_3 respectively. These extension ratios evaluated at a point P on the deformed middle surface S are given by

$$\lambda_1 = \frac{1}{\frac{dz}{d\xi}} \quad , \quad \lambda_2 = \frac{r}{R} \quad , \quad \lambda_3 = \frac{h}{h_o} = \frac{R}{r}\frac{dz}{d\xi} \tag{3}$$

where h_o and h are the thicknesses of the undeformed and the deformed tube respectively and the last equality is derived from the incompressibility assumption of the material, i.e. $\lambda_1 \lambda_2 \lambda_3 = 1$. In these expressions λ_1, λ_2, λ_3, r and z are independent of θ and may be regarded as functions of the single independent variable ξ.

The components of the stress-resultants in the directions ξ and θ will be denoted by T_1 and T_2 respectively. They are given by (Green and Adkins, Ref. 2, p. 150, where $2h_o$ is the thickness of the membrane)

$$T_1 = 2h_o \lambda_3 (\lambda_1^2 - \lambda_3^2)\left(\frac{\partial W}{\partial I_1} + \lambda_2^2 \frac{\partial W}{\partial I_2}\right) \tag{4}$$

$$T_2 = 2h_o \lambda_3 (\lambda_2^2 - \lambda_3^2)\left(\frac{\partial W}{\partial I_1} + \lambda_1^2 \frac{\partial W}{\partial I_2}\right)$$

where $I_1 = \lambda_1^2 + \lambda_2^2 + \lambda_3^2$ and $I_2 = \lambda_1^{-2} + \lambda_2^{-2} + \lambda_3^{-2}$ are two strain-invariants and $W(I_1, I_2)$ is the strain-energy function of the isotropic incompressible material. They are derived from the assumption that the normal stress acting on planes parallel to the middle surface may be neglected in comparison with the other stresses and that the normal stresses in the ξ and θ-directions are constant throughout the thickness. According to these assumptions the extensions λ_1, λ_2 and λ_3 must be treated as independent of the normal coordinate N.

The equations of equilibrium in the absence of body forces are

$$\frac{d}{d\xi}(T_1 r) = T_2 \frac{dr}{d\xi}$$

$$\kappa_1 T_1 + \kappa_2 T_2 = -P \tag{5}$$

where P is the internal pressure and κ_1 and κ_2 are the principal curvatures in the meridional and latitudinal directions respectively. The first equation of (5) gives the equilibrium condition of the membrane in the ξ-direction and the second in the normal direction. Since T_1, T_2, κ_1 and κ_2 are independent of θ, the equilibrium equation in the θ-direction is automatically satisfied. The principal curvatures are given by (Wang, Ref. 3, p. 322)

$$\kappa_1 = \frac{\frac{d^2 r}{dz'^2}}{\left[1 + \left(\frac{dr}{dz'}\right)^2\right]^{3/2}} = \frac{\frac{d^2 r}{d\xi^2}}{\left[1 - \left(\frac{dr}{d\xi}\right)^2\right]^{1/2}}$$

$$\kappa_2 = -\frac{1}{r\left[1 + \left(\frac{dr}{dz'}\right)^2\right]^{1/2}} = -\frac{1}{r}\left[1 - \left(\frac{dr}{d\xi}\right)^2\right]^{1/2} \tag{6}$$

With $(dr)^2 + (dz)^2 = (d\xi)^2$, any one of the three variables r, ξ, z' may be taken as an independent variable and then the other two are regarded as dependent variables. From Eqs. (6), we obtain the following relation between κ_1 and κ_2.

$$\frac{d}{d\xi}(\kappa_2 r) = \kappa_1 \frac{dr}{d\xi} \tag{7}$$

From Eqs. (6) and (7), we get

$$T_1 \frac{d}{d\xi}(\kappa_2 r) + \kappa_2 \frac{d}{d\xi}(T_1 r) = -p \frac{dr}{d\xi}$$

which integrates to the form

$$\kappa_2 T_1 = -\frac{p}{2} - \frac{T}{2\pi r^2} \tag{8}$$

where T is the total force, acting at the ends of the tube, required to keep the tube in static equilibrium. A positive value of T means tension.

3. SIMULTANEOUS EXTENSION AND INFLATION WHICH PRESERVES THE CIRCULAR CYLINDRICAL FORM

The simplest deformation of the cylindrical tube is to elongate the tube and inflate it to one similar to its original shape. From the geometrical consideration, we see that

$$\frac{dr}{d\xi} = 0 \ , \ \kappa_1 = 0 \ , \ \kappa_2 = -\frac{1}{r} = \frac{-1}{\lambda_2 R_0} \ , \tag{9}$$

where r and R are the radii of the tube in the deformed state and undeformed state respectively. Using the above conditions, we derive from Eqs. (4), (5) and (8) the following equations.

$$P = \frac{2h_0}{\lambda_2 R_0}\left(\frac{\lambda_2}{\lambda_1} - \frac{1}{\lambda_1^3\lambda_2^3}\right)\left(\frac{\partial W}{\partial I_1} + \lambda_1^2\frac{\partial W}{\partial I_2}\right)$$

$$T_1 = 2h_0\left(\frac{\lambda_1}{\lambda_2} - \frac{1}{\lambda_1^3\lambda_2^3}\right)\left(\frac{\partial W}{\partial I_1} + \lambda_2^2\frac{\partial W}{\partial I_2}\right) \tag{10}$$

$$T = \frac{2\pi h_0 R_0}{\lambda_1^3\lambda_2^2}\left[2(\lambda_1^4\lambda_2^2 - \lambda_1^2\lambda_2^4 - 1)\frac{\partial W}{\partial I_1} + (\lambda_1^4\lambda_2^4 - 2\lambda_2^2 - \lambda_1^2)\frac{\partial W}{\partial I_2}\right],$$

where P is the pressure necessary to inflate the tube, T_1 is the longitudinal stress resultant per unit length acting on the circumference of the tube and T is the force acting at the ends of the tube to keep it in equilibrium.

Consider the case in which the diameter of the tube is kept constant; i.e. λ_1 is varied but λ_2 is constant. When the elastic properties of the material can be described by a strain-energy function of the form (1), we can differentiate Eq. (10) with respect to λ_1 to obtain

$$\frac{dP}{d\lambda_1} = \frac{2h_o}{\lambda_2 R_o}\left[-\frac{\lambda_2}{\lambda_1^2}\left(1-\frac{3}{\lambda_1^2\lambda_2^4}\right)C_1 + \left(\lambda_2 + \frac{1}{\lambda_1^2\lambda_2^3}\right)C_2\right]. \qquad (11)$$

Since C_1 and C_2 are both non-negative and not simultaneously zero, it follows from Eq. (11) that if $C_1 = 0$, P increases monotonically with λ_1. If $C_2 = 0$ and $1 \leq \lambda_2 < \sqrt[4]{3}$, then P increases to a maximum value when $\lambda_1 = \sqrt{3}/\lambda_2^2$ and then decreases monotonically with λ_1. If $C_2 = 0$ and $\lambda_2 > \sqrt[4]{3}$, P decreases monotonically with λ_1. When neither C_1 nor C_2 is zero, $dP/d\lambda_1 = 0$ when

$$\Gamma a\chi^2 - (a-\Gamma)\chi + 3 = 0 \qquad (12)$$

where $\Gamma = C_2/C_1$, $a = \lambda_2^4$ and $x = \lambda_1^2$. If we assume, furthermore, that Γ is less than one, as is true for most Mooney-Rivlin Solids, Eq. (12) would have two positive real roots for x if its discriminant is positive, which occurs if Γ lies between zero and $(7 - \sqrt{48})/a$. For example, if $\lambda_2 = 1$ (a = 1) and $0 < \Gamma < 7 - \sqrt{48} \sim 1/14$, we find that when λ_1 increases the pressure will first rise, reaching a maximum, then it will fall, reaching a minimum, and rises again at higher extension. For $1 > \Gamma > 7 - \sqrt{48}$, the inflating pressure again increases monotonically with increasing λ_1. On the other hand, $dT/d\lambda_1 > 0$ for any non-negative C_1 and C_2.

Four rubber tubes (cf. Appendix 1) were tested in the laboratory. Three tubes had diameters of 3.79" and one tube had a diameter of 2.88". They were mounted vertically with their ends fixed on two metal cylinders, whose diameter was 3.8", as shown in Fig. 2. A weight T was attached to the lower cylinder and the corresponding extension λ_1 in the vertical direction was taken as the ratio ℓ_f/ℓ_o. The inflating pressure P was measured by a manometer. Using the measured data T and P, the normal force T_1 was calculated from Eq. (8). Two nondimensional quantities P' and T_1' are defined by

$$P' = \frac{PR_o}{2h_o C_1}$$

$$T_1' = \frac{T_1}{2h_o C_1} \qquad (13)$$

The experimental data of P' with $C_1 = 17.8$ psi and $\lambda_2 = 1$ is plotted against λ_1 in Fig. 3. We can see that P' first increases with λ_1 until it reaches a maximum at about $\lambda_1 = 1.9$; then it falls slightly to reach a minimum and then rises again. Curves I, II and III of P' in Fig. 3 were calculated for the strain-energy function $W = C_1 \left[(I_1 - 3) + \Gamma (I_2 - 3) \right]$ under the assumption that $C_1 = 17.8$ psi and $\Gamma = 0$, 0.065 and 0.1 respectively. These curves show different characters as discussed before. There are large gaps between the experimental results and these predictions. In Fig. 4, we plotted the experimental stress resultant T_1' against λ_1. The calculated curves I and III for $\Gamma = 0$ and 0.1 respectively are also plotted in Fig. 4 for comparison. These two curves differ from the experimental data considerably for small λ_1, and the experimental points lie between them for large λ_1. If we choose a larger value for C_1, we would get a better approximation in the range of small λ_1, but worse for large λ_1.

In the simple deformation specified by (9), Eq. (10) can be used to solve for the two unknowns $\partial W/\partial I_1$ and $\partial W/\partial I_2$ as functions of the strain invariants I_1 and I_2 from the experimental data of P and T. If, in addition, $\lambda_2 = 1$, then I_1 is equal to I_2. Some simple calculations show that the values of $\partial W/\partial I_1$ only vary slightly as I_1 and I_2 increase. On the other hand, the values of $\partial W/\partial I_2$ do drop rapidly as I_1 and I_2 increase. The former condition implies that we can approximate the function $W(I_1, I_2)$ by a linear functional of I_1. This suggests that we may use Eq. (2) to describe the stress-strain relation of our rubber tubes:

$$W = C_1 (I_1 - 3) + f(I_2 - 3) \qquad (2)$$

It turned out that Eq. (2) does give a better approximation to our experimental data. A physical constant $C_1 = 17.8$ psi was obtained from Eq. (10) by using experimental values of P and T at $\lambda_1 = 2.9$. The variations of I_2 and $1/C_1 \ \partial W/\partial I_2$ are shown in Table 1 and Fig. 7. With the values of $1/C_1 \ \partial W/\partial I_2$ given in the third column of Table 1, the values of P' and T_1 were calculated according to Eq. (10), and are listed also in Table 1. The calculated results of P' were plotted in Fig. 3 (curve IV) and that of T_1' in Fig. 4 (curve IV). We see that the fall of P' after it passed the maximum is mainly due to the decrease of $1/C_1 \ \partial W/\partial I_2$ as I_2 increases.

When $\lambda_2 = 1.315$, measured values of P' and T_1' were plotted in Figs. 5 and 6 respectively, P' starts at a finite value, increases slightly as the extension increases. The maximum of P' is reached at $\lambda_1 = 1.12$. It decreases furthermore and then rises again at higher extensions.

Values of P' calculated for W in the form of (1) and $\Gamma = 0$, 0.065 and 0.1 are plotted in Fig. 5 as curves I, II and III respectively. In Fig. 6, T_1' so calculated was plotted against λ_1 in curves I and III for $\Gamma = 0$ and 0.1 respectively. These curves differ largely from the experimental data. On the other hand, if we assume W in the form of Eq. (2) and calculate the strain invariant I_2 at each extension ratio λ_1 and use the corresponding values for $\partial W/\partial I_2/C_1$ from Fig. 7 to evaluate P', T_2' and T_1', the results of Table 2 are obtained. It gives curves IV in Figs. 5 and 6. Again a better approximation is obtained under the form (2).

Thus we conclude that Eq. (2) gives a better description for the elastic properties of our rubber tubes than Eq. (1).

4. SYMMETRIC STRETCHING AND DISTENSION OF A THIN CIRCULAR CYLINDRICAL TUBE INTO A SHELL OF REVOLUTION

For more complicated deformation of cylindrical tubes the analytical difficulty is such that we have to assume the strain energy in the form of (1) to make some progress. From Eqs. (1) and (2), we derive

$$T_1 = 2h_0 C_1 \left(\frac{\lambda_1 R_0}{r} - \frac{R_0^3}{\lambda_1^3 r^3}\right)\left(1 + \frac{\Gamma r^2}{R^2}\right)$$

(14)

$$T_2 = 2h_0 C_1 \left(\frac{r}{\lambda_1 R_0} - \frac{R_0^3}{\lambda_1^3 r^3}\right)\left(1 + \Gamma \lambda_1^2\right) ,$$

where $\Gamma = C_2/C_1$. From the first equation of (5) and Eq. (9), we obtain

$$\lambda_1 \frac{d\lambda_1}{d\xi} - \frac{r}{R_0}\frac{dr}{d\xi} + 3R_0^2\left(\frac{1}{\lambda_1^3 r^2}\frac{d\lambda_1}{d\xi} + \frac{1}{\lambda_1^2 r^3}\frac{dr}{d\xi}\right)$$

$$+\Gamma\left\{\frac{1}{R_0^2}\left(r\lambda_1^2\frac{dr}{d\xi} + r^2\lambda_1^2\frac{d\lambda_1}{d\xi}\right) + \frac{3}{\lambda_1^3}\frac{d\lambda_1}{d\xi} + \frac{R_0^2}{r^3}\frac{dr}{d\xi}\right\} = 0$$

which integrates to the form

$$\lambda_1^2 - \frac{r^2}{R_0^2} - \frac{3R_0^2}{\lambda_1^2 r^2} + \Gamma\left(\frac{r^2\lambda_1^2}{R_0^2} - \frac{3}{\lambda_1^2} - \frac{R_0^2}{r^2}\right) = B \qquad (15)$$

where B is a constant. If this equation is solved for λ_1 as a function of r, then the normal forces T_1, T_2 and the principal curvatures κ_1 and κ_2 can all be expressed in terms of r. This suggests that it is more convenient to use r instead of ξ as the independent variable. From Eq. (3) and the second equation of (6), we have the following relations between z, z' and r for the case in which there is no circumferential elongation at the ends of the tube and $P > 0$ *.

$$Z = \int_0^Z \frac{dZ}{d\xi} d\xi = \int_{R_0}^r \frac{dr}{\lambda_1 (1 - \kappa_2^2 r^2)^{1/2}}$$

(16)

$$Z' = \int_0^{Z'} \frac{dz'}{d\xi} d\xi = \int_{R_0}^r \frac{-\kappa_2 r\, dr}{(1 - \kappa_2^2 r^2)^{1/2}}$$

---

* This kind of deformation is easier to discuss and can be generalized to other possible cases without any difficulty.

These equations specify the deformation between the end and the equator of the tube completely when we know the two integration constants B and T and the pressure P.

Before discussing how to determine the unknown constants B and T, let us examine the conditions that are appropriate for solving the problem. Under the assumption of symmetric deformation, no shear stress resultant acts at the ends of the tube. In finite deformation, however, the slope of the membrane at the ends is unknown and the direction of action of the stress resultant T_1 at the ends is unknown. But the total force T acting at the ends of the tube may be specified. It will be shown that by specifying T and the initial length of the tube ℓ_o, constant B can be determined. Another possible set of conditions is to specify the initial length ℓ_o and final length ℓ_f of the tube. The numerical method of solving these constants is discussed in Appendix 2.

Solutions for two types of deformations, namely the stretching of cylindrical tubes, and the distension of cylindrical tubes, were worked out and compared with experimental results. They will be discussed separately:

A. Stretching of Cylindrical Tubes

Thin circular cylindrical tubes were stretched without internal pressure. The observations of the stretched tube were made with an optical cathetometer with horizontal and vertical travels. Rubber tubes were inked with horizontal lines about a quarter inch apart, as shown in Fig. 2.

One rubber tube (R = 1.895") gave the deformed profiles as shown in Fig. 8, another tube (R = 1.44") gave the deformed profile as shown in Fig. 9. Their initial lengths ℓ_o were 3 times of their radii.

The meridional extension ratio λ_1 was readily obtained from the observed data. If $\xi_2 - \xi_1$ is the length of the arc P_1P_2 (cf. Fig. 8) and $z_2 - z_1$ is the corresponding measured intercept on the undeformed tube, then

$$\lambda_1 = \frac{\xi_2 - \xi_1}{z_2 - z_1} \tag{17}$$

is the mean meridional extension ratio over the interval P_1P_2. This was taken to be the meridional elongation at the point midway between P_1 and P_2 in the undeformed state. The data obtained from the measurements of the two tubes mentioned above were presented in Figs. 10 and 11, which show λ_1 plotted against z-axis of the undeformed state.

We discuss first the special case in which there is no change in diameter at the ends of the tube, i.e. $(\lambda_2)_{z'=0, \ell_f} = 1$. For the theoretical calculations, the initial length of the tube ℓ_o is taken to be 3 and the radius R_o to be 1.

Four numerical solutions have been worked out. They are calculated for $R_o = 1$, $\ell_o = 3$, $P' = 0$ and (1) $\ell_f = 3.98$, $\Gamma = 0$; (2) $\ell_f = 3.98$, $\Gamma = 0.46$; (3) $\ell_f = 5.98$, $\Gamma = 0$; (4) $\ell_f = 5.98$, $\Gamma = 0.31$. The values of r, λ_1 and z' were shown in Tables 3 and 4. We observe that the calculations are very insensitive to the chosen values of Γ. This insensitivity is caused by the flatness at the equator such that a slight change in r_m would affect ℓ_o and ℓ_f largely

and compensate for the change of ℓ_o and ℓ_f due to the change of . In Fig. 8, are plotted deformed profiles I for $\ell_f = 3.98$, $\Gamma = 0.46$ and II for $\ell_f = 5.98$, $\Gamma = 0.31$. The calculated values of $_1$ of these two cases were plotted against the z-axis of the undeformed state in Fig. 9. Since the values of I_1 and I_2 vary only slightly along the tube, as we can see from Fig. 12, it might be a good approximation to set $\partial W/\partial I_1$ and $\partial W/\partial I_2$ as constants evaluated at the mean values of I_1 and I_2. From the discussion in Section 3 and the $\partial W/\partial I_2$ vs. I_2 plot in Fig. 7, we take $\partial W/\partial I_1$ to be the constant C_1 and $\partial W/\partial I_2/C_1 = \Gamma = 0.46$ for $\ell_f = 3.98$, where I_2 is about 3.25. We also take $\Gamma = 0.31$ for $\ell_f = 5.98$, where I_2 is about 4.35. Therefore, curves I and II obtained by this first order approximation for the derivatives of the strain-energy function would still yield good agreement between the theoretical result and nondimensionalized experimental result in this type of deformation as shown in Figs. 8 and 10. From Fig. 13, we observe that T_1 falls steadily as we progress outwards from the equator, while T_2 increases steadily toward the ends. Calculated deformation profiles and λ_1 were plotted in Figs. 9 and 11 for the case of an initial circumferential elongation $\lambda_2 = 1.315$ at the ends. It also shows good agreement with the experiment.

B. Distension of Cylindrical Tubes

The ends of the tube were rigidly fixed and we inflated it by internal pressure P. One tube was used for this type of deformation. It had a diameter of 3.79" and initial length 5.69" (three times of its radius). λ_{1m} and r_m were measured at the equator for certain inflating pressures. The result is shown in Table 5. We see that the increase of inflating pressure is followed

by a fall as distension proceeded. The deformed profiles and the meridional extension ratios all along the tube were measured for two different inflating pressures. After being nondimensionalized by $PR_o/2h_oC_1$ where C_1 was again to be taken as 17.8 psi, they are 1.24 and 1.315. The results are plotted in Figs. 14 and 15.

For the numerical calculations, we chose R = 1, $\ell_o = \ell_f$ = 3 and the following sets of P' and Γ : (1) P' = 1.315, Γ = 0.15; (2) P' = 1.24, Γ = 0.1; (3) P' = 1.24, Γ = 0.08 and (4) P' = 1.315, Γ = 0.1. The deformed profiles and the extension ratio λ_1 are plotted in Figs. 16 and 17 respectively. One can see immediately that the theoretical results do depend strongly on the chosen values of Γ. Using a smaller Γ, we obtain a larger deformation at lower inflating pressure as shown by curves I and II in Fig. 16. As discussed earlier in Section 3, the apparent value of $\partial W/\partial I_2/C_1$, which is for a Rivlin-Mooney material, does not remain constant for the particular latex rubber used in our experiment. Fig. 7 shows that Γ may be considered as decreasing as I_2 increases. One may surmise that the fall of pressure observed in the experiments is caused by the fall of the value of Γ at increased deformation.

In Fig. 18, T_1' and T_2' are plotted against z and in Fig. 19, κ_1 and κ_2 are plotted against z. T_1' and T_2' decrease steadily as we go toward the end from the equator, except that T_1 rises slightly near the ends. κ_2 remains constant on most of the tube, but drops near the ends.

Curves I and III in Figs. 14 and 15 were chosen to fit the experimental deformed profiles and curves of λ_1. From Fig. 20, we notice that the value of I_2 varies considerably with the axial coordinate. Therefore the approximation that $\partial W/\partial I_2/C_1$ is a constant throughout the tube would not be valid in such a deformation.

In the above calculation, Γ was considered as a constant parameter chosen to fit the experimental data and it has no relation with the considerations presented in Section 3. We see from Fig. 14 that the calculated deformations are flatter than the experimental deformation profiles and that the curves of λ_1 in Fig. 15 only show a qualitative agreement with the experimental results.

REFERENCES

1. Adkins, J. E. and R. S. Rivlin, "Large Elastic Deformations of Isotropic Materials, IX, The Deformation of Thin Shells", Phil. Trans. A, 244, p. 505, 1952.
2. Green, A. E. and J. E. Adkins, Large Elastic Deformations, Oxford at the Clarendon Press, Chap. IV, 1960.
3. Wang, Chi-Teh, Applied Elasticity, p. 322, McGraw-Hill, New York, 1953.
4. Green, A. E. and W. Zerna, Theoretical Elasticity, Oxford at the Clarendon Press, 1954.
5. Rivlin, R. S. and D. W. Saunders, "Large Elastic Deformations of Isotropic Materials, VII, Experiments on the Deformation of Rubber", Phil. Trans. A, 243, p. 251, 1951.
6. Rivlin, R. S. and A. G. Thomas, "Large Elastic Deformations of Isotropic Materials, VIII, Strain Distribution Round a Hole in a Sheet", Phil. Trans. A., 243, p. 289, 1951.

APPENDIX 1

THE PREPARATION OF RUBBER TUBES

Glass tubes of 3" to 4" diameter were dipped in a rubber latex dispersion (No. 74 latex molding compound). The tubes were taken out and put into coagulant (No. 541 coagulant) to solidify the latex. They were first washed in fluent water for 2 to 3 hours, dried at room temperature, then for 2 hours at 160° F and finally vulcanized for 25 to 35 minutes at 220° F in a hot air oven. A layer of thickness 0.015" to 0.025" was obtained and its variation over the rubber tube is less than 2.5 percent.

APPENDIX 2

A NUMERICAL METHOD OF SOLVING EQUATION (16)

Suppose that ℓ_o and ℓ_f are given. We obtain from Eq. (16)

$$\ell_o = 2 \int_{R_o}^{r_m} \frac{dr}{\lambda_1 (1-K_2^2 r^2)^{1/2}}$$

$$\ell_f = 2 \int_{R_o}^{r_m} \frac{-K_2 r\, dr}{(1-K_2^2 r^2)^{1/2}} \qquad \text{(A.1)}$$

where r_m is the maximum radius at the equator $z' = \ell_f/2$.

The integrands of Eq. (A.1) are very complicated functions of r, and the integrals cannot be expressed in closed form. An iteration method can be used. First, certain values for λ_1 and r at the equator of the tube are assumed and designated as λ_{1m} and r_m respectively. Since $dr/d\xi = 0$ at the equator, Eq. (6) implies that $(K_2) = \ell_f/2,\ r = r_m = -1/r_m$. The constants B and T can then

be obtained from Eqs. (8) and (15), and the integrals (A.1) can be evaluated numerically by a high-speed computer. Readjusting the values of λ_{1m} and r_m and repeating the numerical procedure, we can make these integrals to have the given values ℓ_o and ℓ_f respectively. When ℓ_o and T are given, Eq. (8) provides a relation between λ_{1m} and r_m, and numerical solution can be found by assuming a suitable set of λ_{1m} and r_m that satisfy the given relation and proceed with the iteration method as in the previous case.

Near the equator, there is a square root singularity and we calculate $\Delta\xi$ from the following Taylor expansion

$$\Delta r = \frac{1}{2}\left[\frac{d^2r}{d\xi^2}\right]_{r=r_m}\Delta\xi^2 = \frac{1}{2}[K_1]_{r=r_m}\Delta\xi^2 \qquad \text{(A. 2)}$$

where $\Delta\xi$ must be a sifficiently small value to insure the rapid convergence of Eq. (A. 2). Substituting Eq. (A. 2) into Eq. (A.1) we obtain two approximate formulas for ℓ_o and ℓ_f

$$\ell_o = 2\int_{R_o}^{r_m-\Delta r}\frac{dr}{\lambda_1(1-K_2^2r^2)^{1/2}} + 2\left[\frac{2\Delta r}{[\lambda_1 K_1]_{r=r_m}}\right] \qquad \text{(A. 3)}$$

$$\ell_f = 2\int_{R_o}^{r_m-\Delta r}\frac{-K_2 r\,dr}{(1-K_2^2r^2)^{1/2}} + 2\left[\frac{2\Delta r}{[K_1]_{r=r_m}}\right]$$

If λ_1 and r/R_o are large throughout the whole tube, we may neglect the term $R_o^3/(\lambda_1^3 r^3)$ in Eq. (15) in comparison with $\lambda_1 R_o/r$ and

$r/\lambda_1 R_o$. For example, when $\lambda_1 = r/R_o = 2$, $R_o^3/(\lambda_1^3 r^3) = 1/64$ may be considered as a negligible quantity. In this case, the following approximate stress-strain relations hold:

$$T_1 = 2h_o C_1 \frac{\lambda_1 R_o}{r}\left(1 + \frac{I' r^2}{R_o^2}\right) \tag{A.4}$$

$$T_2 = 2h_o C_1 \frac{r}{\lambda_1 R_o}\left(1 + I'\lambda_1^2\right)$$

A substitution of (A.4) into the first equation of (5) and an integration yields the relation

$$\lambda_1^2 = \frac{B' R_o^2 + r^2}{R_o^2 + I' r^2} \tag{A.5}$$

where B' is a constant. Eq. (A.5) can be obtained also by neglecting the higher order terms in Eq. (15). Using Eqs. (A.4) and (A.5), we derive from Eq. (8)

$$K_2 r = -\frac{P' r^2 + 2T' R_o^2}{2\left[(R_o^2 + I' r^2)(B' R_o^2 + r^2)\right]^{1/2}} \tag{A.6}$$

where $P' = PR/(2h_o C_1)$ and $T' = T/(2\pi h_o C_1 R_o)$. Eqs. (16) now become for $0 \leq z \leq \ell_o/2$ and $0 \leq z' \leq \ell_f/2$

$$Z = \int_{r_e}^{r} \frac{2(R_o^2 + I' r^2)\, dr}{\left\{\left[(4I' - P'^2) r^2 - D\right](r^2 - r_m^2)\right\}^{1/2}} \qquad (A.7)$$

$$Z' = \int_{r_e}^{r} \frac{(P' r^2 + 2T' R_o^2)\, dr}{\left\{\left[(4I' - P'^2) r^2 - D\right](r^2 - r_m^2)\right\}^{1/2}}$$

where $D = 4(B' - T'^2) R_o^4 / r_m^2$ and r_e is the known radius at the ends of the tube. These two equations can be transformed into elliptical integrals of the first and second kind when all the constants are given. After setting $r = r_m$ into Eq. (A.7), we obtain two transcendental equations to determine r_m and λ_{lm} when ℓ_o and ℓ_f are given.

When there is tangential elongation at the ends of the tube, a slight modification of the numerical procedure will provide a solution of the problem.

TABLE 1

The variations of $(1/C_1)/\partial W/\partial I_2)$, P' and T_1' with λ_1, for a tube of constant diameter uniformly stretched longitudinally.

λ_1	I_2	$\frac{1}{C_1}\frac{\partial W}{\partial I_2}$	$T_1' = \frac{T_1}{2h_o C_1}$	$P' = \frac{PR}{2h_o C_1}$
1.15	3.079	0.500	0.739	0.352
1.3	3.282	0.465	1.238	0.561
1.45	3.578	0.416	1.589	0.678
1.6	3.951	0.365	1.851	0.737
1.9	4.887	0.279	2.244	0.773
2.2	6.047	0.213	2.555	0.732
2.5	7.410	0.173	2.858	0.699
2.8	8.968	0.149	3.165	0.676
3.1	10.71	0.130	3.465	0.650
3.4	12.65	0.114	3.759	0.623
3.7	14.76	0.110	4.085	0.628
4.0	17.06	0.107	4.411	0.636

TABLE 2

The variation of $(1/C_1)/(\partial W/\partial I_2)$, T_1', P_1'' with λ_1 for a circular tube uniformly stretches both longitudinally and circumferentially with $\lambda_2 = 1.315$.

λ_1	I_2	$\frac{1}{C_1}\frac{\partial W}{\partial I_2}$	$T_1' = \frac{T_1}{2h_o C_1}$	$P'' = \frac{2^{PR}}{2h_o C_1}$
1.0	3.308	0.465	0.579	1.282
1.15	3.621	0.410	1.000	1.318
1.3	4.092	0.349	1.264	1.290
1.45	4.690	0.293	1.444	1.233
1.6	5.396	0.243	1.576	1.159
1.9	7.098	0.179	1.808	1.034
2.2	9.154	0.147	2.047	0.952
2.8	14.26	0.111	2.511	0.837
3.4	20.65	0.0845	2.951	0.743
3.7	24.32	0.075	3.169	0.703
4.0	28.32	0.072	3.413	0.693
4.3	32.61	0.074	3.682	0.711

TABLE 3

Calculated values of r, λ_1 and z' for a circular tube stretched longitudinally without internal pressure $\ell_o = 3$, $\ell_f = 3.98$, P' = 0, R = 1

$\Gamma = 0.0$			$\Gamma = 0.46$		
T' = 0.8023, B = -1.1380			T' = 1.1017, B = - 1.8239		
r	λ_1	z'	r	λ_1	z'
1.0	1.2901	0.0	1.0	1.2696	0.0
0.9925	1.2924	0.0327	0.9909	1.2744	0.0353
0.9850	1.2948	0.0673	0.9818	1.2793	0.0730
0.9759	1.2979	0.1117	0.9708	1.2854	0.1221
0.9699	1.3000	0.1433	0.9589	1.2922	0.1810
0.9515	1.3068	0.2517	0.9451	1.3005	0.2584
0.9423	1.3105	0.3145	0.9359	1.3062	0.3170
0.9331	1.3143	0.3848	0.9267	1.3121	0.3828
0.9239	1.3183	0.4646	0.9175	1.3181	0.4578
0.9147	1.3225	0.5573	0.9083	1.3243	0.5452
0.9055	1.3268	0.6677	0.8991	1.3306	0.6500
0.8963	1.3313	0.8047	0.8899	1.3372	1.7813
0.8871	1.3360	0.9865	0.8807	1.3439	0.9578
0.8779	1.3408	1.2648	0.8715	1.3508	1.2347
0.9726	1.3437	1.5458	0.8662	1.3549	1.5228
0.8699	1.3452	1.9852	0.8635	1.3570	1.9903

TABLE 4

Calculated values of r, λ_1 and z' for a circular tube stretched longitudinally without internal pressure $\ell_o = 3$, $\ell_f = 5.98$, R = 1, P' = 0 .

$\Gamma = 0.0$			$\Gamma = 0.31$		
T' = 1.7994 , B = 2.1949			T' = 2.1207 , B = 2.1716		
r	λ_1	z'	r	λ_1	z'
1.0	1.9884	0.0	1.0	1.8740	0.0
0.9836	1.9869	0.0637	0.9808	1.8821	0.0546
0.9590	1.9855	0.1659	0.9520	1.8952	0.1433
0.9344	1.9850	0.2778	0.9231	1.9093	0.2418
0.9098	1.9855	0.4014	0.8943	1.9247	0.3526
0.8852	1.9870	0.5398	0.8655	1.9414	0.4797
0.8606	1.9897	0.6976	0.8366	1.9595	0.6289
0.8360	1.9935	0.8817	0.8078	1.9793	0.8105
0.8222	1.9962	1.0005	0.7940	1.9894	0.9138
0.8084	1.9992	1.1343	0.7802	1.9999	1.0321
0.7900	2.0040	1.3452	0.7618	2.0146	1.2232
0.7762	2.0081	1.5393	0.7480	2.0262	1.4049
0.7624	2.0126	1.7847	0.7342	2.0383	1.6439
0.7486	2.0175	2.1324	0.7204	2.0510	2.0034
0.7414	2.0203	2.4196	0.7132	2.0578	2.3194
0.7374	2.0219	2.6941	0.7092	2.0616	2.6352
0.7360	2.0025	2.9888	0.7078	2.0630	2.9836

TABLE 5

Measured internal pressure P', radius r_m/R and the extension ratio λ_{1m} at the equator of a circular tube which is inflated by P' while its ends are fixed with no circumferential elongation, $C_1 = 17.8$ psi.

$P' = \frac{PR}{2h_o C_1}$	r_m/R	λ_{1m}
0.724	1.2	1.023
1.09	1.37	1.035
1.23	1.39	1.05
1.352	1.475	1.08
1.38	1.54	1.13
1.385	1.665	1.215
1.315	1.82	1.355
1.24	2.14	1.815

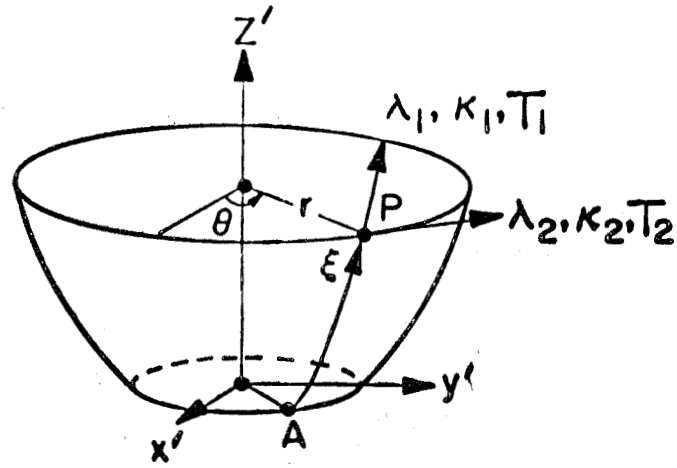

Fig. 1 Middle Surface Defining the Deformed Tube.

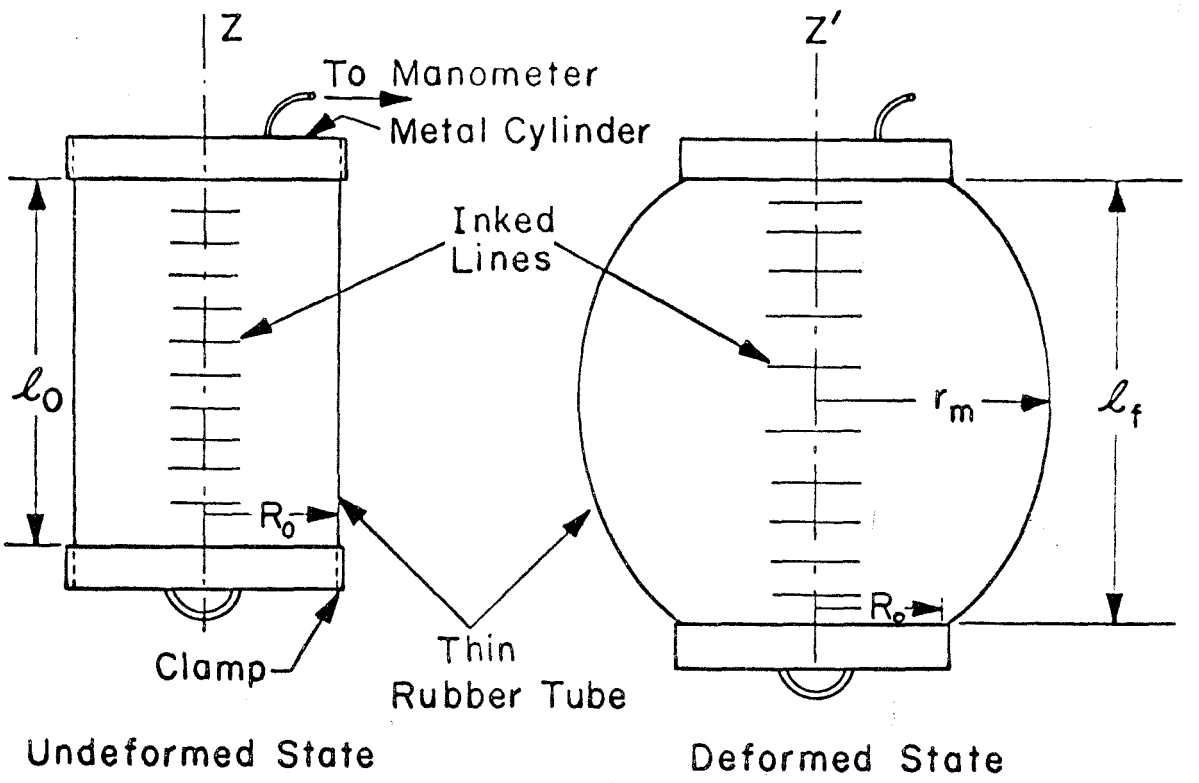

Fig. 2 Mounting of Rubber Tube for Inflation.

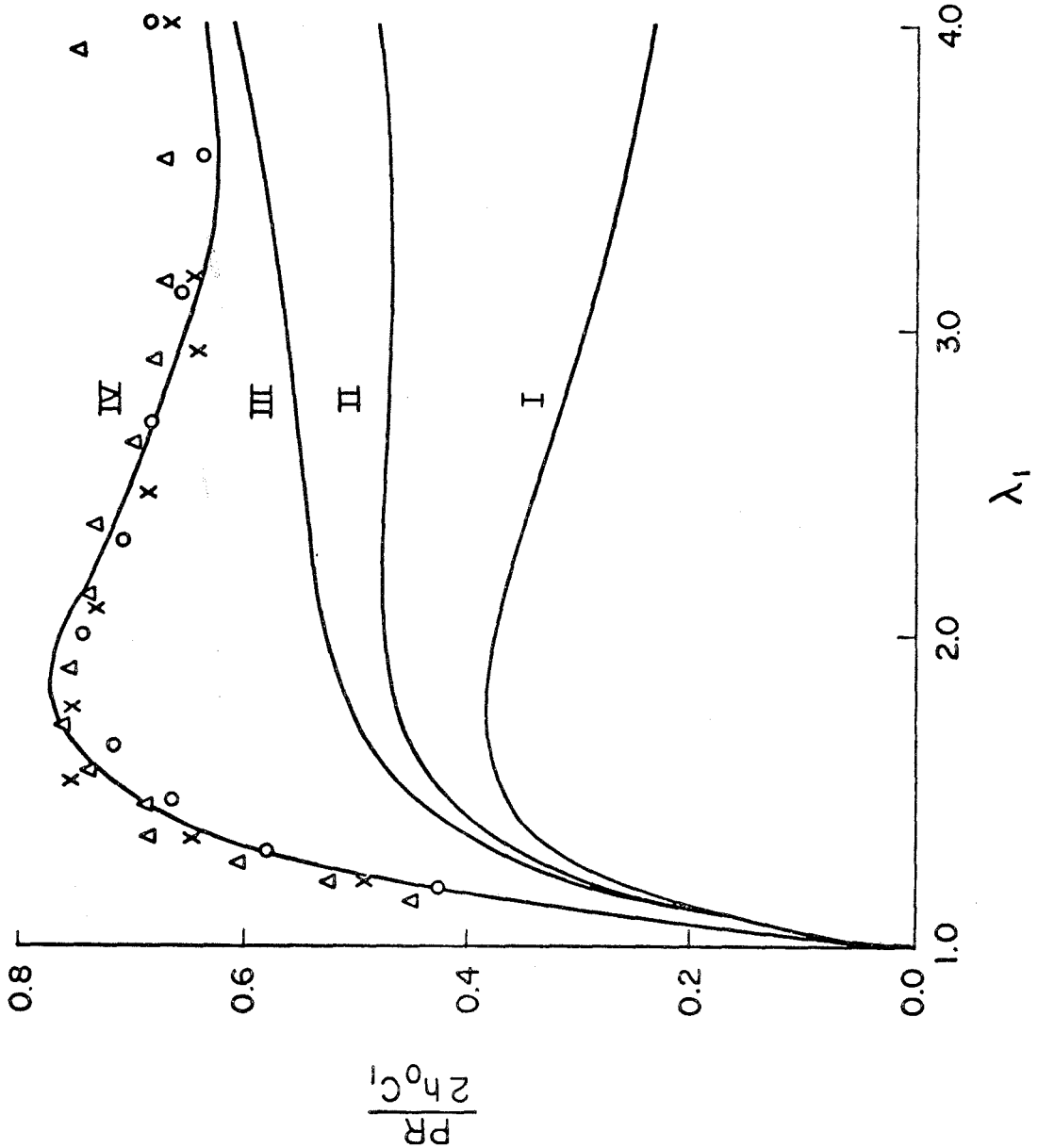

Fig. 3 Variation of pressure P as function of λ_1 for $\lambda_2 = 1$. Curve I, $\Gamma = 0$; Curve II, $\Gamma = 0.065$; Curve III, $\Gamma = 0.1$; Curve IV, $(1/C_1)(\partial w/\partial I_2)$ varying in manner of Fig. 7 and the experimental result (cf. Fig. 4).

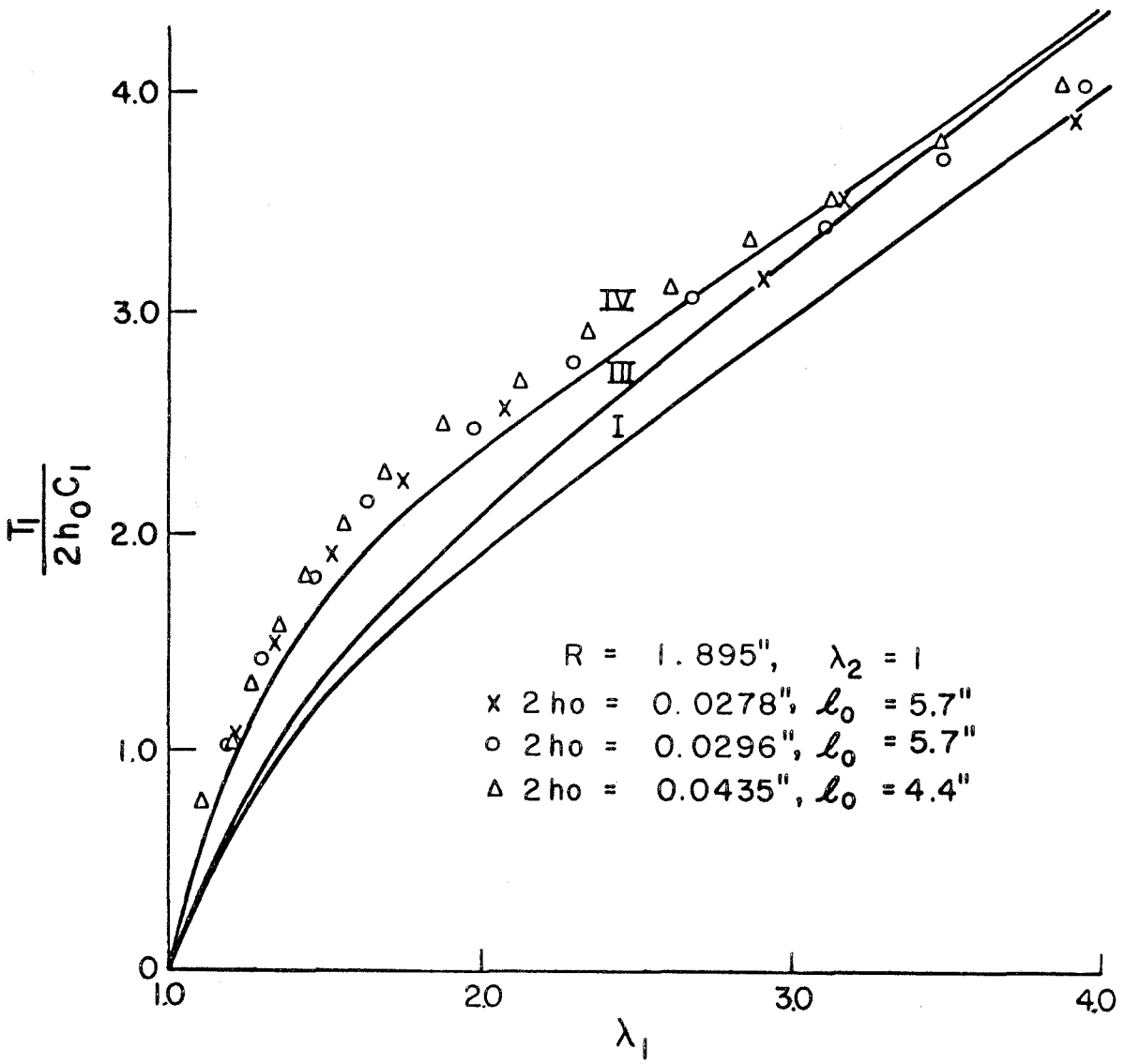

Fig. 4 Variation of longitudinal stress resultant T_1 as function of λ_1 for $\lambda_2 = 1$. Curve I, $\Gamma = 0$, Curve III, $\Gamma = 0.1$; Curve IV, $(1/C_1)(\partial w/\partial I_2)$ varying in manner of Fig. 7 and the nondimensionalized experimental result with $C_1 = 17.8$ psi.

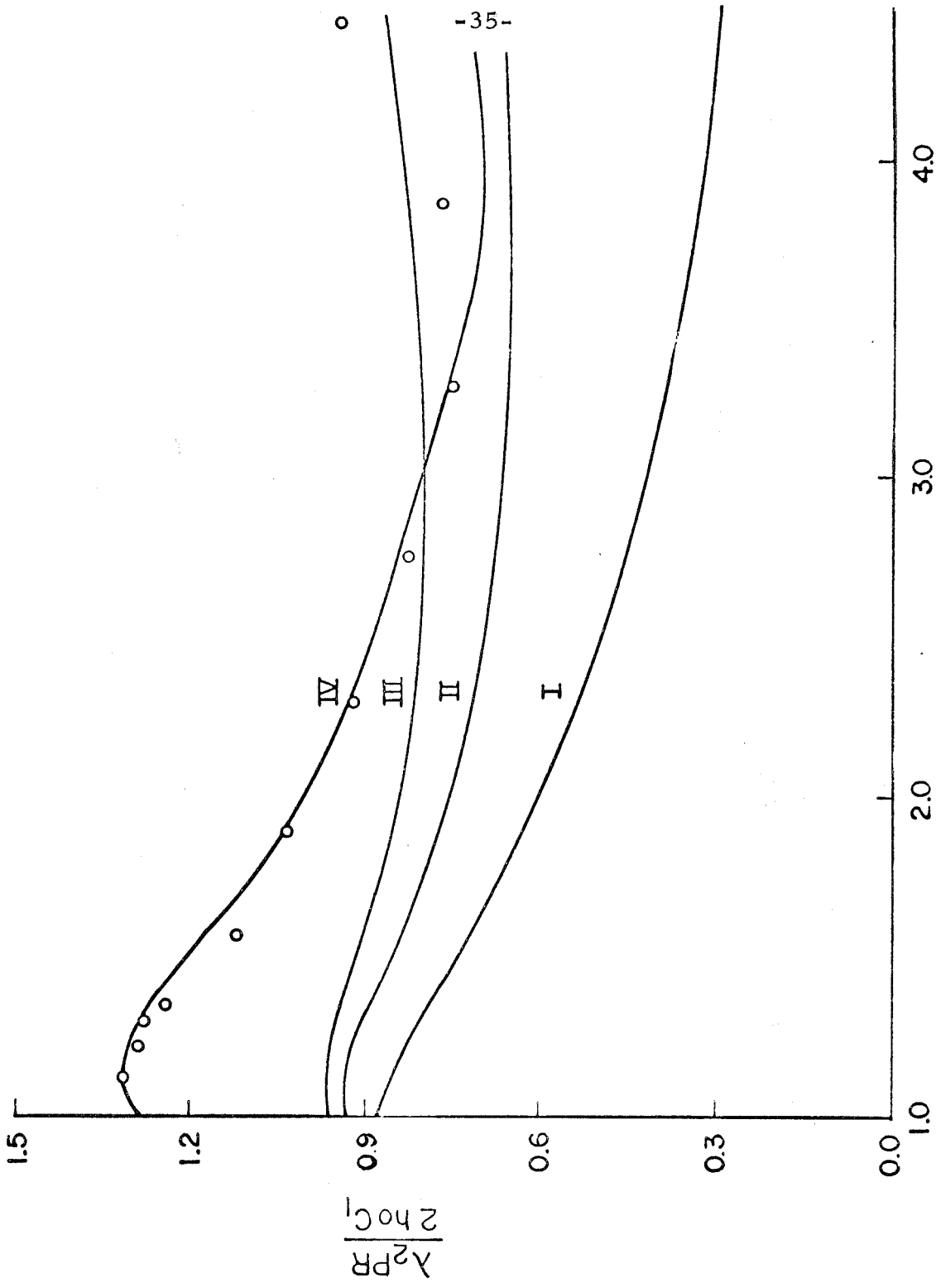

Fig. 5 Variation of pressure P as function of λ_1 for $\lambda_2 = 1.315$. Curve I, $\Gamma = 0$; Curve II, $\Gamma = .065$, Curve III, = 0.1, Curve IV, $(1/C_1)(\partial w/\partial I_2)$ varying in manner of Fig. 7 and experimental result.

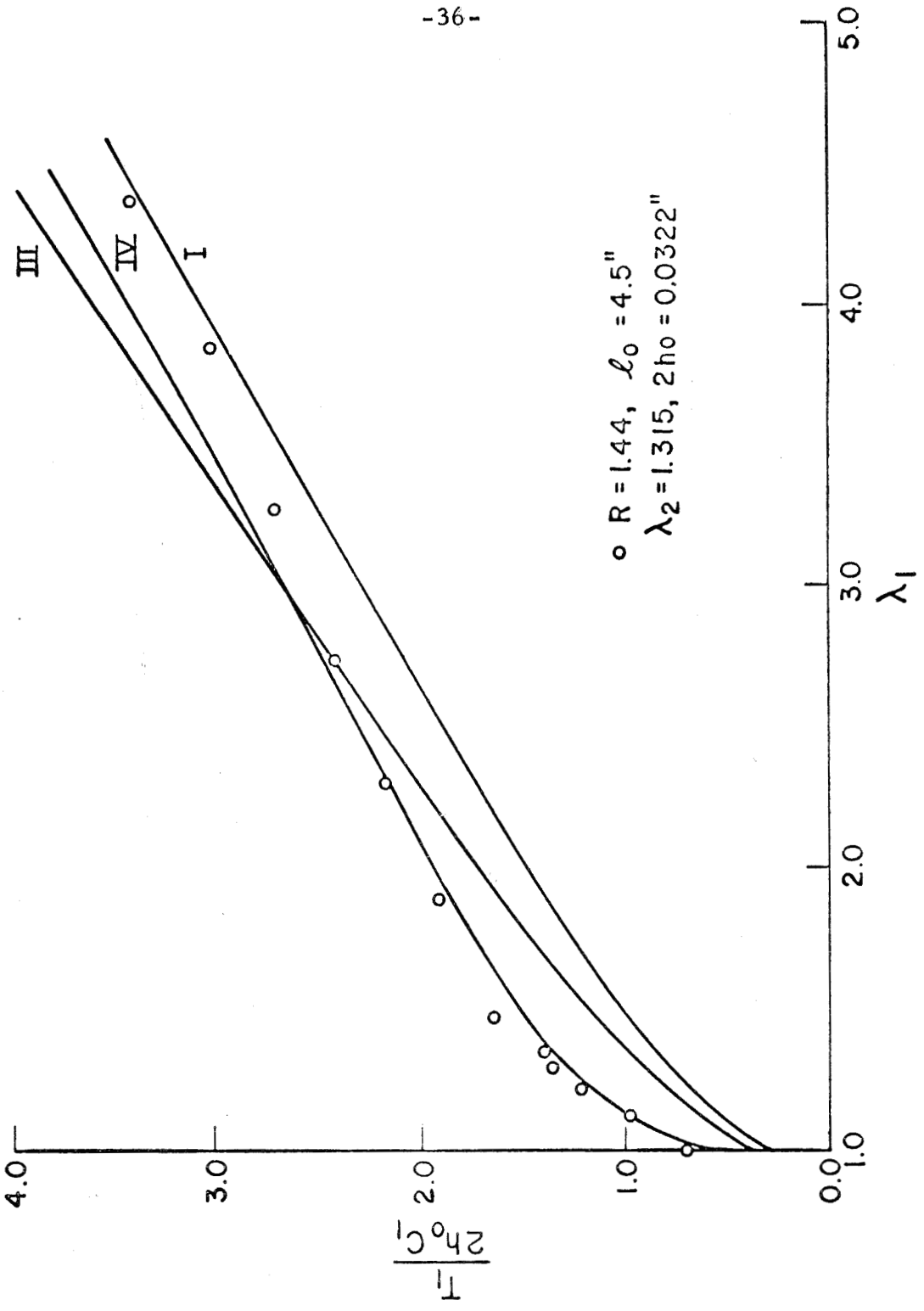

Fig. 6 Variation of longitudinal stress resultant T_1 as function of $\frac{1}{2h_o C_1}$ for $\lambda_2 = 1.315$. Curve I, $\Gamma = 0$; Curve III, $\Gamma = 0.1$, Curve IV, $(1/C_1)(\partial w/\partial I_2)$ varying in manner of Fig. 7 and the nondimensionalized experimental result with $C_1 = 17.8$ psi.

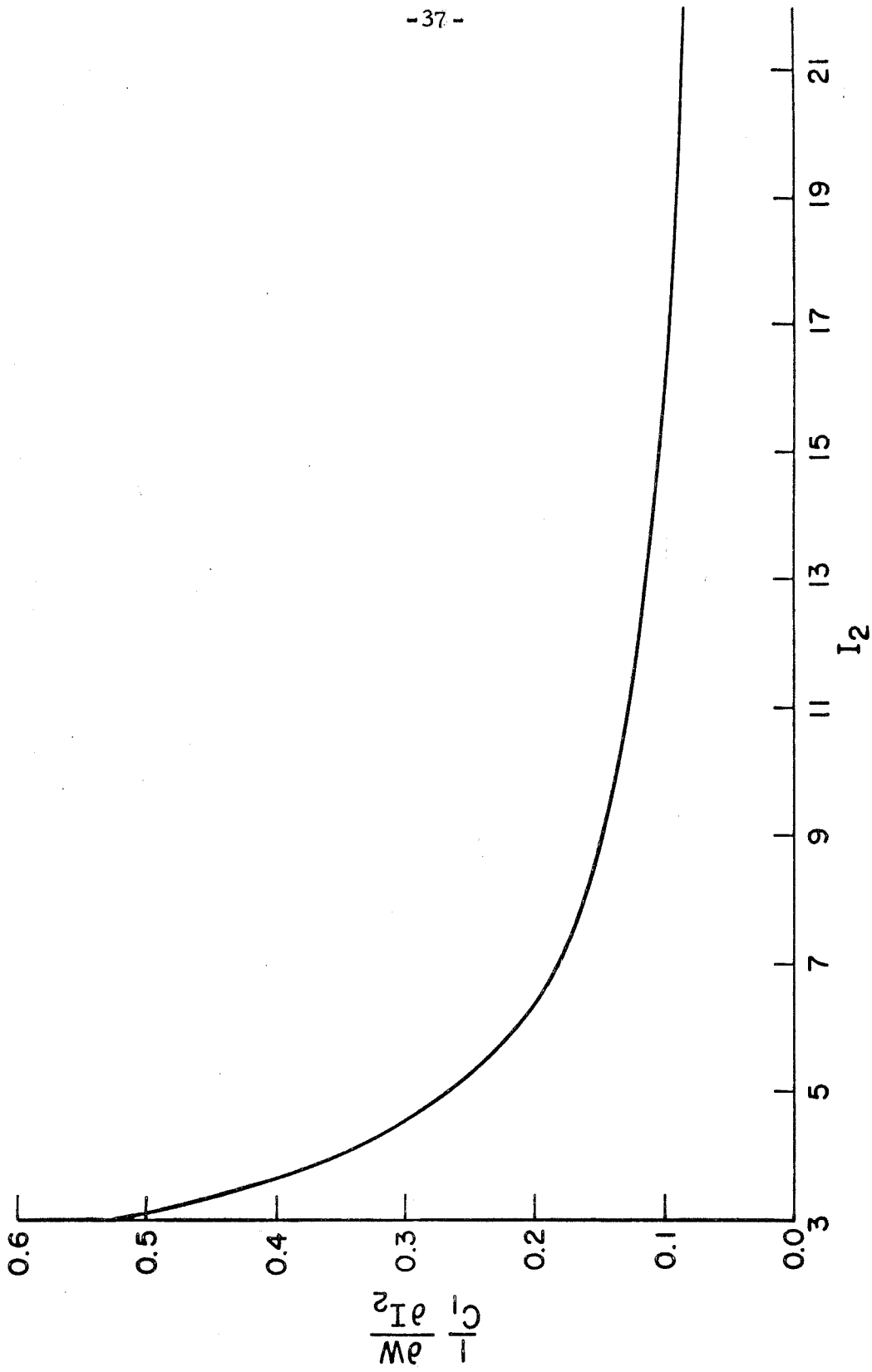

Fig. 7 Variation of $(\partial W/\partial I_2)/C_1$ versus I_2.

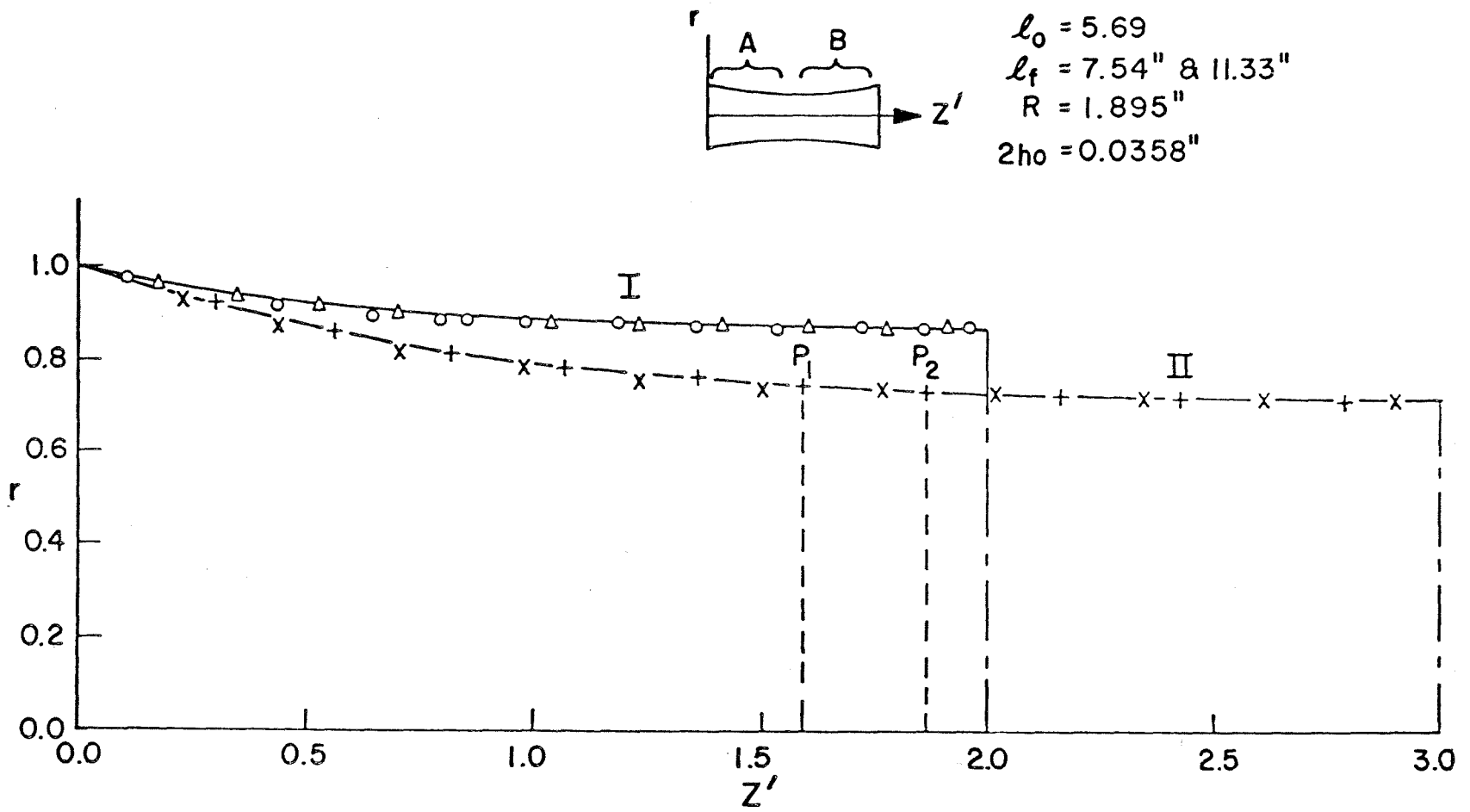

Fig. 8 Calculated deformed profiles for R = r_e = 1 , P = 0, ℓ_o = 3. Curve I, ℓ_f = 3.98, Γ = 0.46; Curve II, ℓ_f = 5.98, Γ = 0.31. Corresponding experimental results (0, x of A part; Δ, + of B part).

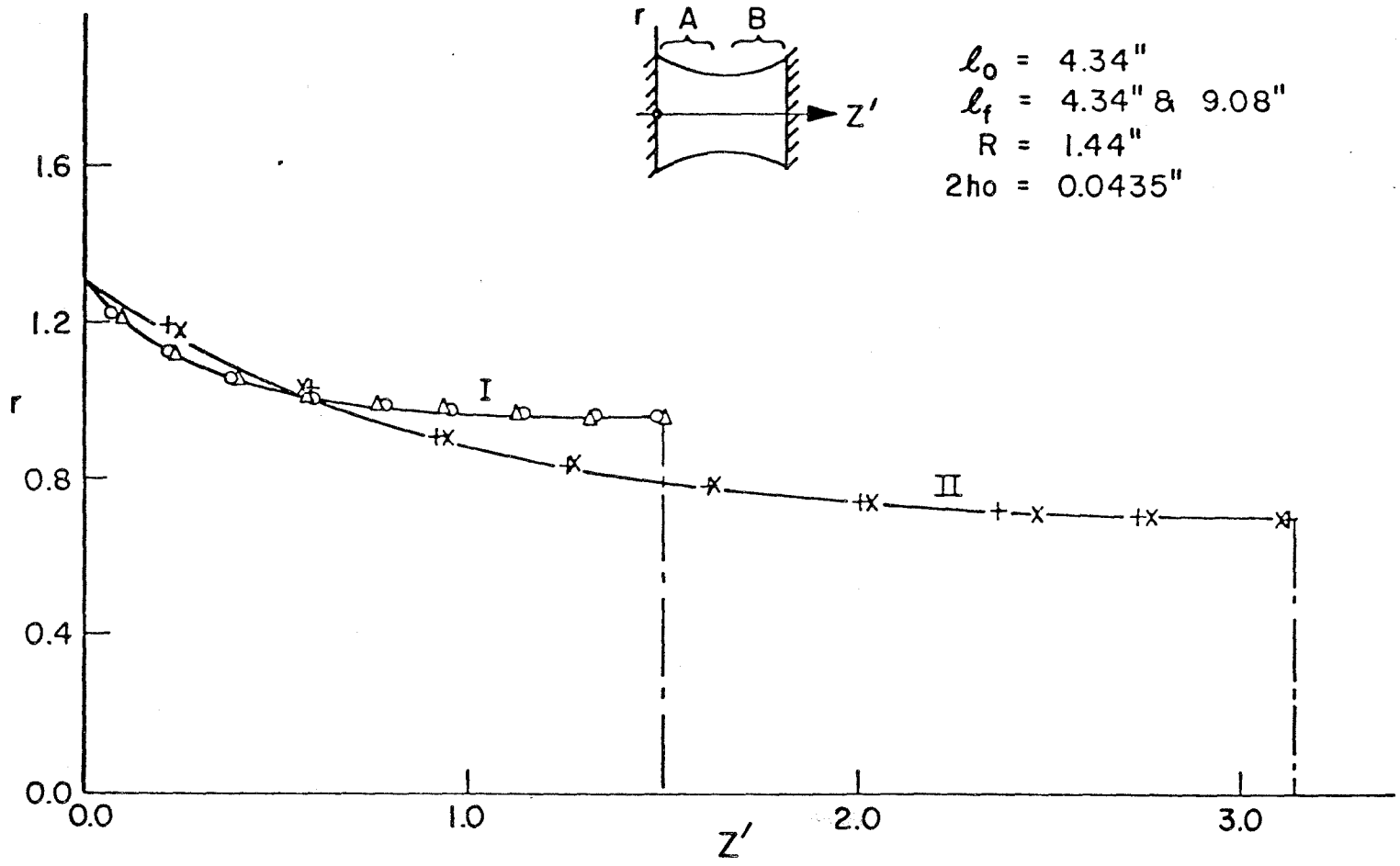

Fig. 9 Calculated deformed profiles for R = 1, r_e = 1.315, P = 0, ℓ_o = 3. Curve I, ℓ_f = 3, Γ = 0.52; Curve II, ℓ_f = 6.28, Γ = 0.3. Corresponding experimental results (0, x of A part; Δ, + of B part).

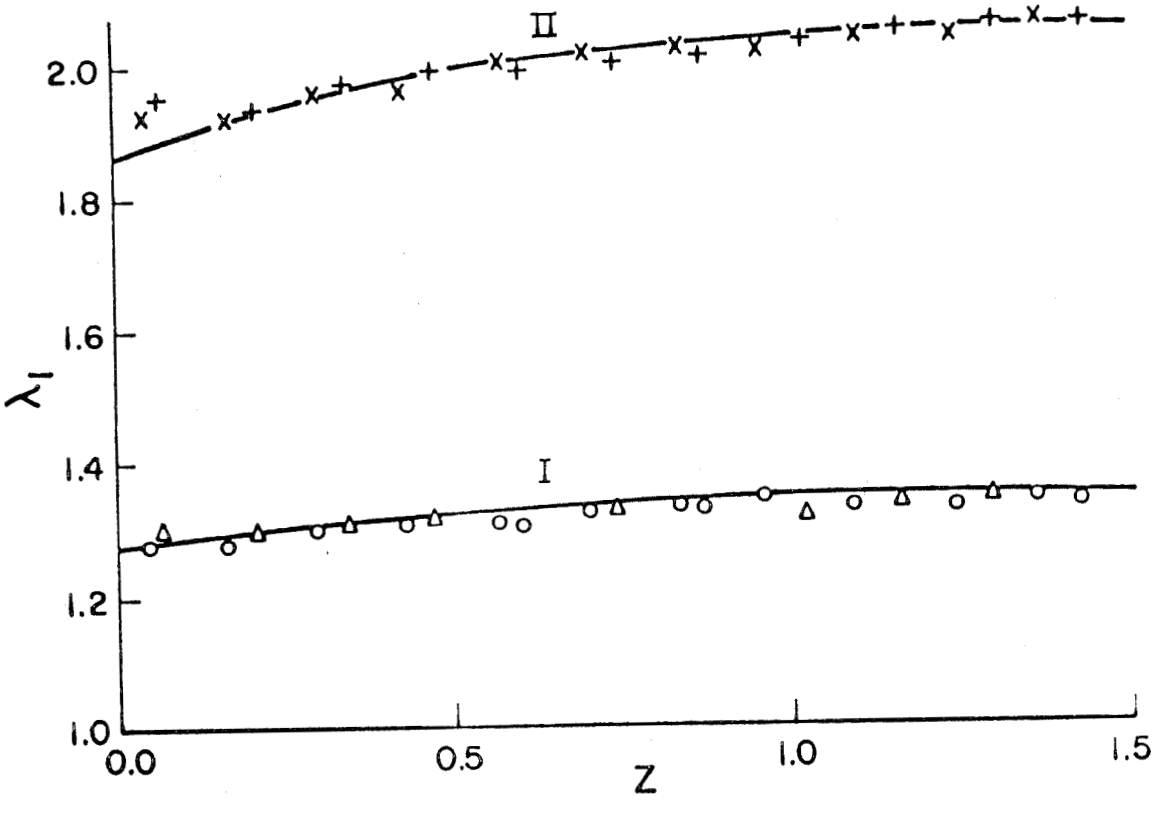

Fig. 10 Calculated λ_1 plotted against z-axis of undeformed state (cf. Fig. 8) as compared with experimental data.

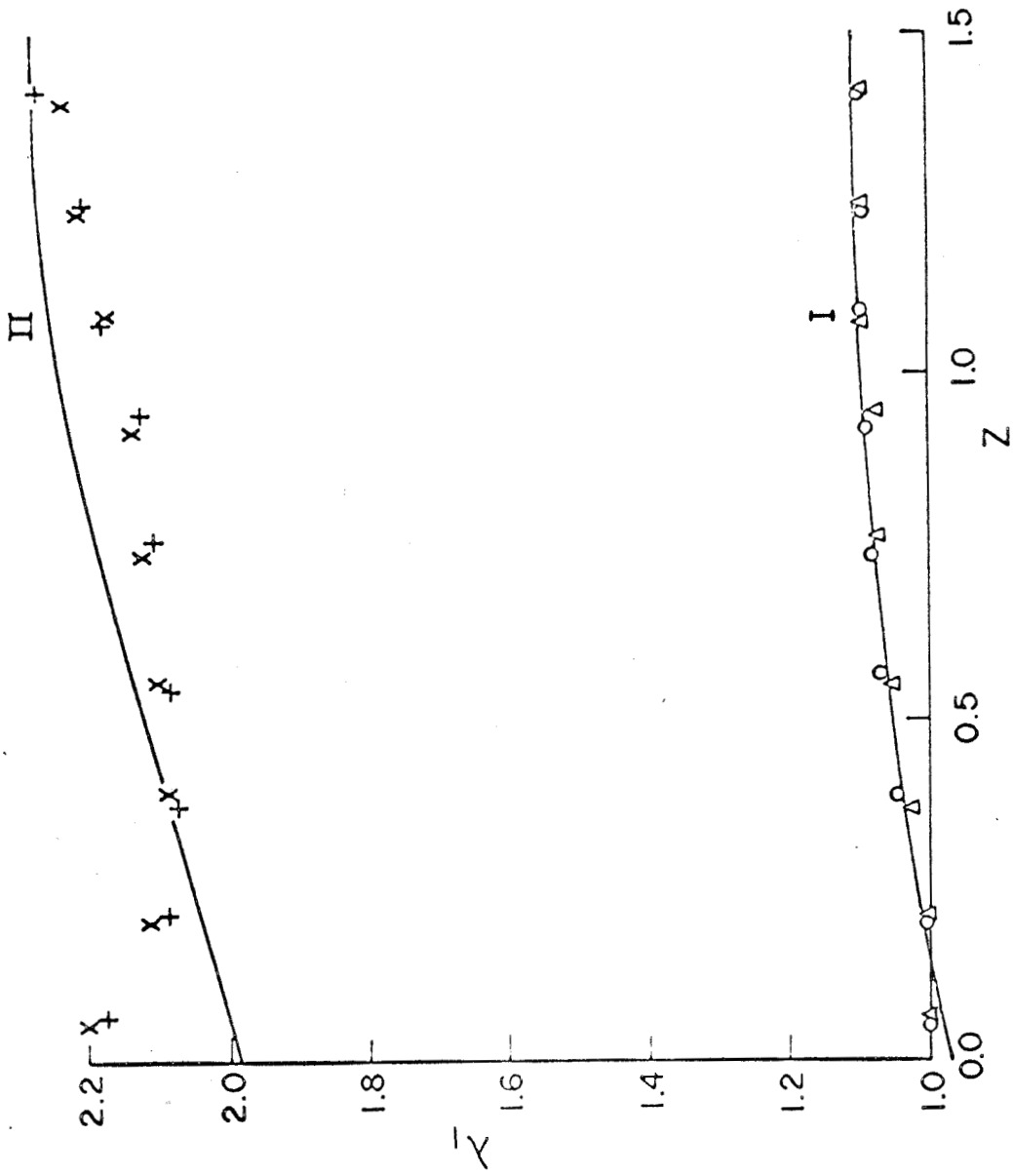

Fig. 11 Calculated λ_1 plotted against z-axis of the undeformed state as compared with the experimental data (cf. Fig. 9).

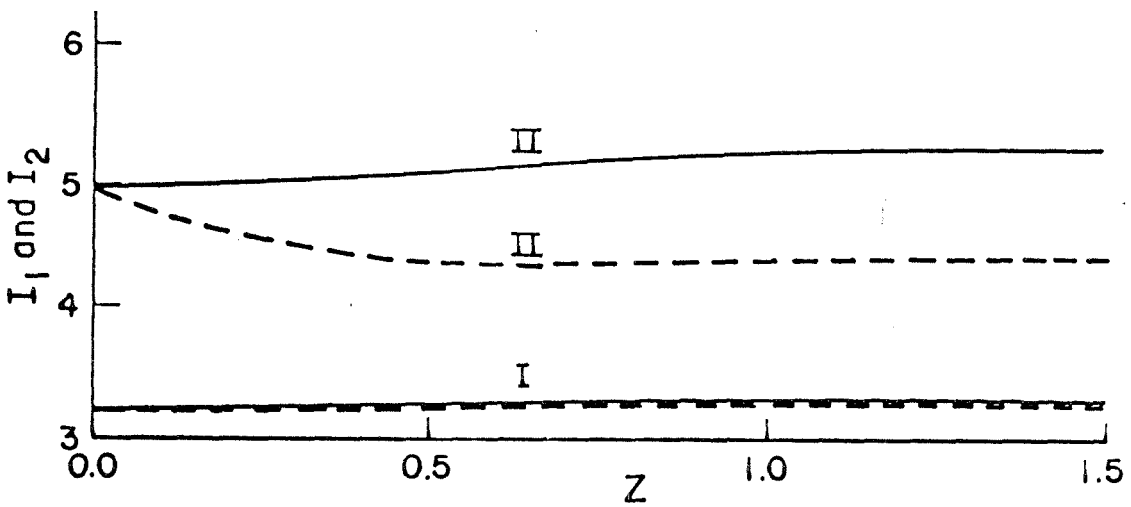

Fig. 12 Calculated I_1 (solid lines) and I_2 (broken lines) plotted against the z-axis (cf. Fig. 8).

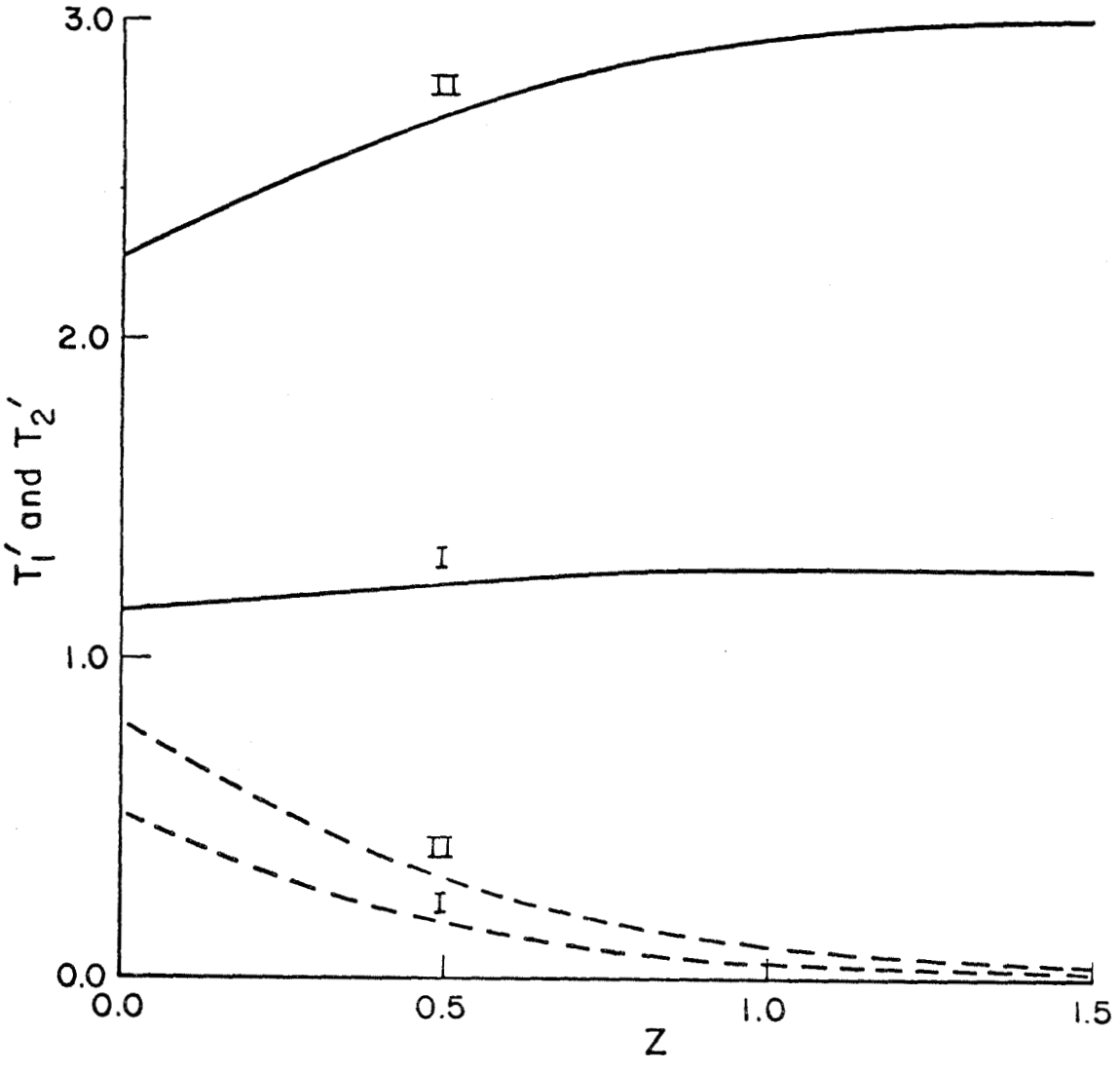

Fig. 13 Calculated stress-resultants T_1' (solid lines) and T_2' (broken lines) plotted against the z-axis (cf. Fig. 8).

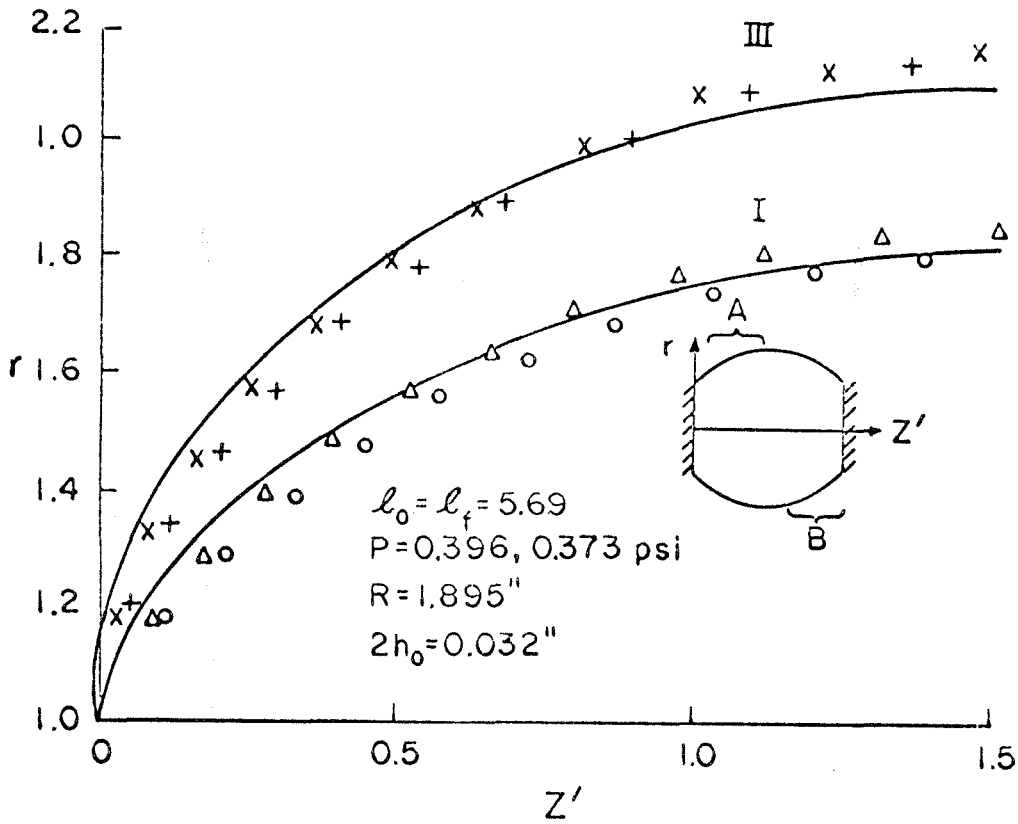

Fig. 14 Calculated deformed profiles I and III from Fig. 16 and the experimental results (Δ, 0, $P' = 1.315$; x, +, $P' = 1.24$; Δ, x of A part; 0, + of B part) with $C_1 = 17.8$ psi.

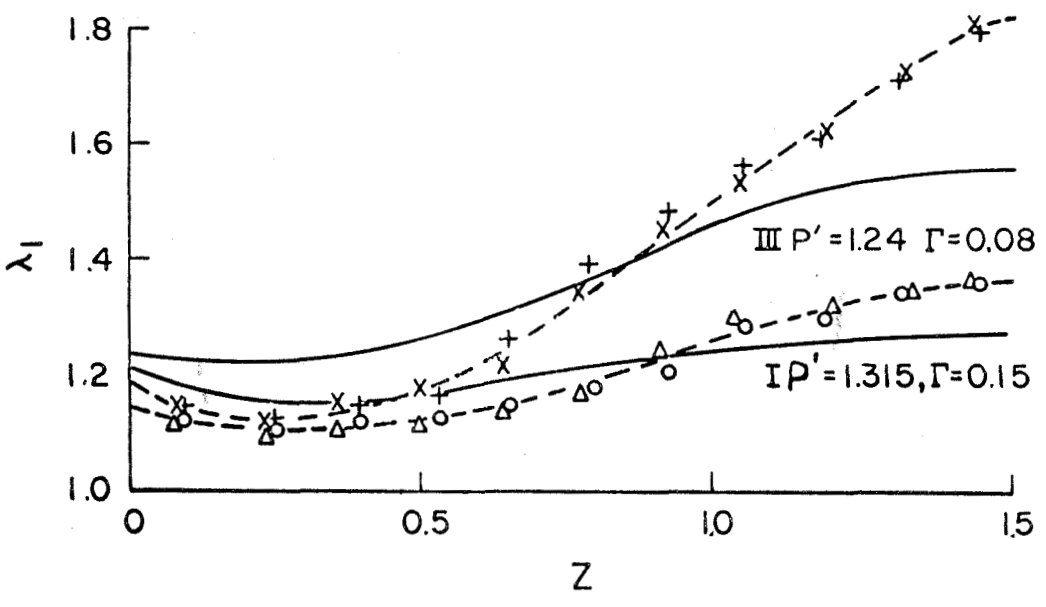

Fig. 15 Calculated (λ_1, z) Curves I and III from Fig. 17 and the experimental results (broken lines) at corresponding pressures (cf. Fig. 14).

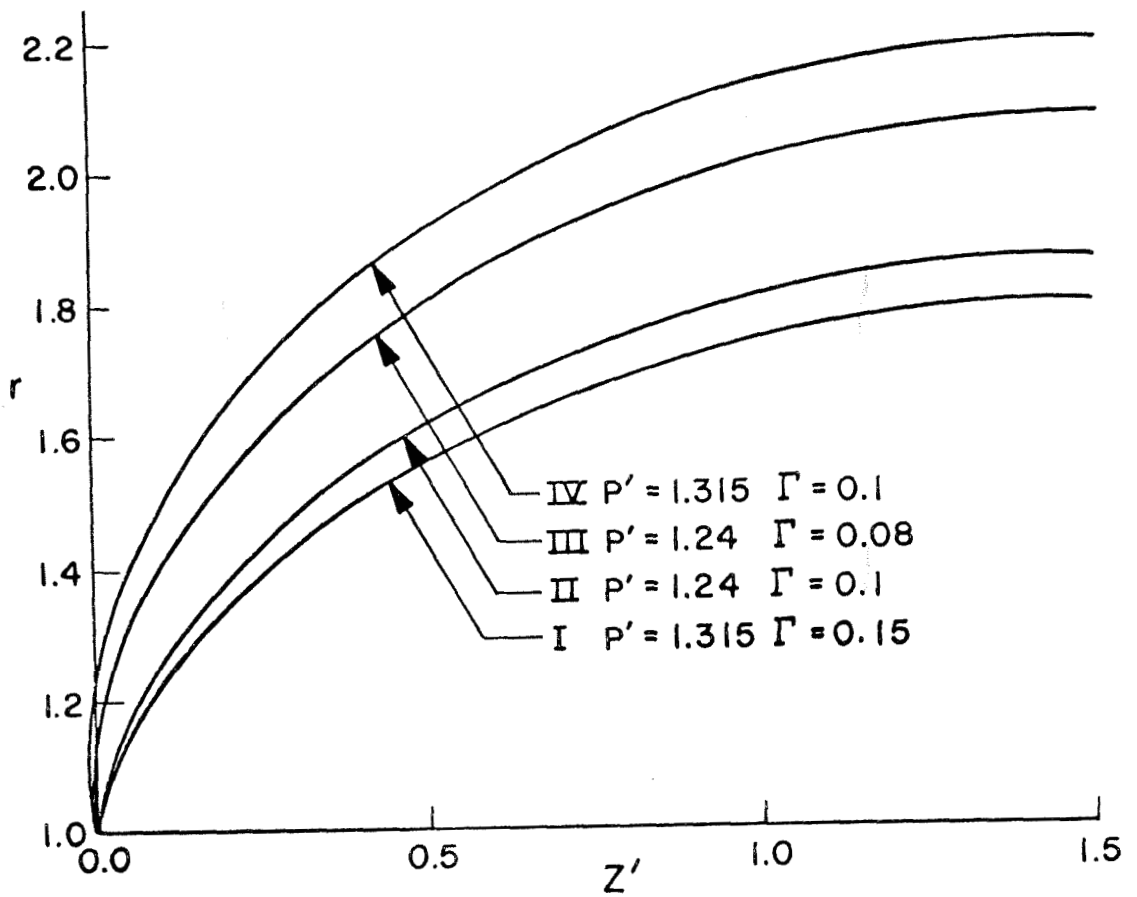

Fig. 16 Calculated deformed profiles for R = 1, $\ell_o = \ell_f = 3$.

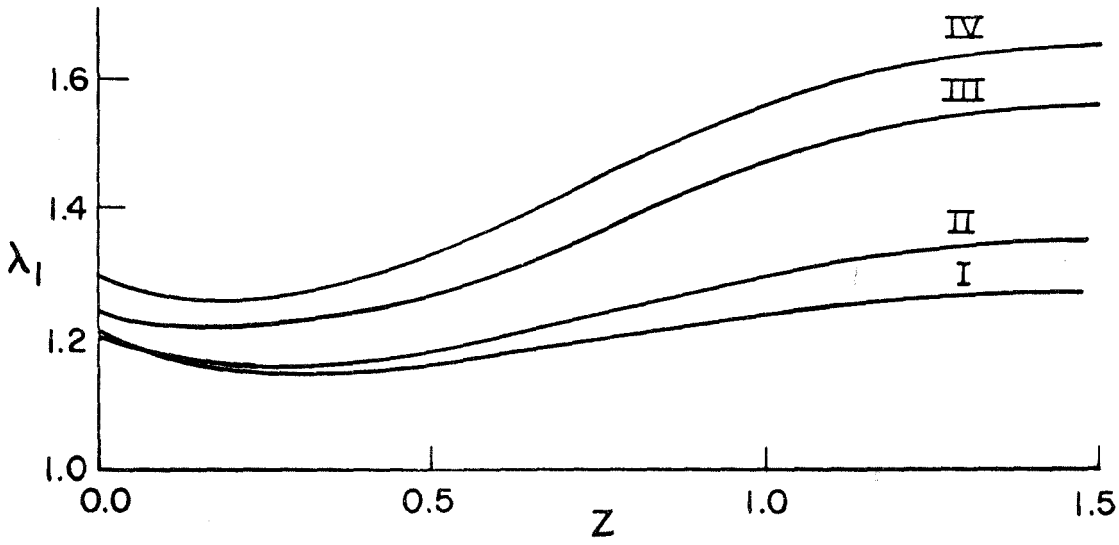

Fig. 17 Calculated λ_1 plotted against the z-axis of the undeformed state (cf. Fig. 16).

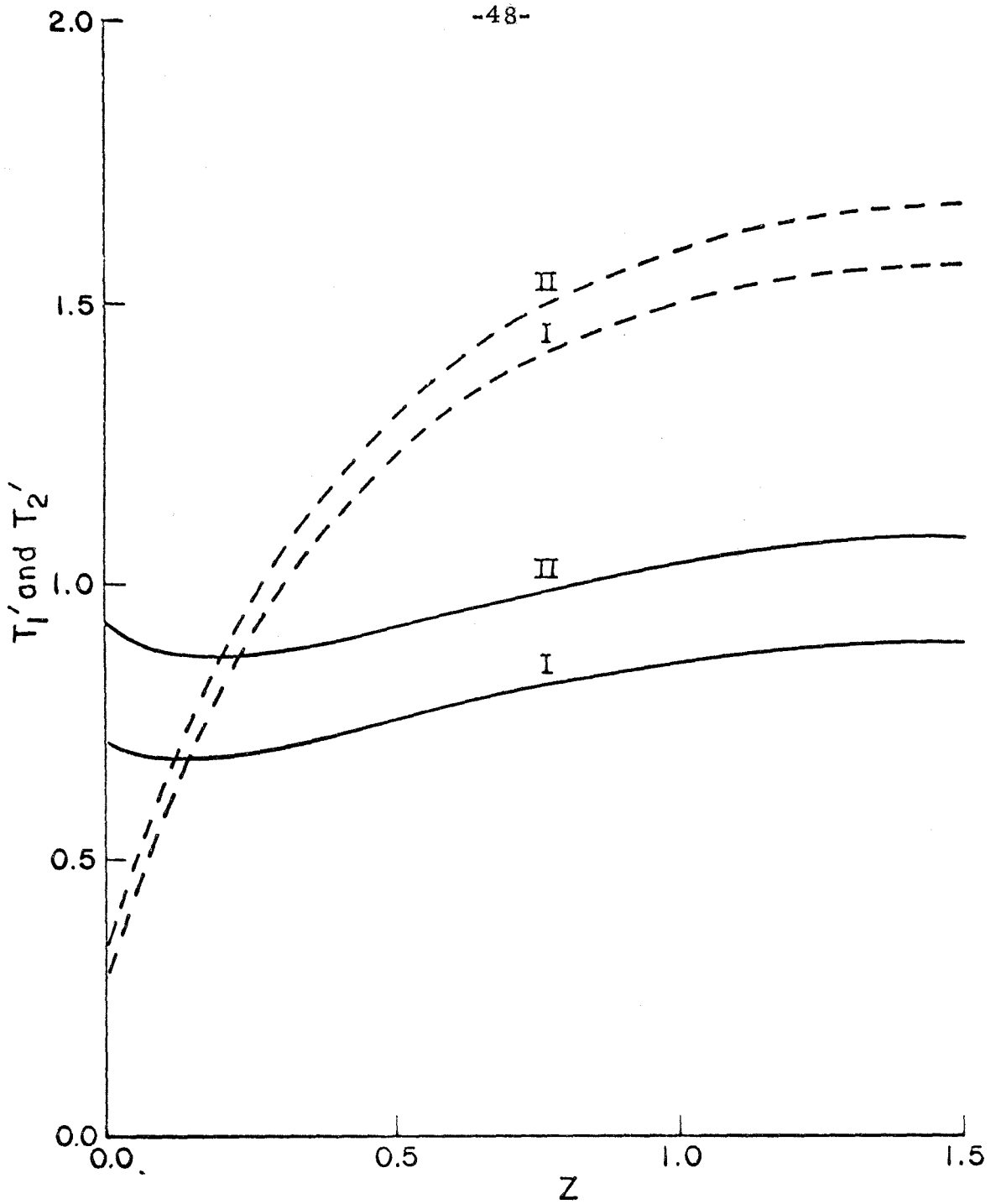

Fig. 18 Calculated stress-resultants T_1' (solid lines) and T_2' (broken lines) for R = 1, $\ell_o = \ell_f = 3, \Gamma' = 0.1$, Curve I, $P' = 1.24$; Curve II, $P' = 1.315$.

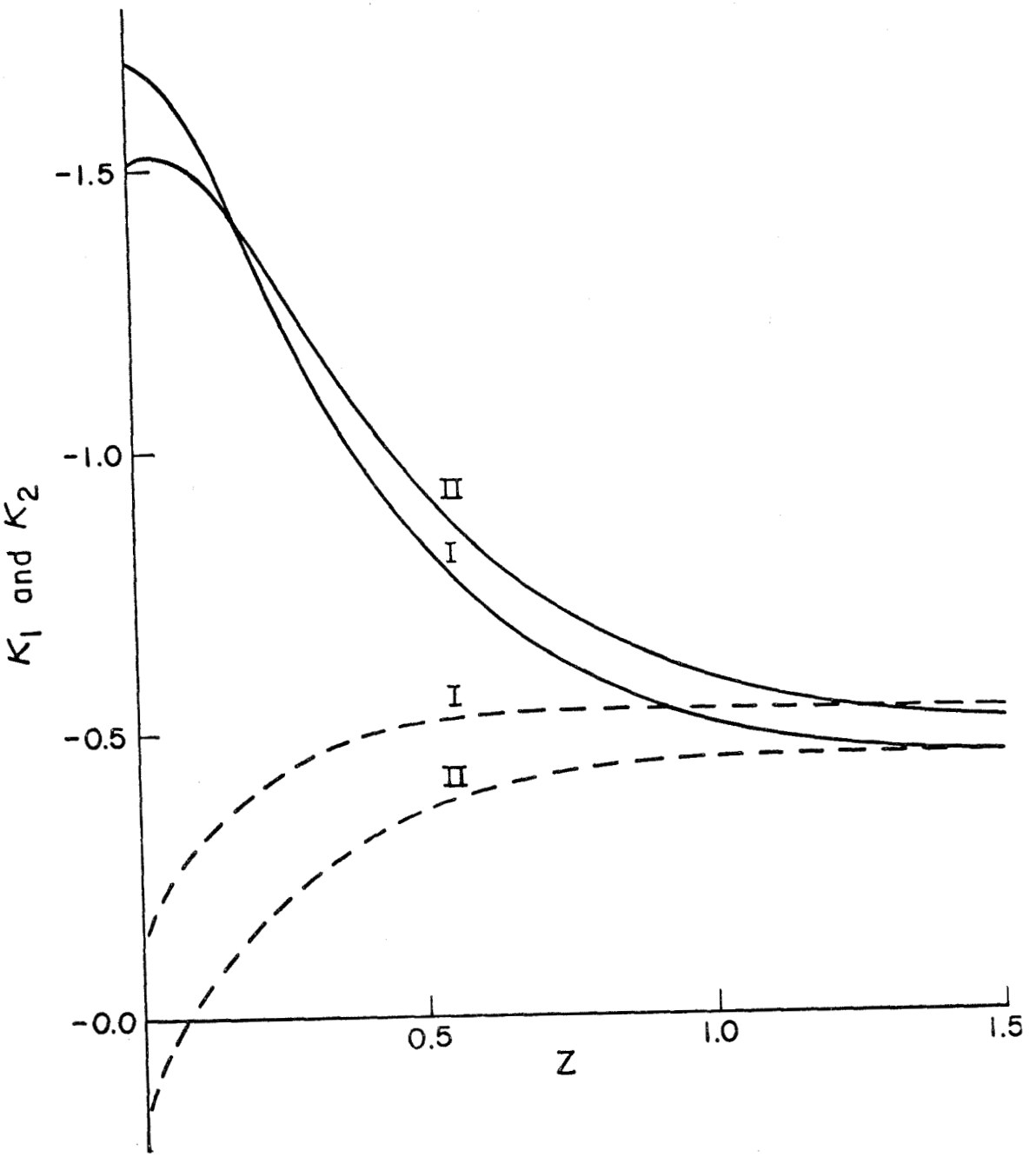

Fig. 19 Calculated principal curvatures K_1 (solid lines) and K_2 (broken lines) against the z-axis with the radius of the undeformed tube to be unit length (cf. Fig. 16).

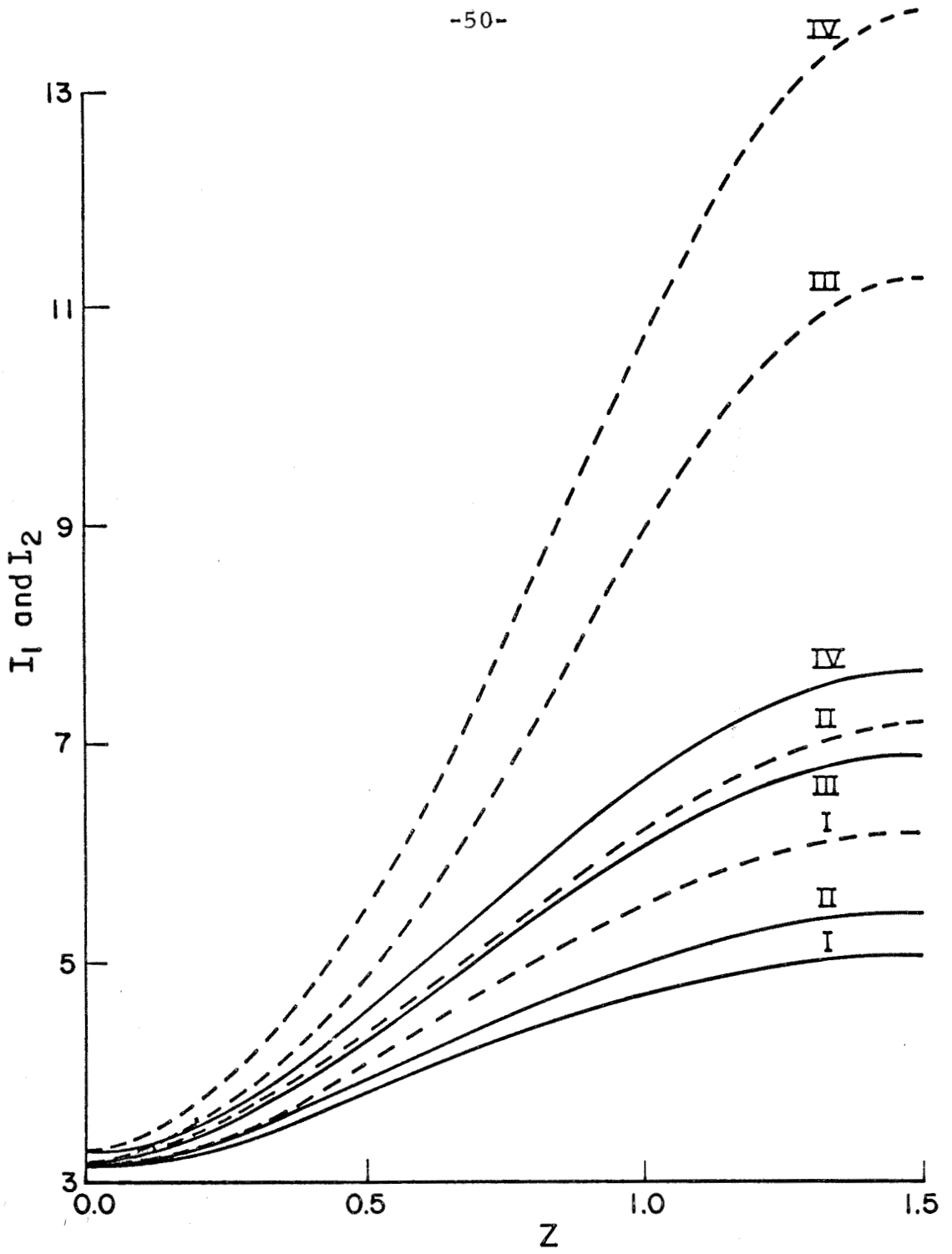

Fig. 20 Calculated I_1 (solid lines) and I_2 (broken lines) plotted against the z-axis (cf. Fig. 16).

PART II

EXPERIMENTAL STUDIES ON THE MECHANICAL PROPERTIES OF LARGE BLOOD VESSELS

TABLE OF CONTENTS

LIST OF SYMBOLS

A	state of vessel in which the vessel diameter equals to the mean of the outside diameters of the vessel near the lower and upper supports
A_o, A_A, A_N	cross-sectional area of the undeformed vessel, of the vessel at state A and at the natural state respectively
e_{11}, e_{22}	strain increments in the longitudinal and lateral directions respectively, induced by an infinitesimal deformation superimposed on a finite deformation
d	outside diameter at the mid-portion
d_A	mean of the outside diameters of the vessel near the lower and upper supports
d_N	outside diameter of the vessel at the natural state
d_o	outside diameter of the vessel at the undeformed state
h_o, h_A, h_N	thicknesses of the undeformed vessel, of the vessel at state A and at the natural state respectively
$k_{11}, k_{12}, k_{21}, k_{22}$	elastic constants, Eq. (9)
ℓ_o, ℓ	length of the undeformed and deformed vessel respectively
ℓ_N	length of the vessel at the natural state

P	internal pressure
s_1, s_2	Lagrangian stresses in the longitudinal and lateral directions respectively. They are referred to the undeformed state for carotid arteries, jugular veins and to the state A for mesenteries and femoral arteries
T_1, T_2	stress resultants per unit length in the meridional and latitudinal directions of the vessel wall respectively
T	force, acting at the ends of the vessel, required to keep the vessel in equilibrium
β	$= h_o \times 1\ cm/A_o$
λ_1	principal extension ratio referred to the undeformed state associated with meridians. For carotid arteries and jugular veins $\lambda_1 = \ell/\ell_o$
$\bar{\lambda}_1$, $\bar{\lambda}_2$	principal extension ratios, referred to the natural length ℓ_N and the reference diameter d_A, $= \ell/\ell_N$ and d/d_A, respectively
λ_{1N}	ratio of the natural length to the undeformed length

PART II

EXPERIMENTAL STUDIES ON THE MECHANICAL PROPERTIES OF LARGE BLOOD VESSELS

1. INTRODUCTION

Most works on the mechanical properties of large arteries are confined to separate measurements of either the circumferential (Ref. 1) or the longitudinal (Ref. 2) elastic behavior. These measurements are insufficient to treat the mechanics of vessel walls. Studies have also been made on strips and rings cut from large vessels (Ref. 3), but the interpretation of the elastic properties of these specimens in views of the fibrous structure is questionable.

Histological studies show that the most important elastic material in the vessel wall is net-like elastin and collagen fibers. A model in which all fibers are arranged in the circumferential direction was used by Bergel (Ref. 1) to explain qualitatively the lateral distensibility of vessels. However, the details of such a model still await a full understanding of the structure and the mechanics of these vessels.

It is the objective of the present paper to report the measurement of the overall mechanics of the large blood vessels of the dog. Our experiments consisted of the longitudinal stretching test, the lateral distensibility test and the repeated-strain test.

The first two tests were designed to determine the stresses as functions of one of the extension ratios. The last one was designed to investigate hysteresis and the effect of strain rate. In the longitudinal stretching test, the blood vessel was stretched very slowly in the longitudinal direction. By adjusting the internal pressure as a vessel was stretched, the diameter of the vessel was held constant. In the lateral distensibility test, vessels were inflated or contracted by changing the pressure step by step while the ends of the vessels were fixed. The relationship between stresses and strains can be determined from these data. In the repeated-strain tests, the vessels were stretched longitudinally as a sinusoidal function of time while the pressure was held constant.

In the experiments named above, fresh specimens were taken from anesthetized dogs and were immediately mounted on the testing chamber for testing in stretching and inflation. The chamber was temperature regulated by circulating Ringer-Tyrode solution. An optical comparator which provides a magnification factor ranging from 10 to 100 was used to measure the diameter change of the vessels. The force, pressure and longitudinal strain were recorded by an elaborate set-up to be described below.

2. EXPERIMENTAL METHOD

In this section, the method of preparing the test specimens, the experimental procedure and the data reduction method are presented.

A. Preparation of the Specimen

The blood vessels used (carotid, femoral, mesenteric arteries and jugular veins) were taken from anesthetized dogs. A carotid artery in situ is shown in Fig. 1. Before the removal of advent tissues, a rough estimation of the diameter of the vessel in situ was obtained by measurement with a caliber and by photography. This diameter is designated the natural diameter d_N. The vessel would shrink to about two thirds of its natural diameter after the advent tissue was gently peeled off. Two ink marks, about 5 cm apart, were marked on a portion of the vessel. This portion was selected on the basis of uniformity of cross-sectional size and scarcity of side branches. If any branches were present, they were ligated and cut close to the parent vessel. The distance between the marks was measured with a caliber when the neck of the dog rested on the operating table. This length is designated the natural length ℓ_N. The physical meaning of this natural length is clear; however, its numerical value is somewhat debatable since the neck assumed different positions, the length between the marks could be changed by 0.5 cm. The marked segment of the vessel was then cut at points about 7 mm beyond the marks and rinsed in a warm Ringer-Tyrode solution.

The distance between the marks and the diameter of the relaxed vessel were measured (Fig. 2) and are designated as the relaxed or undeformed length ℓ_o and the relaxed or undeformed diameter d_o respectively. The length variation due to neck movement noted above amounts to about 20 percent of the undeformed length ℓ_o. Because of the small dimensions of mesenteric and femoral arteries, we had to fasten them to the cones before cutting them out of the animal body. The undeformed dimensions of the mesenteric and femoral arteries were not measured.

The specimen was then mounted on cones of suitable diameters. Fig. 3 shows the mounting device and the cones used for carotid arteries, mesenteries, etc. Two grooves were cut on the cylindrical portion of the cone to secure the attachment of the vessel. Black silk thread was used to tighten the vessel on the grooves. The threads were tied right on the marks and served as markers of the vessel length. The specimen was held vertically in a Lucite chamber circulating with a warm Ringer-Tyrode solution (38° C). The lower support was connected with the pressure system. During the test, there was no circulation inside of the vessel. Fifteen minutes of time was required to complete the transfer of the specimen from the animal body to the testing chamber to start the test.

After each test, the average cross-sectional area in the undeformed state was determined by weighing the specimen, cut at the marks and bisected longitudinally, first in water and then in air. The weight in air was weighed with the inner and outer surfaces dried with Kimwipes paper. Questions may be raised as to the proper degree of dryness the surface should have, but it is

estimated that with all uncertainties included, this method may entail an error of no more than five percent in cross-sectional area. The cross-sectional area in the natural state is then computed by assuming the vessel wall is incompressible.

B. Testing Apparatus

The tests were carried out in the specially designed apparatus shown in Fig. 4. The position of the chamber, the location of the specimen, etc. are indicated in Fig. 5. A light source (not shown in Fig. 4) was situated in front of the chamber, so that any change of diameter could be recorded by measuring the shadow the vessel cast on the comparator screen. The comparator used was a Kodak optical comparator and it could provide a magnification factor ranging from 10 to 100.

A motor was used to stretch the vessel in the longitudinal direction. In the normal configuration, the vessel can be stretched at a constant strain rate. With an eccentric device, the vessel can be stretched sinusoidally in time at a fixed amplitude. In most of our experiments a very small strain rate (0.05 cm/cm/min) was imposed.

A linear differential transformer with a reliable displacement range of 1.25 cm was used to measure the longitudinal translation of the upper end of the specimen. This differential transformer consisted of a core and a casing. The core was connected in series with the upper end of the blood vessel specimen.

The casing was fixed on the rigid frame. A set of flexures was designed to center and to free the core in the casing, and thus it was possible to eliminate any sliding friction between the core and the casing. The electrical output of the differential transformer was monitored by a Moseley X-Y plotter and was frequently calibrated with a micro-comparator. An example of the linear relation between the displacement and the electric output is shown in Fig. 6. As the lower end of the blood vessel specimen was fixed to the bottom of the bath, the differential transformer provided the data on elongation.

The force needed to stretch the vessel was measured by a force transducer which consisted of two steel arms in the form of a horseshoe. On one arm of the force transducer four strain gauges (SR-4) with a gauge factor 1.69 were mounted on both sides of a thinner section with a thickness of about 0.03 inches. The gauges were connected to a Wheatstone bridge. This gave the bending moment at the section and hence the force applied on the ends of the force transducer. The output of the bridge was amplified by a factor of 100 to 1100 with a Leeds and Northrup D.C. amplifier whose output was monitored on a Brown potentiometer and the Moseley X-Y plotter. Fig. 6 also shows the linear output of the force transducer which was calibrated by adding weights on its ends.

The pressure changes were produced with a hand bulb and a reservoir bottle connected to the vessel through the lower support and were measured by a Statham pressure gauge, a mercury manometer and/or a water manometer. For the carotid arteries, the mercury manometer was used. The water manometer was sometimes used for the jugular veins and the smaller arteries. The output of the Statham gauge was monitored on another Moseley X-Y plotter.

In order to see if any phase lag existed in the set-up of the force transducer and the differential transformer, the following repeated-strain tests were carried out with two linear steel springs in place of the test specimen, the outputs of the force and the displacement were monitored by the Moseley plotter as the Y- and X- inputs respectively. The rigidity of the stronger spring was approximately equal to the longitudinal rigidity of a carotid artery and that of the weaker spring was approximately equal to the rigidity of the mesenteries and femoral arteries. The motor was driven at about 1 cycle per minute with an eccentric amplitude of 2 mm. The responses of these two springs and the one with open end are shown in Fig. 7. The last one was used to measure the elasticity and the frictional resistance of the mechanical set-up. It is seen that the outputs were quite linear and the hysteresis was negligible.

Before carrying out the tests, the differential transformer was calibrated by translating its core at a known distance (0.35 cm), the force transducer by adding weights (40 gm) on the part R shown in Fig. 5 when the end was free and the Statham gauge by the mercury manometer with a range of 20 cm Hg.

C. Test Procedure

C.1 Torsional Test

It is desired to determine first whether the overall mechanical behavior of the blood vessel is axisymmetric. One test in this direction is to see whether the vessel has a tendency to twist when it is subjected to a longitudinal stretching and to an internal

inflation. We therefore replaced the part "J" shown in Fig. 4 by a thread (8 pound-test fishing line) which has a very low torsional rigidity. The lower end of the blood vessel being fixed, any twist in the blood vessel will turn the upper support through an angle. By rotating the part R shown in Fig. 5, the torque needed to restore the vessel back to the state of symmetrical deformation can be measured. Experiments with four carotid arteries gave no indication of twisting when the vessels were subjected to longitudinal extension and inflation. Hence the axisymmetry of the test specimens may be assumed.

C.2 Longitudinal Stretching Test

The test specimen was adjusted to have a length of about 10 percent less than the natural length. Some vessels were inflated to the natural or in situ diameters, d_N. Other vessels were inflated only to have a diameter d_A equal to the mean of the diameters of the vessel near the upper and lower supports. These diameters were measured on the screen of the comparator. In the following description, the state of the vessel in which this mean diameter is obtained is called the state A.

Without pressure control, the diameter of the vessel contracted in the lateral direction as the vessel was stretched longitudinally. To maintain a constant diameter, the pressure was continuously adjusted. After the vessel was stretched to a proper limit, it was manually and slowly relaxed back to its starting configuration. Without such a careful relaxation a significant deviation in

the force reading (about 10 percent of total force) at large extension ratios would result for the next run.*

Typical data of the force vs. longitudinal extension ratio (λ_1) and the pressure vs. λ_1 recorded for three successive runs are shown in Figs. 8 and 9 respectively. In these figures the vertical axis is shifted for each run to separate the curves more clearly. Note the resemblance of T - λ_1 curves of the second and the third runs and their difference from the first run. This changing behavior at the first few stress cycles seems to be a general behavior of blood vessels. For this reason, the blood vessel was stretched and relaxed several times around its natural length prior to the routine data taking. This procedure enabled us to obtain repeatable results in T after a few cycles.

C. 3 Lateral Distensibility Test

The length of vessels was set at the natural length or 5 percent less than the natural length . The vessels were distended by changing the internal pressure. Their diameter was decreased from the diameter d_A at a proper pressure decrement to a state at which the differential pressure is nearly zero, then increased by steps to a certain maximum pressure, and finally decreased back to d_A. For some vessels, only the inflation part was performed.

---

*The vessels had been stretched at different constant strain rate. Because of the uncertainty in this relaxation technique, those data are not presented.

Since the force transducer was about a hundred times stiffer than the blood vessels, the ends of the test specimen may be regarded as fixed during the inflation test and the deformation of the vessels in the lateral distensibility test could be regarded as an inflation without any stretching in the longitudinal direction. Furthermore, since the length-to-diameter ratio of the test specimens is of order 10, the specimen is a long circular cylinder and the deformation at the middle section may be regarded as a uniform cylindrical inflation.

C.4 Repeated-Strain Test

Vessels were stretched longitudinally at a rate from 0.2 to 7 cycles per minute. The stretching limits could be adjusted by changing the eccentricity of the driven motor. During the entire test, a zero pressure level was maintained. The outputs of displacement and force were monitored on a Moseley X-Y plotter. It resulted in continuous curves as shown in Fig. 10.

As stated previously, the vessel length in situ varied over a range of about 20 percent of the undeformed length. In this repeated-strain test the vessels were stretched within these recorded variations. At first they were stretched between the two limits of the recorded variations, and then several successive small loops were tested. Each small loop had a range of about 3 percent of the undeformed length.

D. Method of Data Reduction

To study the blood vessel wall as a three dimensional body in all its detail is a formidable task. Structural non-uniformity in the blood vessel wall is well known. A detailed study to determine the structural organization of the collagen fibers, elastin layers and endothelial cells is in progress at the Cardio-Vascular Research Laboratory by the method of differential enzymatic digestion. These studies show that a proper model for the blood vessel wall is a fiber-reinforced structure, with the collagen fibers arranged in different directions in different layers, very much like fiber-reinforced rocket bodies.

When the mechanical properties of each component material (collagen, elastin, endothelial, etc. in vivo) are known, and when the geometric relationship (relative size and architecture) and the interaction mechanism between each of these components (adhesion, friction, weldability, breaking strength, yield point etc.) are determined, then it may be possible to compute the overall properties of the blood vessel. Without this detailed information one cannot predict the overall properties. However, it is possible to measure the overall mechanical properties. The results will be useful for hemodynamic applications directly, and will serve as basic information for future detailed structural studies.

With the determination of the overall properties as our objective, the blood vessel is considered as a circular cylindrical tube of uniform cross-section with a diameter-to-thickness ratio ranging from 7.6 to 21. Strictly speaking, the vessels tested must be considered as thick-walled cylinders. But the difficulty in analysis and the lack of detailed information about fiber-structure suggest that

at the present level, the variations of stresses and strains across the thickness should be neglected. The blood vessel is then treated as a thin-walled tube, with a nominal diameter taken to be the outside diameter of the vessel. Our data analysis will be based on this model, which must be remembered whenever our results are used.

The change of excised length before and after the vessel was stretched and relaxed several times was not significant. This was observed for the proximal and distal segments of the right and left carotid arteries of a god. It demonstrates that the undeformed state, at which the vessel is free of external forces, is unique. Therefore, it is proper to choose the excised length and diameter as the basic reference length in the calculation of extension ratios. However, because of the difficulty of obtaining an accurate measurement of the diameter in the relaxed state, the diameter d_A is taken as the reference diameter of the thin cylindrical tube in the data analysis.

The vessels used were rather long, with length-to-diameter ratios of about 10, hence the fact that the ends of the vessel are fixed on the cones introduces a negligible error if we approximate the longitudinal extension ratio at the middle portion of the vessel by the ratio of the total length of the undeformed vessel and the undeformed length. Thus the following longitudinal and lateral extension ratios λ_1 and $\bar{\lambda}_2$ can be used to characterize the strains of the middle portion of the vessel.

$$\lambda_1 = \frac{\ell}{\ell_o} \qquad (1)$$

$$\bar{\lambda}_2 = \frac{d}{d_A}$$

where $\underline{\ell}$ is the total length of the deformed vessel and $\underline{d}$ is the outside diameter of its mid-portion. In the longitudinal stretching test, the diameter of the vessel was kept constant, hence $\bar{\lambda}_2$ = constant and the only variable in strain is the longitudinal extension ratio λ_1. In the lateral distensibility tests the longitudinal extension λ_1 was kept constant and the deformation of the vessel is characterized by the ratio λ_2. In the repeated-strain tests the deformation was rather complicated due to the fact that the pressure was fixed so that a lateral extension accompanied any longitudinal extension. However, it is sufficient to use the longitudinal extension ratio λ_1 to specify the deformed state.

Our instruments recorded the total force T applied at the ends of the vessel and the internal differential pressure p. The longitudinal stress-resultant T_1 acting on the cross-sectional area of the vessel is given by the formula (cf. Eqs. (8) and (9) of Part I)

$$\pi d T_1 = T + \frac{\pi p d^2}{4} \tag{2}$$

The stress resultant T_2 in the circumferential direction is the well known hoop stress, and is given by the following formula (cf. Eq. (5) of Part I)

$$T_2 = \frac{p d}{2} \tag{3}$$

provided that the small curvature κ_1 in the meridional plane can be neglected. Consider an element of the deformed vessel subjected to the forces dT_1 and dT_2 as shown on the right hand side of Fig. 10.

Let dA, $\overline{dA}$ be the area in the deformed tube on which dT_1 and dT_2 act respectively. Let dA_o and $\overline{dA}_o$ be the areas on the undeformed vessel which correspond to the areas dA, $\overline{dA}$ respectively. We define the Lagrangian stresses as the limiting values of the ratios dT_1/dA_o and $dT_2/\overline{dA}_o$ after dT_1 and dT_2 have been translated parallelly to the undeformed element as shown on the left hand side of Fig. 9. From Eqs. (1) through (3) we obtain the following relations

$$s_1 = \frac{T}{A_o} + \frac{\pi d^2 p}{4 A_o} \tag{4}$$

$$s_2 = \frac{p \lambda_1 d}{2 h_o} = \frac{1}{\beta} \frac{p d \lambda_1 \times 1 cm}{A_o}$$

where s_1 and s_2 are the Lagrangian stresses referred to the undeformed state (stresses based on the undeformed area) in the longitudinal and lateral directions respectively, A_o and h_o are the cross-sectional area and the thickness of the undeformed vessel respectively, and $\beta = h_o \times 1 \text{ cm}/A_o$.

Because of the difficulty of measuring the undeformed dimensions of the femoral arteries and mesenteries, the following extension ratios and stresses are used.

$$\bar{\lambda}_1 = \frac{\ell}{\ell_N} \quad , \quad \bar{\lambda}_2 = \frac{d}{d_A} \tag{5}$$

$$s_1 = \frac{T}{A_N} + \frac{\pi d^2 p}{4 A_N} \, , \quad s_2 = \frac{p d \bar{\lambda}_1}{2 h_N}$$

where A_N and h_N are the cross-sectional area and the thickness of small vessels in their natural state. In the above formula, the stresses are based on the dimensions of the vessel in the natural state and are called the Lagrangian stresses referred to the natural state.

3. TEST RESULTS

The results of the longitudinal stretching and the lateral distensibility tests are presented in Tables 1 and 2 respectively. Nine carotid arteries, four jugular veins, two mesenteries and two femoral arteries were tested. For conciseness, only the data on Lagrangian stresses* are presented. A smoothing technique on the pressure record as shown in Fig. 9 was used in analyzing the data of the longitudinal stretching test. In all the tests, the vessels were either stretched from $\lambda_1 = \lambda_{1N} - 0.1$ to $\lambda_1 = \lambda_{1N} + 0.1$ in the longitudinal direction or distended in a range $\bar{\lambda}_2 = 0.8$ to 1.3 in the lateral direction.

The raw data of three other carotid arteries in a repeated-strain test are presented in Figs. 11, 12, and 13. The Lagrangian stress s_1 is plotted against the longitudinal extension ratio λ_1. Tests were performed within the recorded variations of the vessel length in situ.

The physical dimensions, the natural longitudinal extension ratio λ_{1N}, the natural diameter d_N, the mean diameter d_A, the undeformed cross-section A_o and the thickness at the natural state h_N of carotid arteries and jugular veins are presented in Table 3.

---

* For most of the carotid arteries and the jugular veins, the relaxed diameter of the vessels was not measured. Hence β becomes an unknown constant (Eq.(4)) and it is combined with s_2 in the data reduction. The values of β for four carotid arteries are tabulated in Table 4 and range from 1.04 to 1.96. For the mesentery and the femoral arteries, the stresses are based on the reference state A and the data of s_2 are presented.

The undeformed physical dimensions, the diameter d_o, and the undeformed thickness h_o of the carotid arteries Nos. 8, 9, 11 and 12 are presented in Table 4. For mesenteries and femoral arteries, Table 5 shows the values of the mean diameter d_A, the cross-sectional area A_A and the thickness h_A of the vessels at the state A. The weight of the dogs where the tested vessels came from is shown in Table 6.

Tables 1 and 2 offer the reduced raw data. If it is desired to recover the experimental data on P and T for carotid arteries and jugular veins, one needs only to compute

$$p = \frac{\beta s_2 A_o}{\lambda_1 \bar{\lambda}_2 d_A \times 1cm} \tag{6}$$

$$T = s_1 A_o - \frac{\pi p d_A^2 \bar{\lambda}_2}{4}$$

where s_1, βs_2, λ_1 and $\bar{\lambda}_2$ are the values presented in Tables 1 and 2, and the values of A_o and d_A are presented in Table 3. For mesenteries and femoral arteries one has to use

$$p = \frac{s_2 h_A}{\bar{\lambda}_1 \bar{\lambda}_2 d_A} \tag{6a}$$

$$T = s_1 A_A - \frac{\pi p d_A^2 \bar{\lambda}_2}{4}$$

where s_2 s_2, $\bar{\lambda}_1$ and $\bar{\lambda}_2$ are tabulated in Tables 1 and 2 and d_A, A_A and h_A are tabulated in Table 5.

Figs. 14 to 17 are the straightforward presentations of the data of the carotid arteries Nos. 1 and 8 respectively. In the figures, the Lagrangian stresses s_1 and βs_2 are plotted against the extension ratios λ_1 or $\bar{\lambda}_2$. The paths of experiments are indicated by arrowheads in the figures. For the longitudinal stretching test, only the loading data are presented. On the other hand, the inflation and contraction data of the lateral distensibility test are presented. Hysteresis loops were observed as shown in Fig. 15. Note that the slopes (not closed loops) $\partial s_1/\partial \bar{\lambda}_2$ and $\partial s_2/\partial \bar{\lambda}_2$ are increased upon unloading.

Figs. 11 to 13 are the data monitored on the Moseley X-Y plotter in the repeated-strain test except that the force scale has been modified to the stress scale by

$$s_1 = \frac{T}{A_o} \tag{6b}$$

where A_o is the undeformed cross-sectional area and is presented in Table 3. This formula is obtained by setting $p = 0$ in Eq. (6). The path of experiments is indicated by an arrowhead in the figures. The first and third cycles of the carotid artery No. 10 are shown in Fig. 12. Note the decrease in stress as cycling proceeds. Results of steady-state response of the carotid arteries Nos. 11 and 12 which were stretched at different amplitudes and frequencies are shown in Figs. 12 and 13. One sees that the slope $\partial s_1/\partial \lambda_1$ at an extension ratio λ_1 can depend on the cycling amplitude and the frequency.

4. DISCUSSION

A. Stress-Strain Relationship

In the torsional test we have demonstrated the symmetrical properties of the vessels. Since the Lagrangian stresses s_1, s_2 and the extensional ratio λ_1 and λ_2 are sufficient to prescribe the stress state and the strain state of any symmetrical deformation, a double power series of s_1 and s_2 in terms of λ_1 and λ_2 or their combinations (e.g. $\lambda_1 - 1$ and $\lambda_2 - g$, where $\lambda_1 = 1$, $\lambda_2 = g$ describes the undeformed state) may be used as a stress-strain law to fit the experimental data. However, one can see that the stress-strain relation is highly nonlinear and it is difficult to correlate the coefficients of the power series with the experimental data.

As discussed in Part I, the Rivlin-Saunder's form for the strain-energy function gives a good approximation for latex rubber subjected to large deformation. However, the elastic behavior of latex rubber differs from that of blood vessels. For most of the vessels, the loading curves are rather flat at small extension ratios and then sharply ascendant at large extension ratios as shown in Figs. 14 and 15. On the other hand, the rubber has a higher tangential modulus at small extension ratios and a smaller one at higher extension ratio. Thus the Rivlin-Saunder's form of strain-energy function cannot be used in describing the stress-strain law for the blood vessels. Neither can the Mooney-Rivlin form (cf. Figs. 3 and 4

of Part I) be used. At the present stage, a stress-strain functional, e. g. a strain energy function which is better in the tensorial properties than the previously proposed Taylor's series and which can predict the behavior of the blood vessels as the Rivlin-Saunder's form does on rubber-like materials, is still being sought.

B. Elastic Constants of a Deformed Vessel

Suppose a symmetrical infinitesimal deformation is superimposed on a deformed vessel of which the finite deformation is specified by the extension ratios $(\lambda_1, \bar{\lambda}_2)$. The strain increments are

$$e_{11} = \frac{\Delta\lambda_1}{\lambda_1} \quad , \quad e_{22} = \frac{\Delta\bar{\lambda}_2}{\bar{\lambda}_2} \tag{7}$$

where $\Delta\lambda_1$ and $\Delta\bar{\lambda}_2$ are the increments of the extension ratios due to the additional deformation. Up to the first order approximation of $\Delta\lambda_1$ and $\Delta\bar{\lambda}_2$ the increments of the Lagrangian stresses are

$$\Delta s_1 = \left(\frac{\partial s_1}{\partial \lambda_1}\right)\Delta\lambda_1 + \left(\frac{\partial s_1}{\partial \bar{\lambda}_2}\right)\Delta\bar{\lambda}_2 \tag{8}$$

$$= k_{11}\, e_{11} + k_{12}\, e_{22}$$

$$\Delta \bar{s}_2 = \left(\frac{\partial \bar{s}_2}{\partial \lambda_1}\right)\Delta\lambda_1 + \left(\frac{\partial \bar{s}_2}{\partial \bar{\lambda}_2}\right)\Delta\bar{\lambda}_2$$

$$= k_{21}\, e_{11} + k_{22}\, e_{22} \qquad (8)$$

where

$$k_{11} = \lambda_1 \left(\frac{\partial \bar{s}_1}{\partial \lambda_1}\right) \quad , \quad k_{12} = \bar{\lambda}_2 \left(\frac{\partial \bar{s}_1}{\partial \bar{\lambda}_2}\right)$$

$$k_{21} = \lambda_1 \left(\frac{\partial \bar{s}_2}{\partial \lambda_1}\right) \quad , \quad k_{22} = \bar{\lambda}_2 \left(\frac{\partial \bar{s}_2}{\partial \bar{\lambda}_2}\right) \qquad (9)$$

and are evaluated at $(\lambda_1, \bar{\lambda}_2)$.

Using Eq. (5) of Part I and Eqs. (1) to (2), we have the equilibrium equations of the vessel.

$$k_{11}\frac{de_{11}}{dz} + (k_{12} - \beta^* \bar{s}_2)\frac{de_{22}}{dz} = 0$$

$$k_{21}\, e_{11} + (k_{22} - \bar{s}_2)\, e_{22} - \frac{\bar{s}_1}{\beta^*}\frac{d^2 e_{22}}{dz^2} = \frac{\pi d_A^2}{2A_o}\frac{1}{\beta^*}\Delta p \qquad (10)$$

where z is the axial coordinate of the deformed vessel, Δp is the pressure increment, $\beta^* = \beta \times \pi\, d_A/(\lambda_1 \times 1\ \text{cm})$, and $\bar{s}_1$, $\bar{s}_2$ are the Lagrangian stresses evaluated at $(\lambda_1, \bar{\lambda}_2)$.

In this derivation one sees that the elastic constants k_{11}, k_{12}, k_{21} and k_{22} are a proper choice in representing the response of the vessel to infinitesimal deformation.

To compare the rigidity of a vessel in the longitudinal and lateral directions, it is best to choose two flat square membranes: one membrane has the stress-strain law Eq. (8) and another one is obtained by a 90° rotation of the previous one. Stretching these membranes to a deformation $e_{11} = e$ and $e_{22} = 0$, where e is a small quantity, we see that a larger longitudinal Lagrangian stress s_1 is required on the first one than that on the second one if the inequality $k_{11} > k_{22}$ is true. Therefore it is proper to say that a vessel behaves more rigidly in the longitudinal direction than in the lateral direction, if the elastic constants k_{11} and k_{22} of the vessel satisfy the inequality $k_{11} > k_{22}$.

The distensibility tests of the carotid arteries Nos. 8 and 9 were done to evaluate these elastic constants at several sets of $(\lambda_1, \bar{\lambda}_2)$. Test results are presented in Tables 1 and 2 and in Figs. 16 and 17. Note the overall increases of slope $\partial s_1/\partial \lambda_1$ and $\partial s_2/\partial \bar{\lambda}_1$ as $\bar{\lambda}_2$ increases from 0.9 to 1.0 and then to 1.1 in the longitudinal stretching test (Fig. 16). Similar characteristics are also seen in Fig. 17 for the lateral distensibility test. The computed elastic constants of the carotid arteries Nos. 8 and 9 are presented in Table 7. A smoothing technique on the stress-strain curves is used in measuring their slopes at points of a specific set of extension ratios. One can see that these two arteries behave more rigidly in the longitudinal direction than in the lateral direction in the neighborhood of the natural state. Table 7 also presents the elastic constants for other carotid arteries, jugular veins, mesenteries and femoral arteries.

One can also see that the feature, the tested vessels behaving more rigidly in the longitudinal direction, is true at certain points on the $\lambda_1 - \bar{\lambda}_2$ plane and that their elastic constants are of the same order of magnitude, except that for three jugular veins out of four they have a very small k_{22}.

C. Repeated-Strain Test

In this sub-section we shall discuss qualitatively some of the interesting aspects observed in the repeated-strain test. This test is designed to investigate the dynamic response of vessels at low frequencies.

When the carotid artery No. 10 was stretched longitudinally between fixed limits at a frequency of 0.2 cycles per minute, we observed a substantial decrease in stress from the first cycle to the third one (Fig. 11). This test consisted of five cycles. The largest decrease occurred in the first cycle and the fourth and the fifth repeated the result of the third one. When we repeated the repeated-strain test after about a five minute pause, the change in stress was much less significant than in the previous test. The fact that the decrease in stress after the vessel has been stretched for several times was also observed in the longitudinal stretching test as shown in Fig. 8. One sees that the second loading curve is lower than the first one for large extension ratios while the third one repeated the second one. Comparable phenomena have been recorded in experiments on repeated-inflation tests of large blood vessels

(Bergel, Ref. 1) and on repeated-strain tests of steel specimens* (Bailey, Ref. 6). The features, the stiffening (higher tangent modulus) at unloading and the decrease in stress as cycling proceeds, are rather similar to the plasticity of metals. When the vessels were cut out from the animal body, they contracted to about two thirds of their natural lengths. This abnormal contraction has been regarded as the principal cause for why a repeatable stress-strain curve or a steady-state response in stretching or in inflation could be achieved only after several cycles have been tested (Figs. 8 and 11). Thus it is useful if one can construct the mechanism of this abnormal contraction on the mechanical properties of blood vessels, e.g. a model with certain elastic-plastic properties of metals. For a "standard linear" model (a viscoelastic material, cf. Appendix 1) the phenomenon of the stress decrease could also be observed as it is suddenly being stretched sinusoidally. However, a change of the initial condition will result in a stress increase. For the three carotid arteries tested the initial conditions of the suddenly imposed sinusoidal excitation were quite arbitrary, but the stress level was always decreased. Thus the decrease in stress of the vessels might not be interpreted as a viscoelastic response.

After two or three cycles of repeated stretchings, the response reaches a steady state in the sense that the hysteresis loops overlap each other for several subsequent runs. Fig. 12 shows the steady-state response of the carotid artery No. 11.

---

* In his experiments, the strain limits were 0 and 6×10^{-3}. The bending moment, applied on the specimen for the first loading cycle was increased from 0 to 120 ft. lb. However, the extrema of the bending moment dropped to -40 and 110 ft. lb. for the third loading cycle. In our test the stress level of the blood vessels is positive.

All loops were run at a frequency of 0.2 cycles per minute. Note that the loading curve of the large hysteresis loop is quite linear. On the other hand, one can see that the slope $\partial s_1/\partial \lambda_1$ could be a nonlinear function of the driven amplitude, the one with a smaller amplitude has a higher slope. This result differs with that of the Voigt model (a linear viscoelastic material, cf. Appendix 1) of which the force-displacement loops would look like ellipses with parallel major and minor axes when the model is driven at different amplitudes or frequencies. Similar results were observed for a rubber tube as shown in Fig. 7.

Steady state responses of the carotid artery No. 12 stretched at different frequencies are shown in Fig. 13. The last small loop (the one on the right hand side of the figure) of the third test had been driven at frequencies 1.1 and 7.1 cycles per minute. No differences on their force readings were observed. On the other hand, when the vessel was repeatedly stretched between large limits at frequencies of 0.2 and 1.1 cycles per minute, the loops cross each other at large extension ratios.

In Bergel's dynamic tests (Ref. 7), he distended the vessels laterally at frequencies from 2 to 18 cycles per second with a mean pressure of 100 mm Hg. The radius changes were less than 3 percent for a pressure change of $\pm$ 5$\sim$10 mm Hg. He showed that the dynamic Young's modulus of the tested carotid arteries changed insignificantly in the above frequency range and its value was about 1.6 times the static Young's modulus which was measured at an internal pressure of 100 mm Hg. In his static test, being similar to our lateral distensibility test, the diameter of the carotid artery

was increased step by step from 0.24 to 0.45 cm. Based on our qualitative result of the carotid arteries tested in the repeated-strain test, one realizes that the oscillation amplitude could be an important nonlinear factor in explaining why the dynamic Young's modulus is larger than the static one as shown in Bergel's test.

5. CONCLUSION

The experimental results of the extensibility test show that the vessel has a smaller tangential modulus at small extension ratios and a higher one at larger extension ratios in both the latitudinal and longitudinal directions. This characteristic differs from ordinary rubber-like materials. In discussing the response of the vessel in the neighborhood of the natural state to infinitesimal deformations, we found that the vessels tested behaved more rigidly in the longitudinal direction than in the latitudinal direction.

Results of the repeated-strain test demonstrate that the dynamic extensibility of the vessel depends more strongly on the driven amplitude than on the driven frequency and the first may be an important factor in explaining the increase in the dynamic modulus over the static one.

REFERENCES

1. Bergel, D. H., "The Static Elastic Properties of the Arterial Wall", J. Physiol., 156, p. 445, 1961.
2. McDonald, D. A., Blood Flow in Arteries, Baltimore, Williams and Wilkins, 1960.
3. Lawton, R. I., "Measurements on the Elasticity and Damping of Isolated Aortic Strips of the Dog", Circulation Res., 3, p. 403, 1955.
4. Burton, A. C., "Relation of Structure to Function of the Tissues of the Wall of Blood Vessels", Physiol. Rev., 34, p. 619, 1954.
5. Fenn, W. O., "Changes in Length of Blood Vessels on Inflation", In Tissue Elasticity, ed. by J. W. Remington, Am. Physiol. Soc., Washington D. C., p. 154, 1957.
6. Bailey, R. W., "Usefulness and Role of Repeated Strain Testing as an Aid to Engineering Design and Practice", International Conference on Fatigue of Metals, Sponsored by the Institute of Mechanical Engineers in co-operation with the American Society of Mechanical Engineers, London and New York, Session 2, Paper 14, 1956.
7. Bergel, D. H., "The Dynamic Elastic Properties of the Arterial Wall", J. Physiol. Soc., 156, p. 458, 1961.
8. Fung, Y. C., Foundations of Solid Mechanics, Prentice-Hall, Englewood Cliffs, New Jersey, 1965.
9. Fung, Y. C., B. W. Zweifach, M. Intagalietta, "Elastic Environment of the Capillary Bed", Circulation Res., (In press).

APPENDIX 1

RELAXATION OF A STANDARD LINEAR MODEL

The standard linear model is (1) a combination of a Voigt Model (a linear spring and a dashpot being parallelly connected) and a spring connected in series, or (2) a parallel combination of a Maxwell model (a spring and a dashpot being connected in series) and a spring. A dashpot behaves as a massless piston moving in a viscous fluid. A sudden change of the deflection of these models

$$\begin{aligned} u &= 0 \qquad && t < 0 \\ &= D \sin \omega t \qquad && t > 0 \quad , \end{aligned} \tag{A.1}$$

where t is the time, ω is the frequency, and D is a constant, will produce the following load

$$F = \frac{E_R D}{1 + \tau_\epsilon^2 \omega^2} \left[(\tau_\epsilon - \tau_\sigma)\, e^{-t/\tau_\epsilon} - \omega(\tau_\epsilon - \tau_\sigma)\cos \omega t + (1 + \tau_\epsilon \tau_\sigma \omega^2) \sin \omega t \right] \tag{A.2}$$

where E_R, τ_ϵ , τ_σ are functions of the spring constants and the coefficient of viscosity of the dashpot. In the above formula, the first term in the bracket is a term of exponential relaxation. If $D(\tau_\epsilon - \tau_\sigma) > 0$ ($(\tau_\epsilon - \tau_\sigma) > 0$ for model (1), < 0 for model (2), and = 0 for Voigt model) hysteresis loops of the model in repeated-strain test decay exponentially to a lower limit. Otherwise, the loops tend to a higher limit. One can see that the decrease or increase in the stress of the standard linear models depends on the sign of D, and hence on the initial condition. More detail on the governing equations of viscoelastic materials can be found in Fung, Foundations of Solid Mechanics, Chapter 1.

TABLE 1

Measured values of the Lagrangian stresses s_1 and βs_2 in the longitudinal stretching tests.

Carotid Artery 1
$\bar{\lambda}_2 = 1.0$

λ_1	s_1	βs_2
1.33	.51	.35
1.39	.75	.40
1.42	.83	.43
1.45	1.06	.49
1.48	1.68	.61
1.495	2.27	.71
1.51	3.301	.84

Carotid Artery 2
$\bar{\lambda}_2 = 1.0$

λ_1	s_1	βs_2
1.5	.36	.11
1.58	.54	.13
1.65	.73	.17
1.69	.93	.24
1.72	1.45	.32
1.74	2.22	.39

Carotid Artery 3
$\bar{\lambda}_2 = 1.0$

λ_1	s_1	βs_2
1.74	0.65	.27
1.79	0.85	.35
1.84	1.28	.46
1.87	1.64	.51
1.90	2.19	.75
1.92	2.90	.93

Carotid Artery 4
$\bar{\lambda}_2 = 1.0$

λ_1	s_1	βs_2
1.59	0.84	0.71
1.64	1.04	0.82
1.67	1.21	0.91
1.70	1.49	1.04
1.72	1.88	1.20
1.74	2.82	1.41
1.75	3.45	1.5

Carotid Artery 5

$\bar{\lambda}_2 = 1.0$

λ_1	s_1	βs_2
1.60	.79	.64
1.68	1.06	.75
1.74	1.44	.92
1.78	1.86	1.04
1.81	2.48	1.29
1.83	3.13	1.52

Carotid Artery 6

$\bar{\lambda}_2 = 1.0$

λ_1	s_1	βs_2
1.67	.61	.59
1.73	.80	.67
1.78	.91	.74
1.82	1.24	.78
1.85	1.77	.87
1.87	2.83	1.09

Carotid Artery 7

$\bar{\lambda}_2 = 1.0$

λ_1	s_1	βs_2
1.69	.66	.76
1.75	.88	.85
1.79	1.19	1.07
1.82	1.90	1.34
1.84	2.91	1.60
1.85	3.52	1.71
1.86	4.57	1.98

Carotid Artery 8

λ_1	s_1	βs_2
$\bar{\lambda}_2 = 0.9$		
1.575	.88	.13
1.600	1.09	.16
1.626	1.31	.18
1.651	1.55	.20
1.675	1.85	.22
1.702	2.15	.24
$\bar{\lambda}_2 = 1.0$		
1.575	.90	.39
1.600	1.10	.43
1.626	1.35	.46
1.651	1.63	.49
1.675	1.96	.53
1.702	2.39	.56
1.727	3.24	.68
$\bar{\lambda}_2 = 1.1$		
1.575	.94	1.01
1.600	1.20	1.05
1.626	1.48	1.12
1.651	1.86	1.19
1.675	2.42	1.25
1.702	3.16	1.39

Carotid Artery 9

λ_1	s_1	βs_2
$\bar{\lambda}_2 = 0.9$		
1.62	.39	.06
1.66	.58	.08
1.70	.75	.11
1.73	.88	.12
1.75	1.02	.13
1.77	1.14	.14
$\bar{\lambda}_2 = 1.0$		
1.62	.39	.16
1.66	.57	.19
1.70	.74	.20
1.73	.90	.23
1.75	1.08	.29
1.77	1.29	.33
$\bar{\lambda}_2 = 1.1$		
1.62	.44	.33
1.66	.61	.37
1.70	.82	.41
1.73	.99	.46
1.75	1.20	.54
1.77	1.50	.68

Jugular Vein 13

$\bar{\lambda}_2 = 1.0$

λ_1	s_1	βs_2
1.80	.30	.39
1.90	.43	.32
1.98	.59	.35
2.04	.77	.40
2.08	1.32	.51
2.11	2.62	.78

Jugular Vein 14

$\bar{\lambda}_2 = 1.0$

λ_1	s_1	βs_2
1.95	.12	.11
2.05	.18	.12
2.15	.26	.15
2.23	.34	.19
2.29	.45	.22
2.35	.61	.26

Jugular Vein 15

$\bar{\lambda}_2 = 1.0$

λ_1	s_1	βs_2
1.66	.23	.06
1.69	.31	.08
1.72	.39	.10
1.75	.47	.14
1.77	.53	.16
1.785	.62	.24

Jugular Vein 16

$\bar{\lambda}_2 = 1.0$

λ_1	s_1	βs_2
1.76	.20	.02
1.82	.33	.03
1.86	.43	.04
1.90	.59	.05
1.92	.78	.08
1.93	.93	.11

Mesentery 17
$\bar{\lambda}_2 = 1.0$

$\bar{\lambda}_1$	s_1	s_2
0.87	1.40	0.34
0.91	2.01	0.51
0.95	2.49	0.63
0.99	3.08	0.83
1.02	3.92	1.11
1.05	5.17	1.40

Mesentery 18
$\bar{\lambda}_2 = 1.0$

$\bar{\lambda}_1$	s_1	s_2
0.91	.39	.18
0.95	.64	.65
0.99	.91	1.00
1.03	1.15	1.54
1.06	1.31	1.88
1.09	1.46	1.98

Femoral Artery 19
$\bar{\lambda}_2 = 1.0$

$\bar{\lambda}_1$	s_1	s_2
0.85	.51	0.44
o.89	1.35	.6 2
0.93	2.16	.79
0.97	2.99	.99
1.00	3.73	1.09

Femoral Artery 20
$\bar{\lambda}_2 = 1.0$

$\bar{\lambda}_1$	s_1	s_2
0.88	.95	0.2
0.94	1. 51	0.23
1.00	2.12	.34
1.06	2.68	.47
1.10	3.08	.64
1.14	3.47	.79

TABLE 2

Measured values of Lagrangian stresses s_1 and βs_2 in the lateral distensibility tests.

Carotid Artery 1 $\lambda_1 = 1.465$			Carotid Artery 2 $\lambda_1 = 1.64$		
$\bar{\lambda}_2$	s_1	βs_2	$\bar{\lambda}_2$	s_1	βs_2
1.008	1.20	.43	.997	.92	0.27
.920	.78	.23	.859	.83	0.09
.829	.63	.11	.983	.91	0.27
.893	.75	.22	1.132	1.21	0.69
.940	1.04	.39	1.181	1.51	0.99
1.020	1.50	.72	1.219	1.80	1.26
1.148	3.16	1.78	1.250	2.24	1.64
1.208	4.26	2.56	1.264	2.61	2.01
1.235	5.12	3.31	1.281	2.96	2.39
1.265	5.94	4.11	1.309	3.62	3.17
1.238	4.40	2.62	1.320	4.25	3.94
1.188	2.88	1.51	1.316	3.72	3.19
1.124	1.69	.82	1.309	3.12	2.45
1.060	1.09	.44	1.288	2.76	2.05
			1.247	1.96	1.29
			1.184	1.28	0.70
			1.112	1.014	0.41
			1.039	.91	0.27

Carotid Artery 3
$\lambda_1 = 1.86$

$\bar{\lambda}_2$	s_1	βs_2
.993	1.37	.68
.86	1.10	.25
.780	1.03	.12
.865	1.09	.25
.989	1.36	.68
1.099	1.84	1.37
1.135	2.14	1.79
1.156	2.45	2.21
1.177	2.84	2.80
1.199	3.30	3.49
1.227	3.86	4.39
1.206	3.35	3.51
1.195	2.56	2.29
1.170	2.25	1.85
1.152	1.93	1.44
1.106	1.65	1.06
1.164	1.43	.73
1.011	1.25	.51

Carotid Artery 4
$\lambda_1 = 1.65$

$\bar{\lambda}_2$	s_1	βs_2
.997	1.20	.79
.976	1.13	.1
.896	1.07	.43
.822	1.01	.29
.711	.95	.11
.798	1.00	.28
.864	1.05	.41
.916	1.11	.57
.993	1.21	.87
1.045	1.36	1.23
1.063	1.53	1.64
1.080	1.79	2.22
1.105	2.16	2.92
1.125	2.61	3.79
1.122	1.95	2.31
1.108	1.65	1.71
1.087	1.49	1.28
1.000	1.16	0.64

Carotid Artery 5
$\lambda_1 = 1.73$

$\bar{\lambda}_2$	s_1	βs_2
1.00	1.34	.85
.93	1.16	.55
.84	1.07	.35
.78	1.05	.23
.71	1.06	.14
.79	1.07	.28
.90	1.13	.50
.99	1.33	.83
1.05	1.57	1.25
1.09	1.80	1.68
1.12	2.11	2.25
1.16	2.52	3.05
1.19	3.09	4.05
1.18	2.61	3.05
1.16	2.26	2.39
1.13	1.87	1.76
1.08	1.56	1.18
.99	1.28	.68

Carotid Artery 6
$\lambda_1 = 1.71$

$\bar{\lambda}_2$	s_1	βs_2
.993	.73	.61
.927	.67	.45
.815	.57	.19
.787	.55	.15
.845	.58	.27
.935	.66	.48
1.000	.77	.66
1.061	.80	.88
1.135	.94	1.30
1.190	1.16	1.92
1.215	1.50	2.76
1.257	2.21	4.09
1.235	1.50	2.52
1.215	1.24	1.87
1.168	1.03	1.31
1.125	.85	.95
1.015	.71	.58

Carotid Artery 7

$\lambda_1 = 1.77$

$\bar{\lambda}_2$	s_1	βs_2
1.004	.77	.85
.860	.59	.44
.796	.55	.34
.738	.51	.25
.652	..48	.11
.731	.52	.24
.792	.56	.36
.867	.62	.53
1.011	.82	.96
1.057	1.67	2.19
1.090	2.55	3.38
1.118	3.23	4.30
1.111	2.71	3.45
1.090	1.89	2.26
1.068	1.24	1.46
1.004	.79	.83

Carotid Artery 8

$\lambda_1 = 1.577$

$\bar{\lambda}_2$	s_1	βs_2
.94	.78	.23
.98	.82	.36
1.01	.85	.44
1.04	.87	.52
1.07	.93	.71
1.10	.95	.83

$\lambda_1 = 1.654$

.88	1.55	.21
.93	1.63	.34
.96	1.73	.50
1.01	1.92	.70
1.07	2.28	1.06

Carotid Artery 9

$\lambda_1 = 1.555$

$\bar{\lambda}_2$	s_1	s_2
.911	.47	.03
.975	.46	.08
1.025	.53	.16
1.085	.56	.27
1.127	.60	.37
1.169	.66	.52
1.212	.74	.71

$\lambda_1 = 1.71$

.898	.82	.086
.958	.86	.16
1.008	.91	.28
1.051	.98	.40
1.102	1.06	.53

Jugular Vein 13

$\lambda_1 = 1.99$

$\bar{\lambda}_2$	s_1	s_2
.949	1.83	.21
.885	1.77	.17
.806	1.73	.13
.719	1.70	.11
.640	1.68	.08
.561	1.65	.03
.712	1.69	.08
.838	1.74	.14
.933	1.82	.20
1.000	2.10	.42
1.067	2.66	.88
1.138	3.96	2.00
1.146	4.71	2.69
1.166	5.55	3.41
1.194	6.44	4.20
1.107	5.67	3.50
1.180	4.89	2.80
1.158	3.20	1.36
1.123	2.36	.66

Jugular Vein 14

$\lambda_1 = 2.08$

$\bar{\lambda}_2$	s_1	βs_2
.990	.15	.05
.893	.14	.04
.784	.14	.03
.704	.13	.01
.811	.13	.02
.924	.14	.03
.993	.15	.04
1.083	.16	.06
1.150	.17	.07
1.256	.21	.11
1.302	.26	.19
1.369	.57	.52
1.336	.29	.20
1.302	.22	.12
1.143	.17	.06
0.990	.15	.04

Jugular Vein 15

$\lambda_1 = 1.72$

$\bar{\lambda}_2$	s_1	βs_2
1.000	.36	.05
.865	.35	.02
.777	.34	.01
.688	.39	.00
.806	.35	.02
.941	.36	.04
1.029	.37	.08
1.094	.41	.17
1.147	.49	.32
1.191	.66	.65
1.182	.52	.34
1.150	.44	.18
1.118	.40	.10
1.000	.36	.39

Jugular Vein 16

$\lambda_1 = 1.87$

$\bar{\lambda}_2$	s_1	βs_2
1.000	.46	.04
.926	.45	.02
.852	.45	.01
.945	.45	.01
.926	.44	.03
1.000	.47	.04
1.063	.48	.06
1.141	.49	.09
1.208	.52	.12
1.264	.57	.17
1.317	.64	.24
1.285	.54	.13
1.211	.49	.07
1.141	.48	.06
1.064	.47	.04
.989	.46	.03

Mesentery 17
$\bar{\lambda}_1 = 1.0$

$\bar{\lambda}_2$	s_1	s_2
.854	2.88	0.16
.888	2.96	0.29
1.003	3.19	0.82
1.038	3.34	1.04
1.061	3.51	1.51

Mesentery 18
$\bar{\lambda}_1 = 0.964$

$\bar{\lambda}_2$	s_1	s_2
.969	0.93	0.40
1.008	0.89	0.62
1.022	0.89	0.70
1.039	0.91	0.92

Femoral Artery 19
$\bar{\lambda}_1 = 0.907$

$\bar{\lambda}_2$	s_1	s_2
.963	2.26	0.28
1.011	2.47	0.73
1.058	2.66	1.06
1.095	3.00	1.88

Femoral Artery 20
$\bar{\lambda}_1 = 0.989$

$\bar{\lambda}_2$	s_1	s_2
.936	2.73	0.11
.963	2.80	0.32
.982	2.86	0.47
1.015	2.94	0.83
1.038	2.96	0.88

TABLE 3

Physical dimensions of the carotid arteries and jugular veins.

Number*	λ_{1N}	d_N (cm)	d_A (cm)	A_o (cm^2)	h_N (cm)	d_N/h_N
			Carotid Arteries			
L.1	1.47		0.506	0.080		
R.2	1.64	0.40	0.462	0.092	0.05	8.0
R.3	1.86		0.452	0.084		
L.4	1.65	0.34	0.460	0.069	0.045	7.6
R.5	1.73	0.38	0.454	0.079	0.044	12.0
L.6	1.71	0.36	0.442	0.076	0.045	8.0
R.7	1.77	0.34	0.442	0.068	0.041	8.3
L.8	1.65	0.44	0.438	0.059	0.030	15.0
R.9	1.71	0.38	0.378	0.065	0.036	11.0
L.10	1.67	0.32		0.056	0.038	8.4
R.11	1.78	0.52		0.068	0.024	22.0
L.12	1.61	0.42		0.052	0.027	16.0
			Jugular Veins			
R.13	1.96	0.34	0.632	0.071	0.048	7.1
L.14	1.68	0.84	0.754	0.21	0.06	14.0
R.15	1.72	0.50	0.524	0.06	0.026	19.0
R.16	1.87	0.36	0.446	0.078	0.041	8.8

* L. signifies left and R. signifies right.

TABLE 4

Undeformed physical dimensions of the carotid arteries Nos. 8, 9, 11 and 12.

Number**	d_o* (cm)	h_o (cm)	d_o/h_o	
L.8	0.32	0.08	4.0	1.23
R.9	0.30	0.04	2.7	1.96
R.11	0.32	0.096	3.3	1.42
R.12	0.34	0.054	6.3	1.04

* Measured by photographic method.

** L. signifies left and R. signifies right.

TABLE 5

Physical dimensions of femoral arteries and mesenteries.

Number*	d_A (cm)	A_N (cm^2)	h_A (cm)	d_A/h_A
M 17	0.138	0.0053	0.014	10.
M 18	0.102	0.0023	0.008	13.
FA 19	0.151	0.0039	0.009	18.
FA 20	0.173	0.0056	0.011	16.

* FA signifies femoral artery and M signifies mesenteries.

TABLE 6

Weight of the experimental dogs.

Specimen	Weight of the dog tested
Carotid artery 1, Carotid artery 2	50 lbs.
Jugular vein 9	
Carotid artery 3	65 lbs.
Carotid artery 4, Carotid artery 5	45 lbs.
Carotid artery 6, Carotid artery 7	45 lbs.
Jugular vein 14	
Carotid artery 8, Carotid artery 9	50 lbs.
Carotid artery 10	40 lbs.
Carotid artery 11, Carotid artery 12	54 lbs.
Jugular vein 15	39 lbs.
Jugular vein 16	40 lbs.
Mesentery 17, Mesentery 18	50 lbs.
Femoral artery 19, Femoral artery 20	45 lbs.

TABLE 7

Measured values of the elastic constants.*

Number**	λ_1***	$\bar{\lambda}_2$	k_{11}	k_{21}	k_{12}	k_{22}
C.A. 8	1.577	1.0	14.	1.8	0.9	2.5
	1.577	1.1	17.	3.7	0.8	3.6
	1.654	0.9	19.	2.1	1.7	2.1
	1.654	1.0	21.	1.9	3.4	3.4
C.A. 9	1.71	0.9	11.	1.4	0.2	0.4
	1.71	1.0	12.	1.4	0.5	1.2
	1.71	1.1	13.	2.6	1.2	1.9
C.A.1	1.465	1.0	15.	5.3	7.1	5.3
C.A.2	1.64	1.0	4.1	2.7	1.2	1.0
C.A.3	1.86	1.0	22.	7.8	3.6	4.8
C.A.4	1.65	1.0	9.9	5.8	3.3	3.2
C.A.5	1.73	1.0	12.	5.2	3.0	5.6
C.A.6	1.71	1.0	4.6	2.2	0.9	2.5
C.A.7	1.77	1.0	12.	7.7	2.4	3.7
J.V.13	1.99	1.0	4.2	1.0	6.4	4.3
J.V.14	2.09	1.0	2.1	0.8	0.1	0.2
J.V.15	1.72	1.0	4.5	1.4	0.1	0.3
J.V.16	1.87	1.0	6.2	0.6	0.1	0.2
M. 17	1.0	1.0	22.	1.1	2.1	4.4
M. 18	0.96	1.0	5.9	11.	2.4	3.2
F.A.19	0.91	1.0	19.	4.0	2.3	5.3
F.A.20	0.99	1.0	9.7	2.5	1.5	7.2

* All constants have the dimension 10^6 dyne/cm^2 (cf. Eq. (9)).

** C.A., carotid artery. J.V., jugular vein. F.A., femoral artery. M., mesentery.

*** For mesenteries and femoral arteries, λ_1 should read as $\bar{\lambda}_1$.

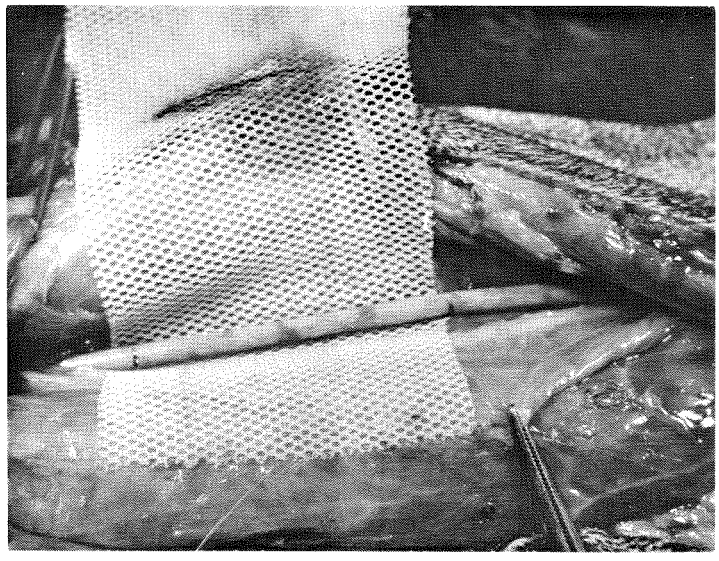

Fig. 1

Carotid artery No. 8 in situ.

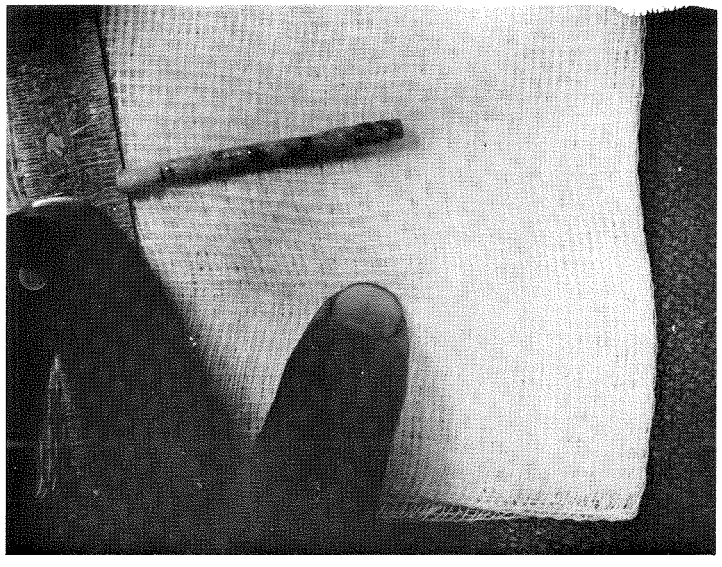

Fig. 2

Excised carotid artery No. 8.

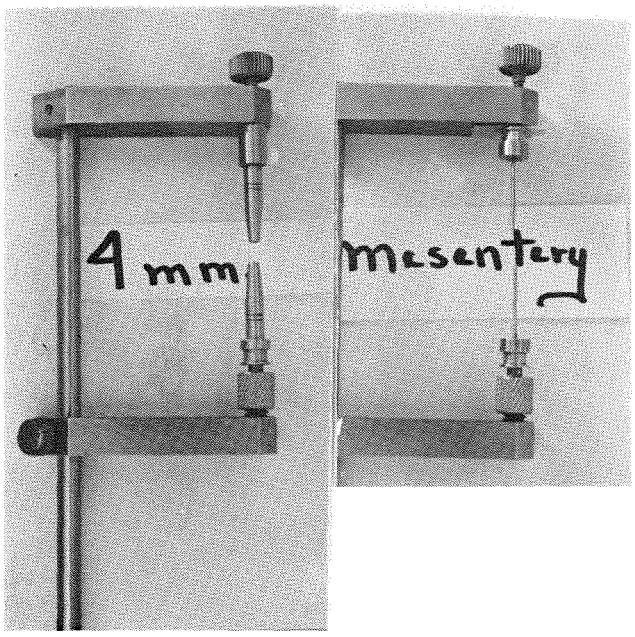

Fig. 3

Mounting device, 4 mm cones (carotid arteries) and 1 mm cones (mesenteries)

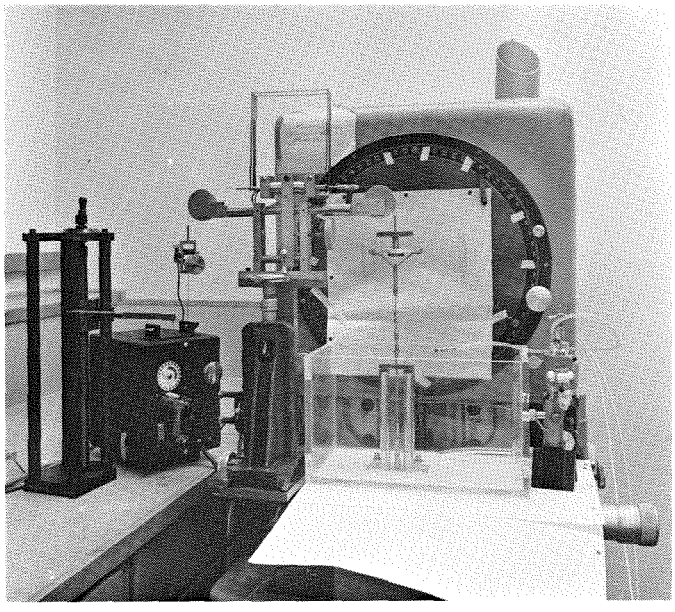

Fig. 4

Testing Appartus

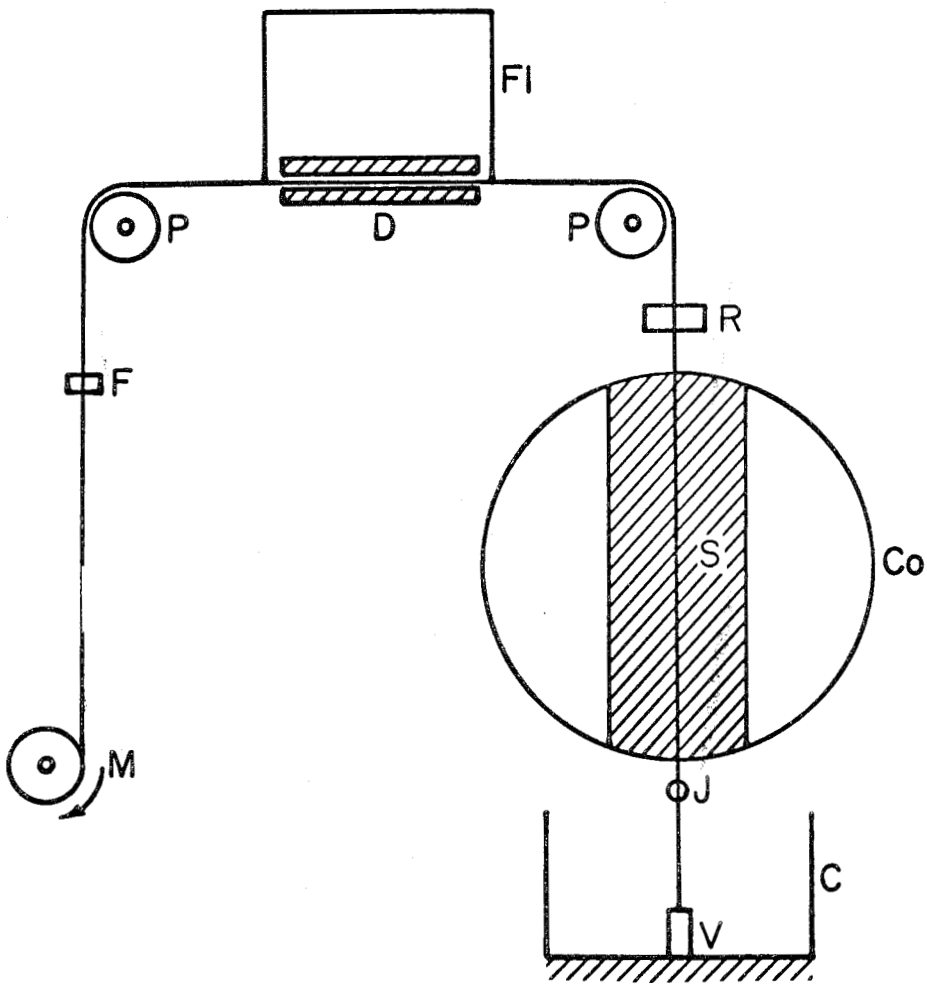

Fig. 5 A diagrammatical set-up of the testing apparatus. C = chamber, CO = comparator screen, D = differential transformer, F = force transducer, Fl = flexure, J = joint, M = motor, P = pulley, R = joint which is free rotate, S = shadow of the vessel, V = vessel.

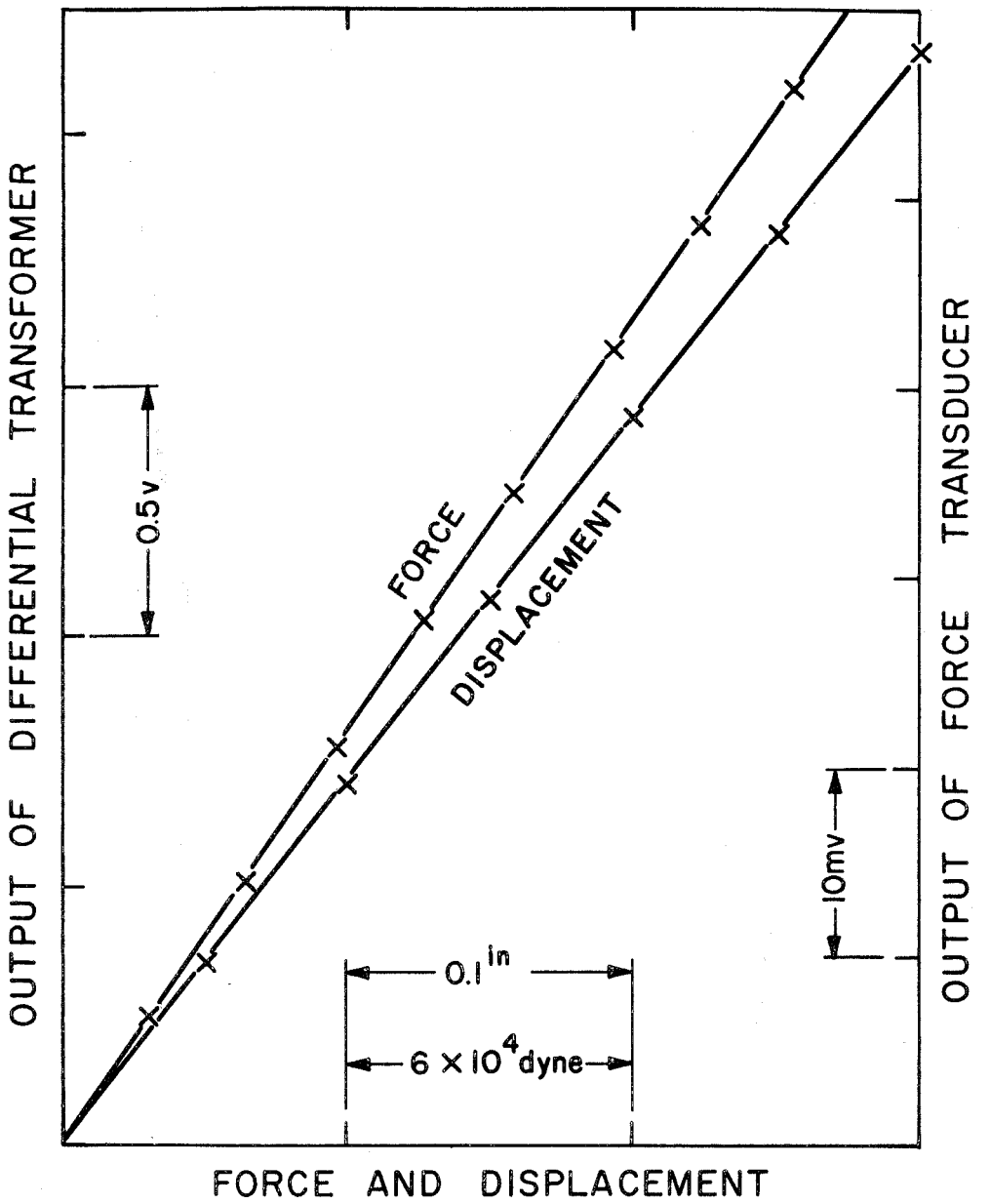

Fig. 6 Static calibration of the outputs of the force transducer (amplified 10^3 times by a Leed-Northrop Amplifier) and the differential transformer (displacement), both of which were monitored on the Moseley plotter. The force transducer was calibrated stepwise by adding weight chips, and the differential transformer was calibrated stepwise by a micro-comparator. No hysteresis was recorded.

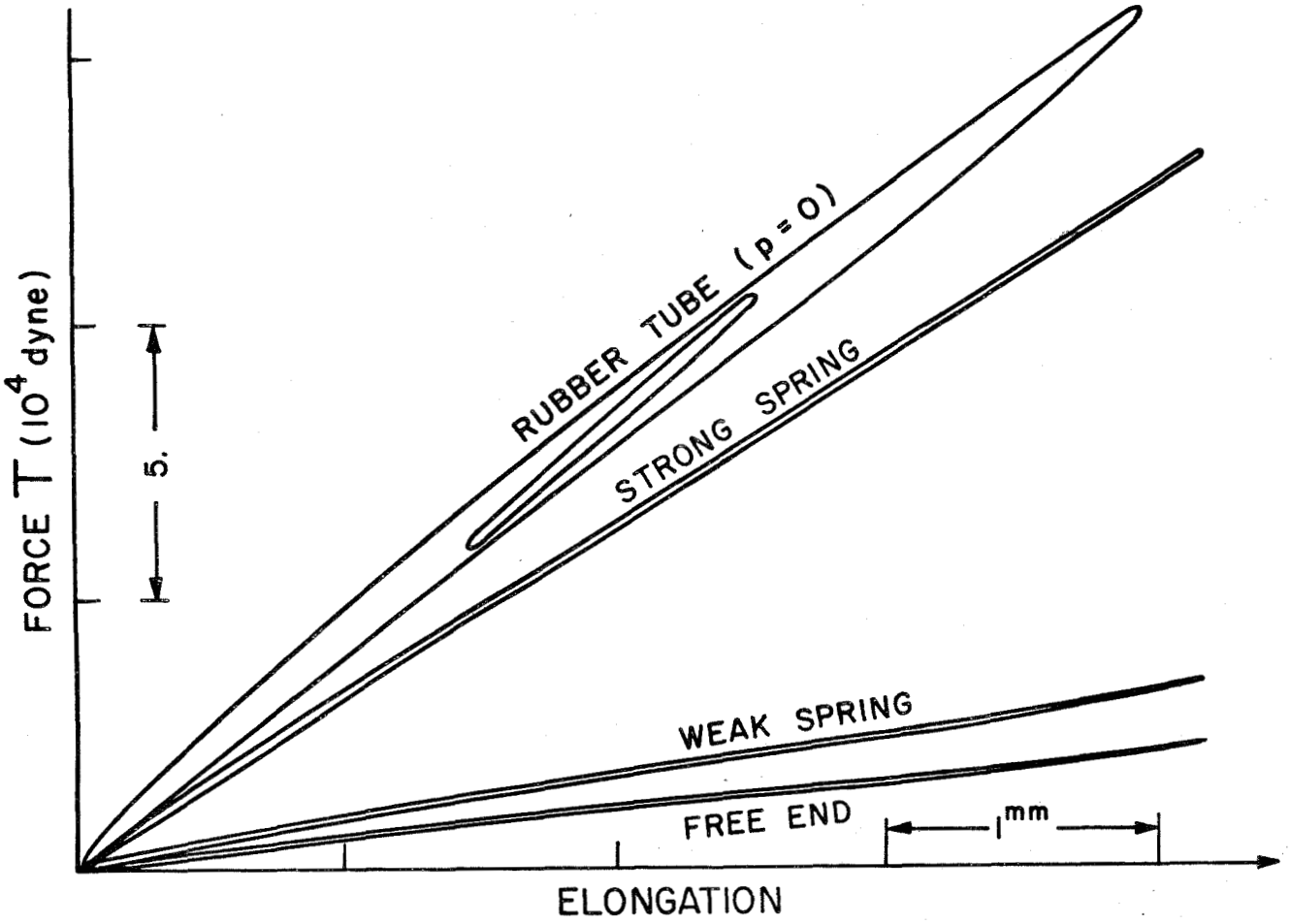

Fig. 7 Hysteresis loops (included the elasticity of the testing apparatus) of springs and a rubber tube in repeated-strain tests. This serves the purpose of calibrating the force-displacement system by those of known elastic properties. The elasticity of the testing apparatus is represented by the free-end plot.

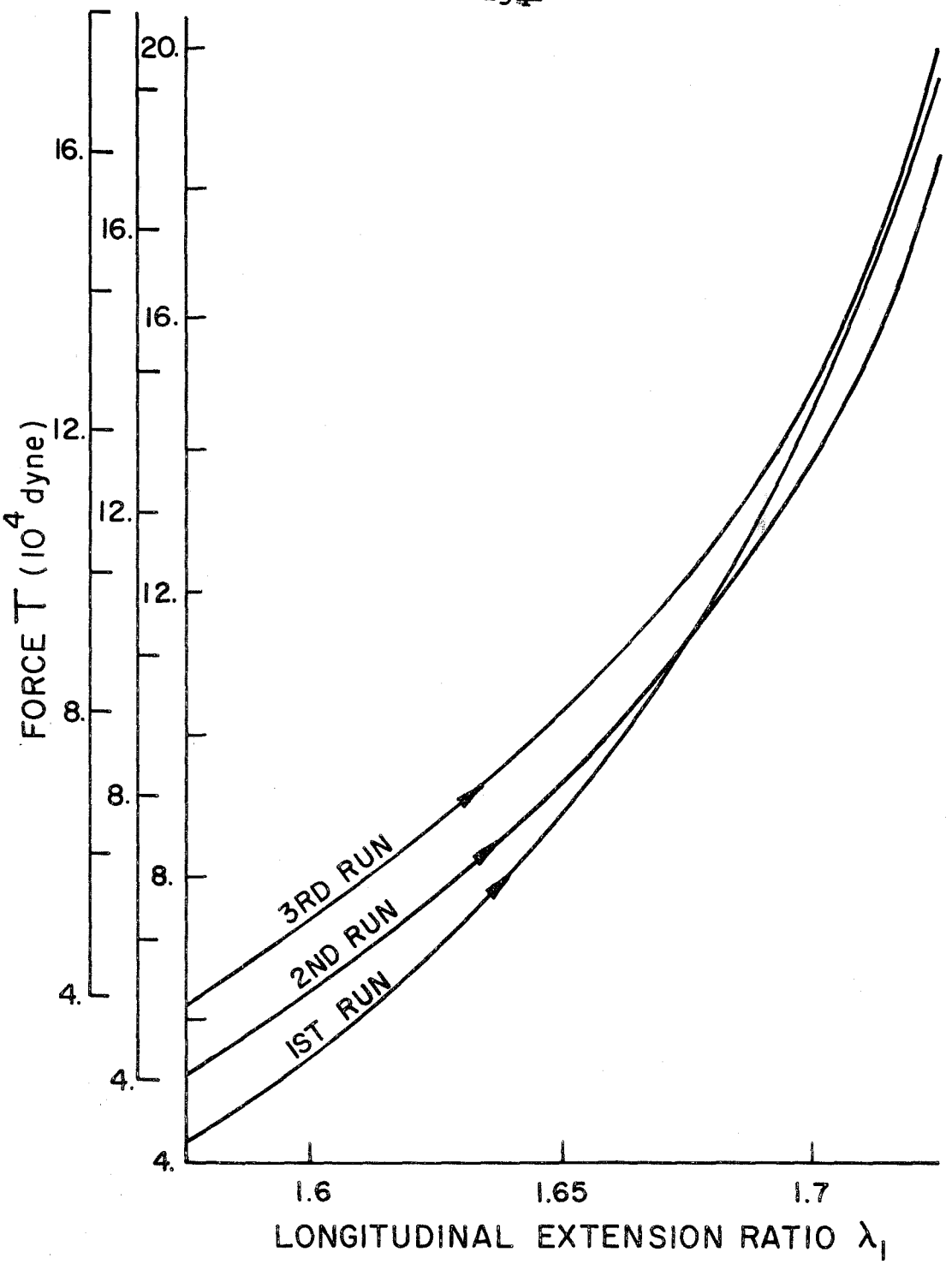

Fig. 8 Force vs. longitudinal extension ratio of the carotid artery No. 8. These are the force-displacement curves monitored on the Moseley X-Y plotter. For clarity the vertical axis is shifted for each run.

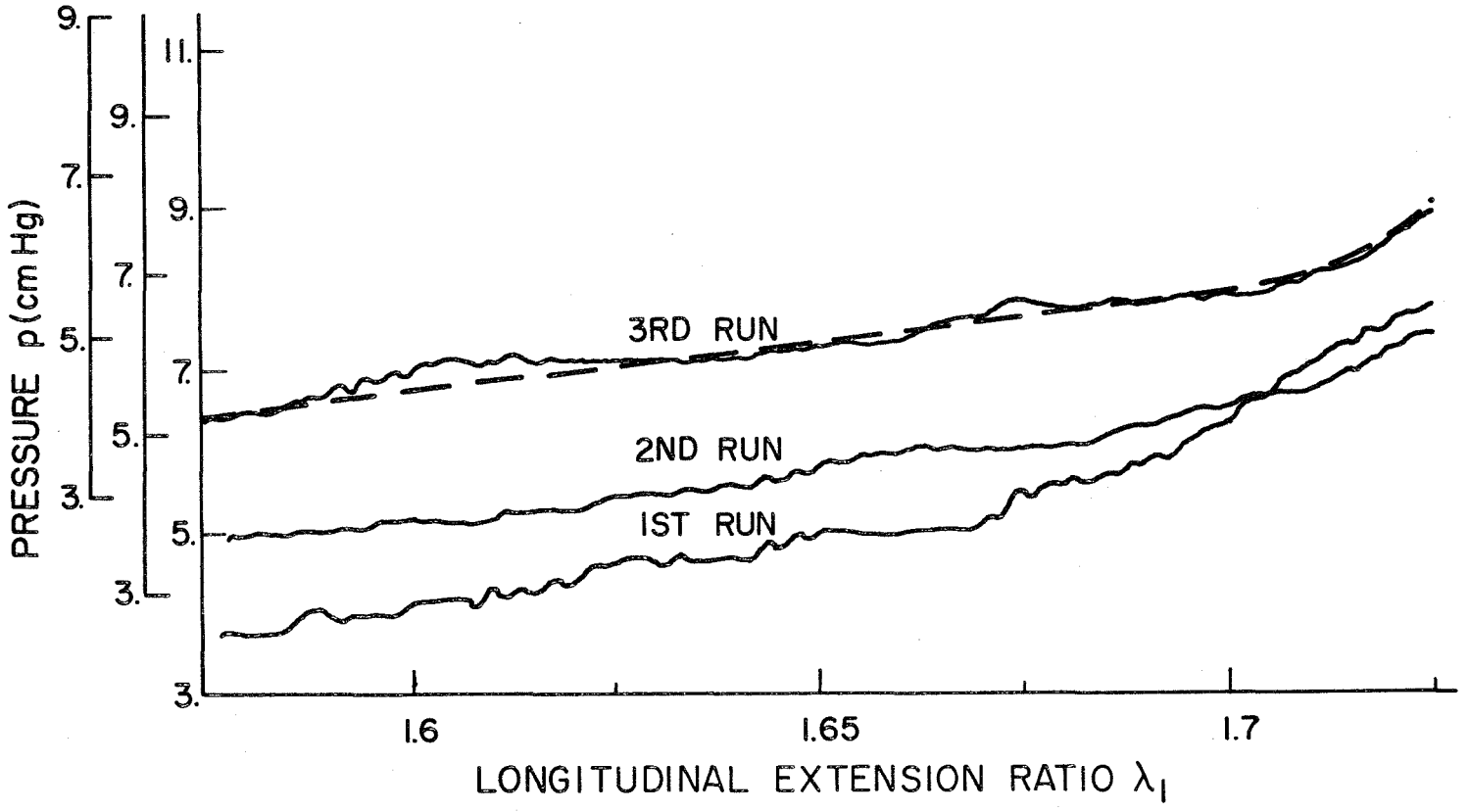

Fig. 9 Pressure vs. longitudinal extension ratio of the carotid artery No. 8. Pressure re ıgs monitored on the Moseley plotter are shown by the solid lines. A smoothing tech ıe (the broken line) is used on the third reading for data reduction. For clarity t' ertical axis is shifted for each run.

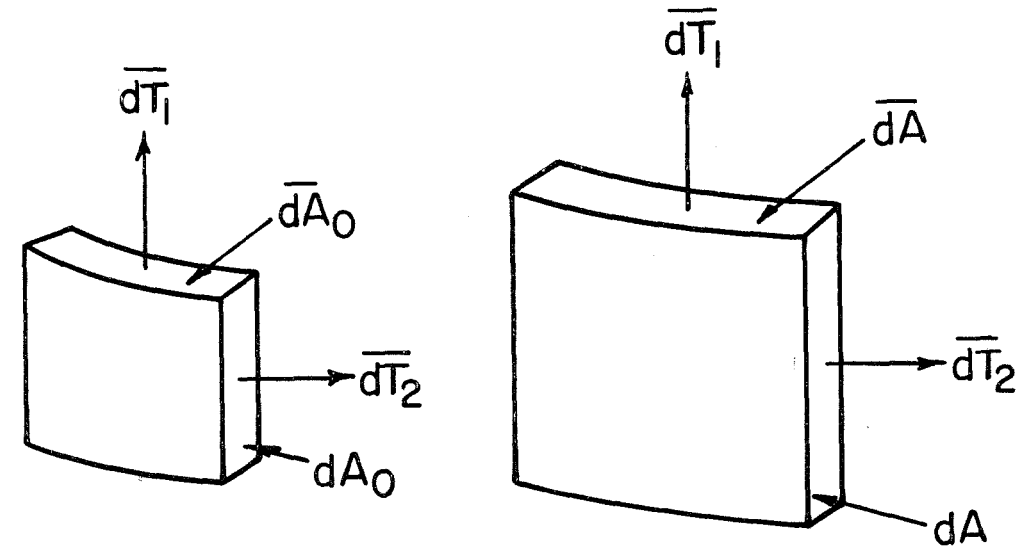

Fig. 10 The correspondence of force vectors in defining Lagrangian stresses. dT_1 and dT_2 are parallelly translated from the deformed state to the corresponding surfaces of the undeformed state.

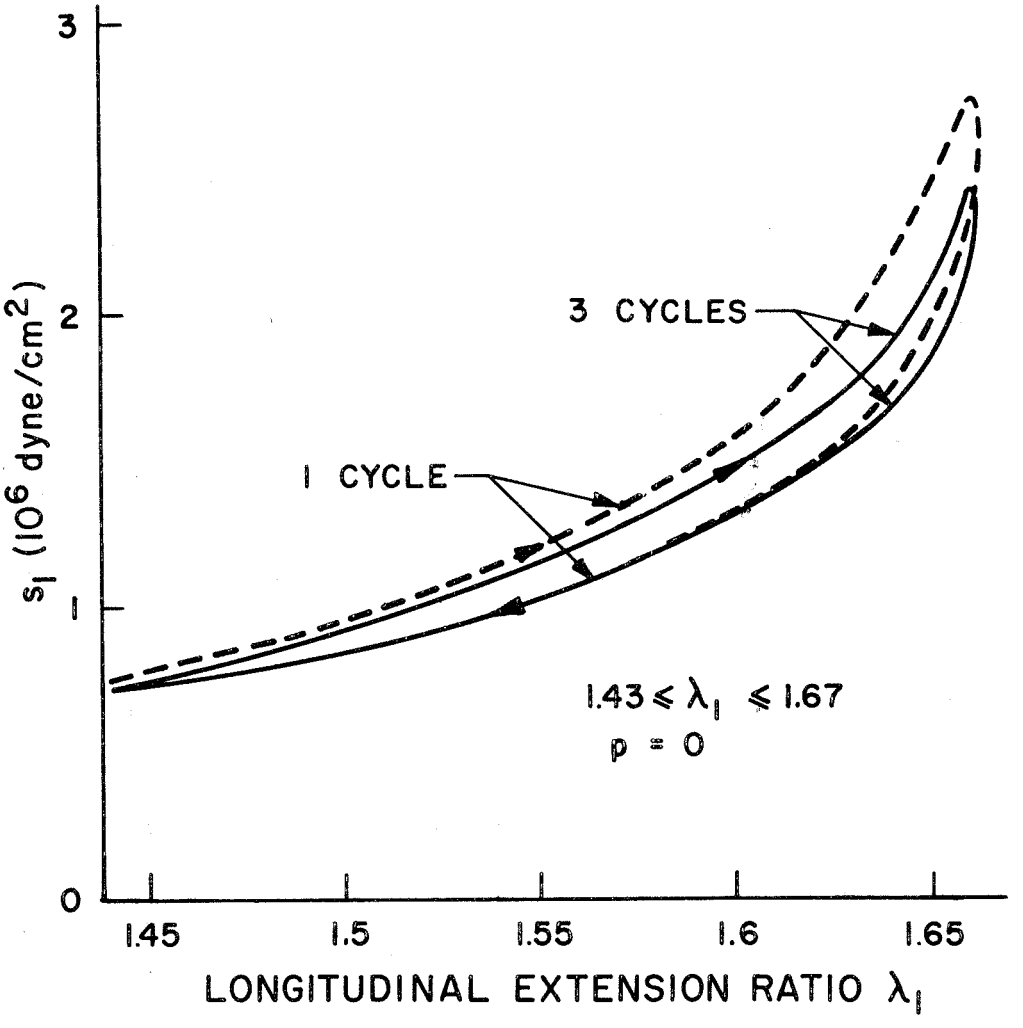

Fig. 11 Hysteresis loops of the repeated-strain test of the carotid artery No. 10. These loops are direct readings on the Moseley X-Y plotter.

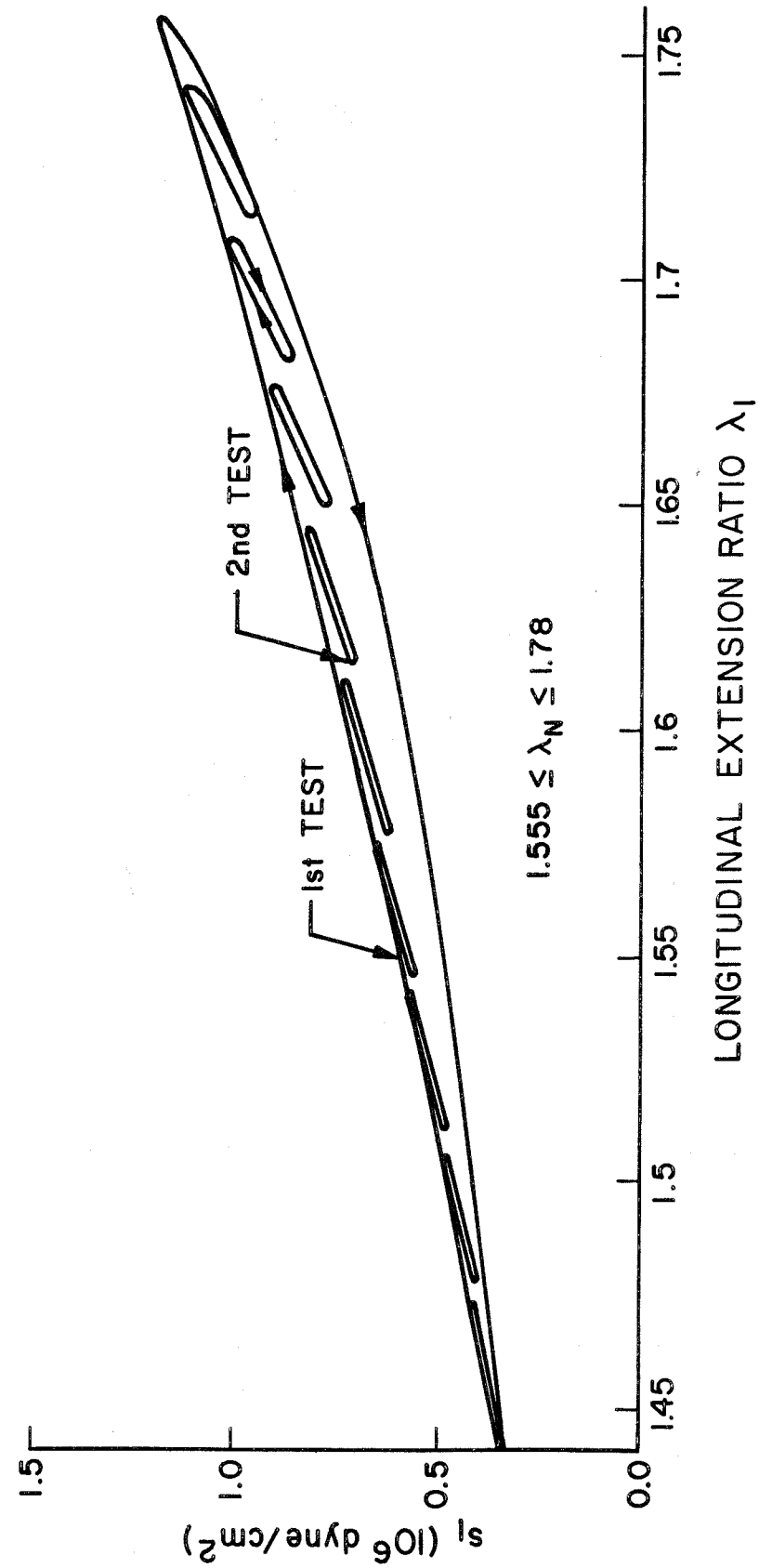

Fig. 12 Hysteresis curves of the repeated-strain test of the carotid artery No. 11. All loops were run at 0.21 cycles per minute.

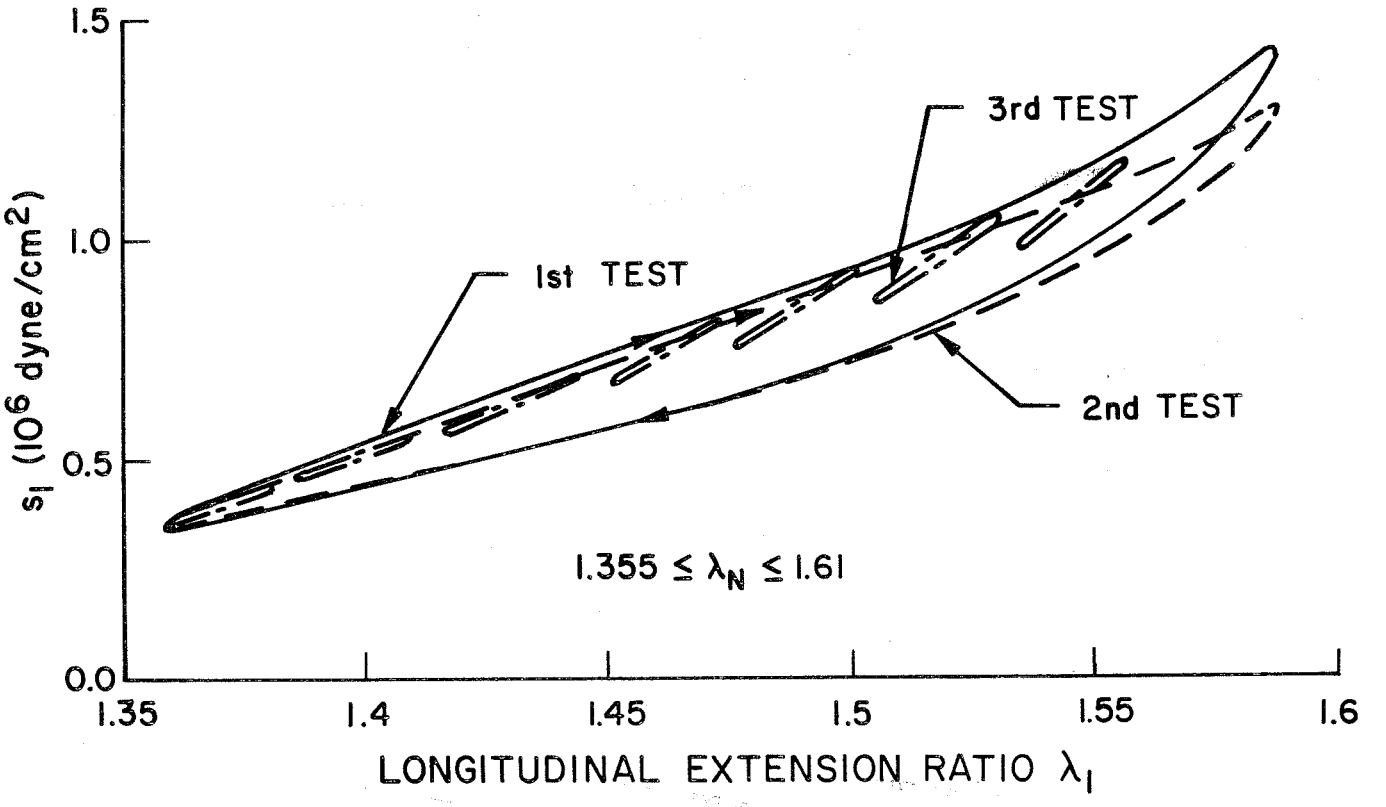

Fig. 13 Hysteresis curves of the repeated-strain test of the carotid artery No. 12. The loops of the first, second and third runs were run at frequencies of 1.1, 0.21 and 1.1 cycles per minute, respectively.

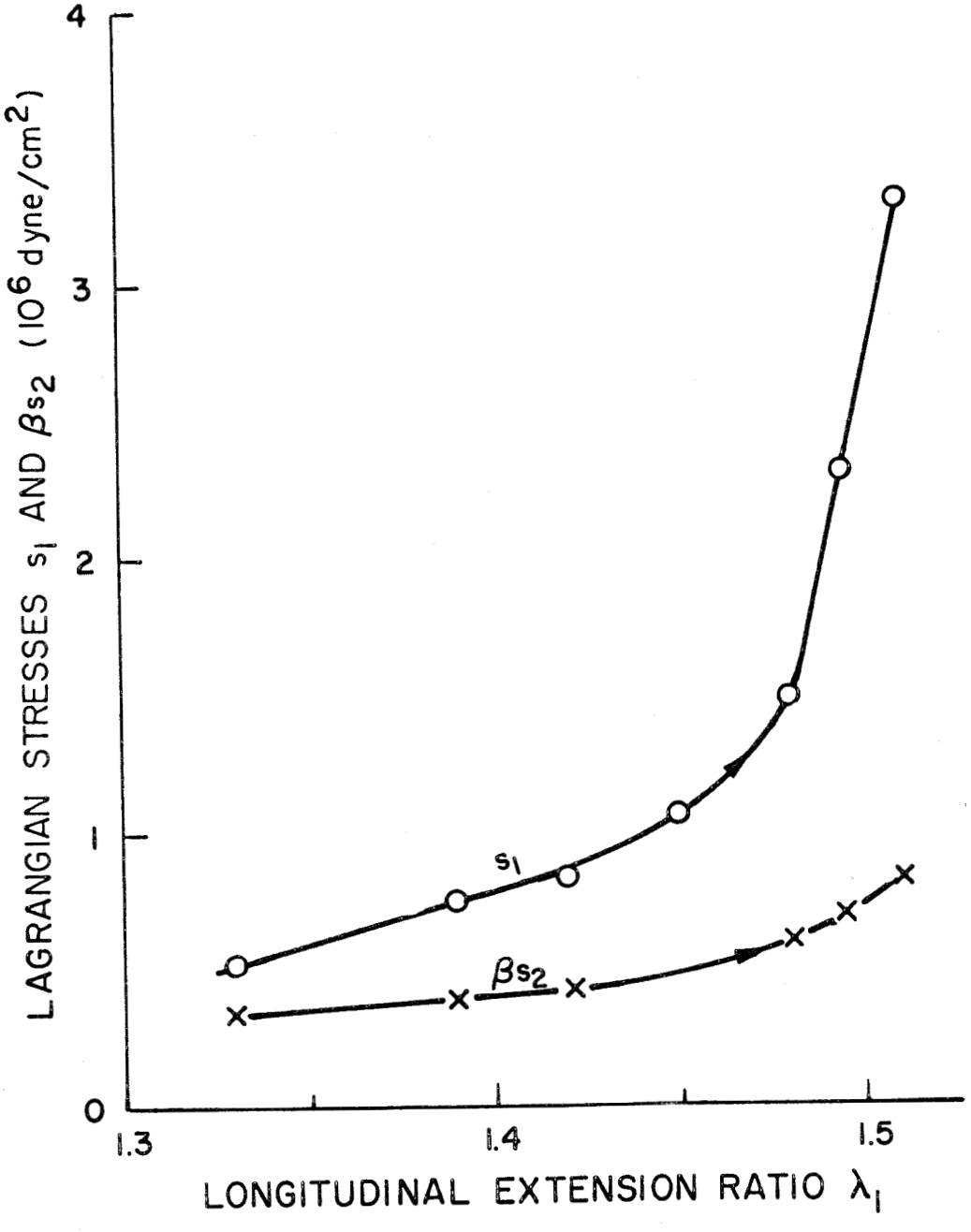

Fig. 14 Lagrangian stresses vs. longitudinal extension ratio of the carotid artery No. 1. The lateral extension ratio λ_2 was 1 .

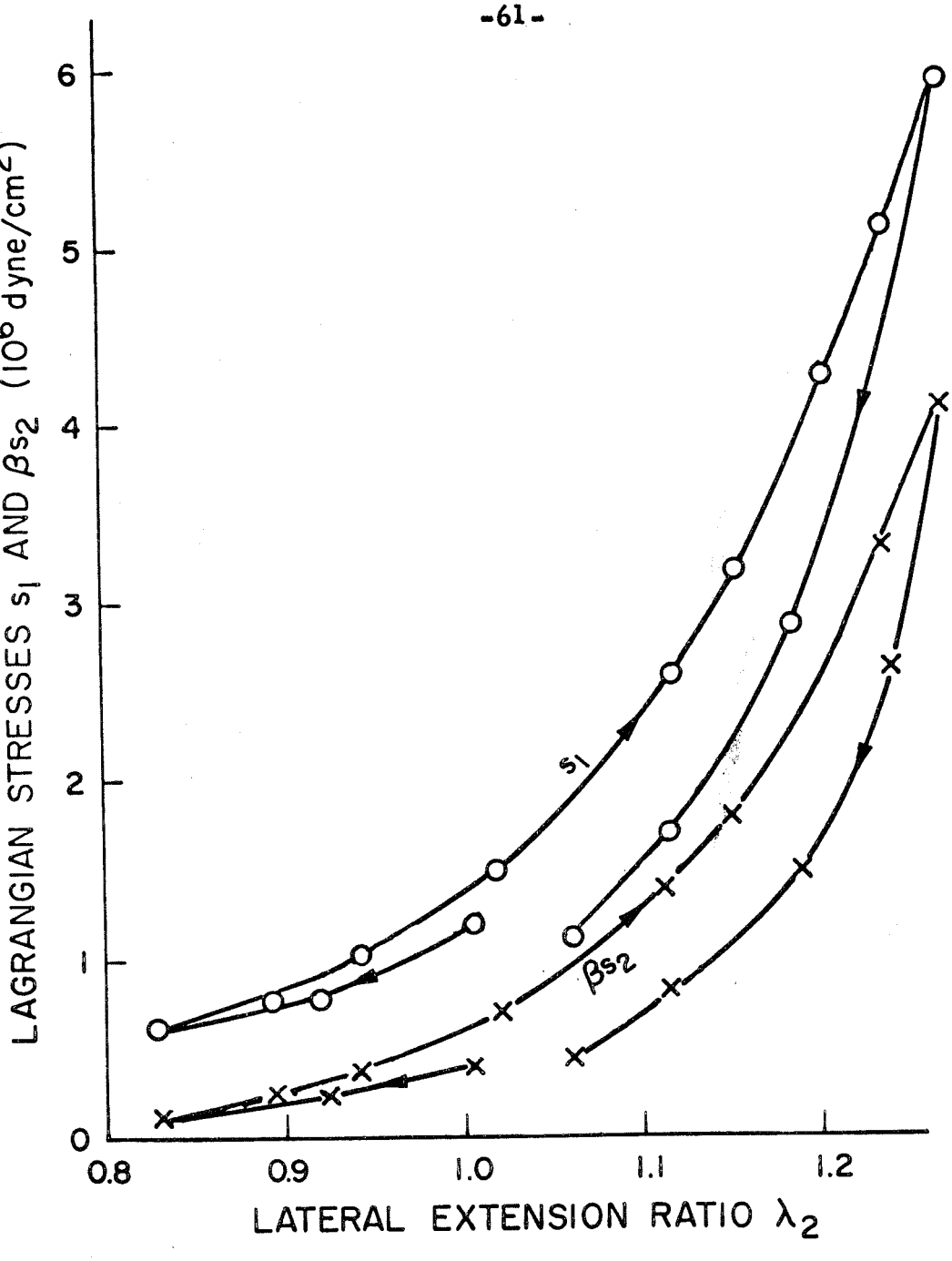

Fig. 15 Lagrangian stresses vs. latitudinal extension ratio of the carotid artery No. 1. The longitudinal extension ratio λ_2 was 1.465.

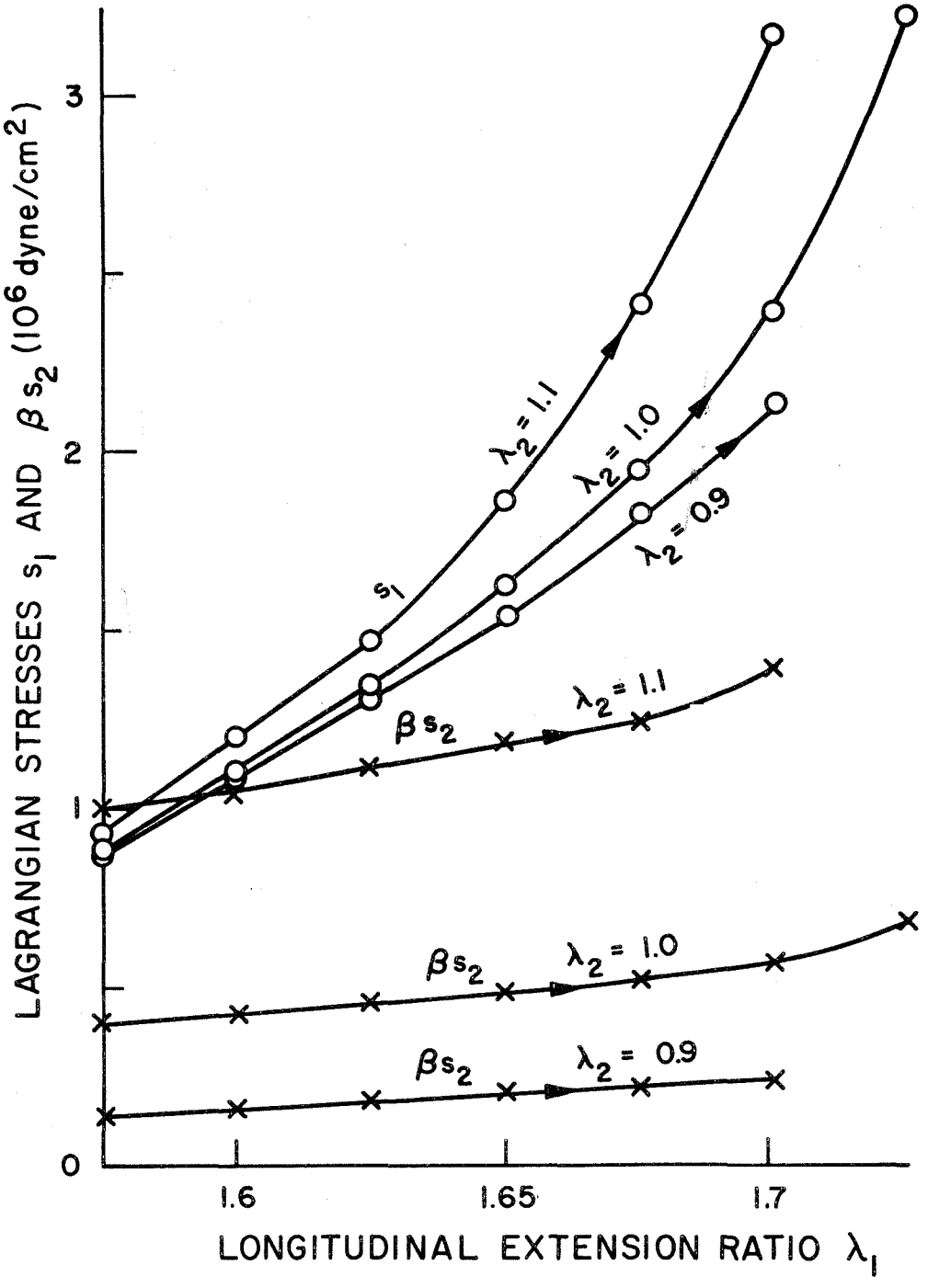

Fig. 16 Lagrangian stresses vs. longitudinal extension ratio of the carotid artery No. 8. The lateral extension ratio λ_2 was kept constant in the stretching test as shown on the curve.

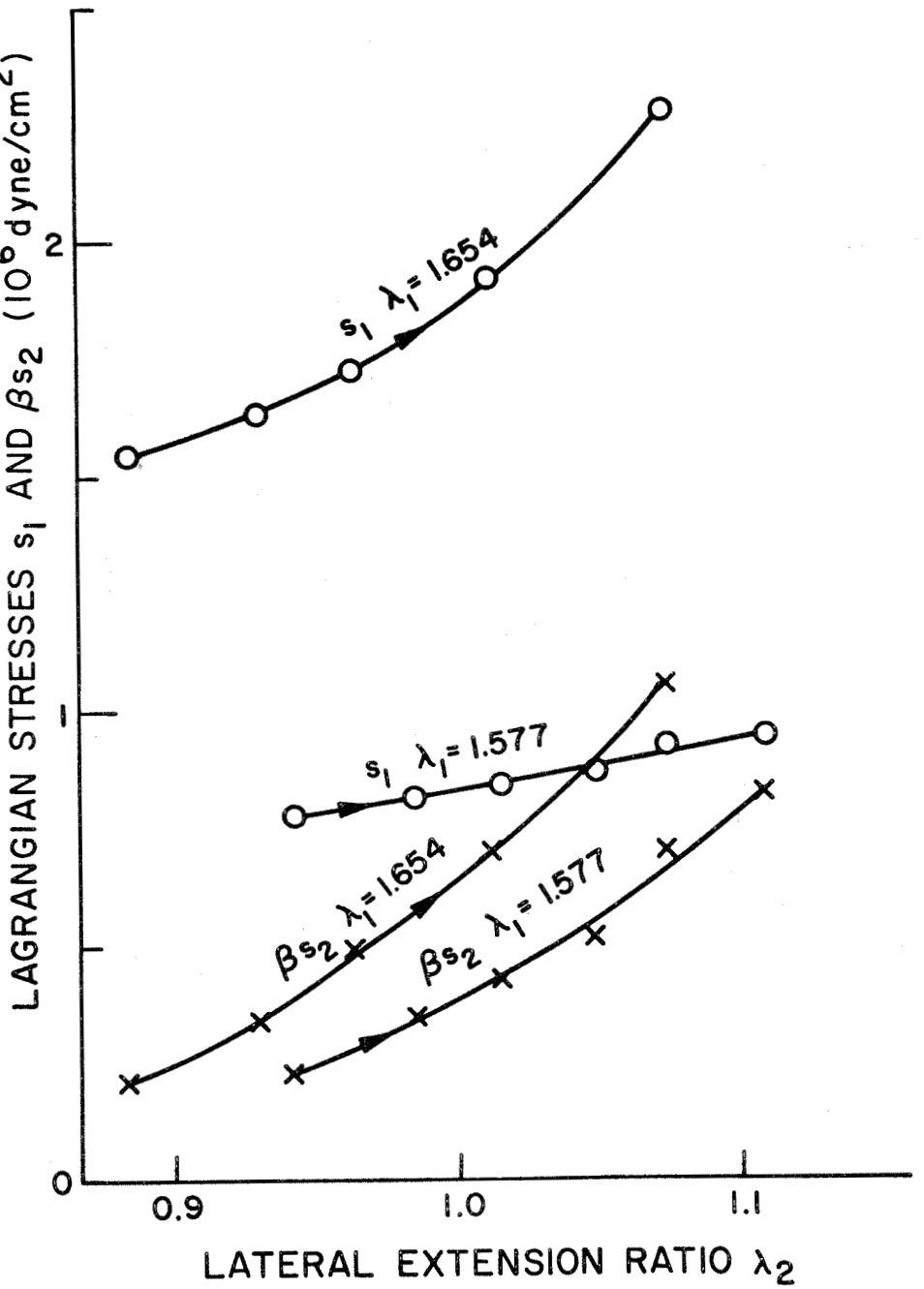

Fig. 17 Lagrangian stresses vs. lateral extension ratio of the carotid artery No. 8. The longitudinal extension ratio λ_1 was kept constant in the distensibility test as shown on the curve.